

# **Pyrolysis Bio-oil as a Renewable Fuel and Source of Chemicals: its Production, Characterization and Stability**

By

© EID MUSA ALSBOU

A thesis submitted to the School of Graduate studies in partial fulfillment of the requirement for the degree of

Doctor of Philosophy

Department of Chemistry  
Faculty of Science  
Memorial University of Newfoundland

July 2014

St. John's, Newfoundland and Labrador

## Abstract

Bio-oil is a liquid fuel that can be produced from various lignocellulosic feedstocks via fast pyrolysis. It is a complex mixture comprised of hundreds of highly oxygenated organic compounds originating from lignin and carbohydrates and is recognized as a clean renewable bio-fuel, an attractive alternative to fossil fuels. It can be easily transported and used directly in boilers and modified turbines or upgraded/fractionated for drop in fuels or chemical production. Proper bio-oil characterization is important in optimizing the pyrolysis process, bio-oil upgrading and utilization, and its stabilization for long-term storage. With this in mind, research has been undertaken to develop better techniques to rapidly profile the composition of whole bio-oil samples, and an accelerated aging study performed to determine why bio-oil is unstable upon storage.

Pyrolysis-GC/MS and TLC-FID were used as tools to differentiate bio-oils of different lignocellulosic biomasses, and among thermal-cracking (upgrading) fractions. Results showed that birch bio-oil had high syringol derivatives compared to pine and barley straw bio-oils which had higher guaiacol and non-methoxy-phenolic compounds, respectively, compared with birch bio-oil. TLC-FID was successful in bio-oil differentiation, showing diagnostic chromatographic profile differences.

Direct infusion-ESI-ion trap MS and ESI-ion trap MS<sup>2</sup> were successfully used in the analysis of forest-residue bio-oil and reference bio-oils from cellulose and hardwood lignin dissolved in methanol:water. NH<sub>4</sub>Cl can be used as a dopant to distinguish carbohydrate-derived products from other bio-oil components. NaOH and NaCl dopants resulted in the highest intensity peaks in negative ion mode and positive mode, respectively. Tandem MS, that is, ESI-Ion Trap MS<sup>2</sup> was a successful tool for the confirmation of

individual target ions such as levoglucosan and cellobiosan and for structural insight into lignin products.

In accelerated aging (at 80 °C for 1, 3 and 7 days) studies, the physical and chemical properties of bio-oil from ash wood (produced from a pilot-scale auger pyrolyzer) and birch wood (lab-scale pyrolyzer) were monitored in order to identify the factors responsible for bio-oil instability. Water content, viscosity, and decomposition temperature (by TGA) increased for both bio-oil samples with aging. Chemical analysis showed reduction in amount of most of the bio-oil components as aging progressed, typically for are olefins and aldehydes. The oils remained a single phase throughout until the 7th day.

## **Acknowledgments**

This work could only have been accomplished through mutual collaboration with different people. I would like to express my special appreciation and thanks to my advisor Dr. Bob Helleur, as you have been a tremendous mentor for me. I would like to thank you for encouraging me throughout my research and allowing me to grow as a research scientist as well as your advice and patient guidance through my study during both research and writing. I would also like to thank Dr. Francesca Kerton and Dr. Sunil Pansare for serving as my committee members. I would especially like to thank the department staff and Linda Winsor (C-CART).

I would like to thank Dr. Erika Merschrod, Dr. Yuming Zhao, and Dr. Paris Georghiou for allowing me to use their laboratory facilities.

I would also like to thank all of my friends and lab-mates, Dr. Mansour Almatarneh, Ahmad Al Shraa, Dr. Iyad Hailat, Dr. Tayel Hujran, Wilson Humphries, Ahmad Al-Rwashdeh, Dr. Khaled Omari, Dr. Osama Al-Hmadneh, Eyad Younes, Dr. Ali Atoom, and Hassan Kofahi who helped, supported me in my study, and encouraged me to strive towards my goal.

I would like to give special thanks to my family. Words cannot express how grateful I am to my mother, Eshbah, and father, Musa, for all the sacrifices you have made on my behalf. Your prayers for me are what have sustained me thus far. I would also like to thank my beloved brothers Abdullah, Ali, Mohammad, Abdurahman and Omar, and sisters Alia, Abla, Esmahan, Fatima and Ishah who have supported my entire life. Thank you for your love.

I would like express appreciation to my beloved wife Etaf who has endured hard times with me and always supported me in the moments when I needed to feel better, and alleviated my anxiety and work pressure. Lastly, I would like to give great thanks to my children, Rafif and Musa, who make my life joyful and beautiful.

Finally, I would like to thank Al-Hussein Bin Talal University, Department of Chemistry and the School of Graduate Studies at Memorial University, BioFuelNet (Canada), and The National Sciences and Engineering Research Council (NSERC) of Canada for their funding Support.

## **Dedication**

To my parents, who spent their lives building a good family and brightening my life with their love and affection.

## Table of Contents

Abstract	ii
Acknowledgements	iv
Dedication	vi
Table of Contents	vii
List of Figures	x
List of Tables	xiii
List of Abbreviations	xv
<hr/>	
<b>Chapter 1: Introduction</b>	<b>1</b>
1.1. Fuel from the renewable sources	2
1.2. Woody feedstock main components	3
1.3. Biomass conversion methods	7
1.4. Thermochemical conversion of biomass	8
1.5. Fast Pyrolysis	10
1.6. Pyrolysis of lignocellulosic biomass	13
1.7. Bio-oil	16
1.8. Bio-oil characterization	19
1.8.1. Physical characterization	20
1.8.2. Chemical characterization	21
1.9. Stability and chemical recovery from bio-oil	26
1.9.1. Stability of bio-oil	26
1.9.2. Chemical recovery from bio-oil	28
1.10. Objectives of this study	31
1.11. Co-authorship statement	32
1.12. References	33
<hr/>	
<b>Chapter 2: Whole sample analysis of bio-oils and thermal cracking fractions by Py-GC/MS and TLC-FID</b>	<b>37</b>
Summary	38
2.1. Introduction	39
2.1.1. Bio-oil	39
2.1.2. Analysis of bio-oil	41
2.2. Materials and methods	43
2.3. Results and discussion	47
2.3.1. Py-GC/MS	47
2.3.1.1. Bio-oil samples	47
2.3.1.2. Forest residue bio-oil and its thermal cracking fractions	57
2.3.2. TLC-FID analysis	59
2.3.2.1. Bio-oil samples	59
2.3.2.2. Forest residue bio-oil and its thermal cracking fraction	64

2.4. Conclusion	65
2.5. References	66
<b>Chapter 3: Direct infusion mass spectrometric analysis of bio-oil using ESI-Ion Trap MS</b>	<b>69</b>
Summary	70
3.1. Introduction	71
3.2. Materials and methods	76
3.2.1. Samples and materials	76
3.2.2. Py-GC-MS	76
3.2.3. ESI-Ion Trap MS	78
3.2.4. Bio-oil fractionation	78
3.3. Result and discussions	79
3.3.1. Py-GC/MS	79
3.3.2. ESI Ion Trap MS	80
3.3.2.1. Model compounds	80
3.3.2.2. Bio-oil samples	83
3.3.2.3. Bio-oil fractionation	94
3.4. Conclusion	97
3.5. References	98
<b>Chapter 4: Accelerated aging of bio-oil from fast pyrolysis of hardwood</b>	<b>100</b>
Summary	101
4.1. Introduction	102
4.2. Materials and methods	106
4.2.1. Materials	106
4.2.2. Bio-oil samples and accelerated aging	107
4.2.3. Analysis	108
4.2.3.1. Physiochemical properties	108
4.2.3.2. Py-GC/MS analysis	109
4.2.3.3. Thermogravimetric analysis (TGA)	109
4.2.3.4. FTIR analysis	109
4.2.3.5. <sup>13</sup> C-NMR analysis	110
4.3. Results and discussions	110
4.3.1. Fresh bio-oil samples	110
4.3.2. Change in water content	111
4.3.3. Viscosity	111
4.3.4. TGA	112
4.3.5. Py-GC/MS	114
4.3.6. FTIR	121
4.3.7. <sup>13</sup> C-NMR analysis	122
4.3.8. Homogeneity	125
4.4. Conclusion	127



4.5. References	128
<b>Chapter 5: Summary and future work</b>	<b>130</b>
5.1. Summary of research	131
5.2. Future work	134
5.3 References	136
<b>Appendix</b>	<b>138</b>
Supporting Information for Chapter 3	139

## List of Figures

Figure 1.1	Main features of biomass energy technology [ <i>Reproduced with permission from reference (10)</i> ].	3
Figure 1.2	The schematic representation of the main biopolymer components in lignocellulosic biomass.	6
Figure 1.3	Products from thermal conversion of biomass [ <i>Reproduced with permission from references (6, 16)</i> ].	9
Figure 1.4	Proposed mechanism of cellulose pyrolysis (DP: degree of polymerization; compounds symbols can be found in text) [ <i>Adapted with permission from reference (18)</i> ].	15
Figure 2.1	Iatrosan TLC–FID setup.	45
Figure 2.2	TIC of the volatile products of bio-oil obtained from (a) barley straw, (b) pine wood, (c) birch wood and (d) lignin.	50
Figure 2.3	Mass % for residue in Py-cup, water content and GC-detectable in bio-oil obtained from barley straw, pine wood, birch wood lignin and forest residue.	55
Figure 2.4	TIC of the volatile products of forest residue bio-oil and its thermal cracking fractions. (a) Forest residue bio-oil, (b) light fraction, (c) middle fraction and (d) heavy fraction.	58
Figure 2.5	TLC–FID chromatograms of (a) standards, (b) lignin bio-oil, (c) barley straw bio-oil, (d) pine wood bio-oil, and (e) birch wood bio-oil.	61
Figure 2.6	TLC–FID chromatograms of forest residue bio-oil and its thermal cracking fractions. (a) Standards, (b) forest residue bio-oil, (c) light fraction, (d) middle fraction, and (e) heavy fraction.	63
Figure 2.7	Relative peak area for polarity zones on TLC chromatograms obtained for bio-oil from barley straw, pine wood, birch wood, lignin and forest residue.	64
Figure 3.1	GC/MS TIC of bio-oils from a) cellulose, b) lignin and c) forest residue. [LG: levoglucosan, G: guaiacol, S: syringol, and V: vanillin].	80
Figure 3.2	Product ion spectra from the MS <sup>2</sup> analysis for NH <sub>4</sub> <sup>+</sup> and Cl <sup>-</sup> adducts of model carbohydrates.	83
Figure 3.3	Negative ion ESI-Ion Trap mass spectra of bio-oils. *= deprotonated LG; C= carbohydrate-derived; L= lignin-derived.	84
Figure 3.4	Positive ion ESI-Ion Trap mass spectra of different bio-oils. *= sodiated LG.	85
Figure 3.5	Product ion spectra from MS <sup>2</sup> experiments for LG standard in negative ion (a) and positive ion (b); for cellulose's <i>m/z</i> 161 in negative ion (c) and for <i>m/z</i> 185 in positive ion (d) forest residue's <i>m/z</i> 161 in negative ion (e) and <i>m/z</i> 185 positive ion (f) and for cellulose (g) and forest residue bio-oil's (h) <i>m/z</i> 323 in negative ion.	87

Figure 3.6	Product ion spectra from negative ion MS <sup>n</sup> experiments. MS <sup>2</sup> of <i>m/z</i> 151 from (a) lignin bio-oil and (b) forest residue bio-oil and (c) <i>m/z</i> 317 and MS <sup>3</sup> of <i>m/z</i> 163 (d) and <i>m/z</i> 191 (e) from lignin bio-oil's parent ion <i>m/z</i> 317.	89
Figure 3.7	Negative and positive ion ESI mass spectra of the various doped cellulose bio-oil samples. * = sodiated levoglucosan <i>m/z</i> 185; ** = sodiated <i>m/z</i> 203 (glucose); AM = ammoniated carbohydrate products.	91
Figure 3.8	Negative and positive ion ESI MS spectra of various doped forest residue bio-oil samples. * = sodiated levoglucosan <i>m/z</i> 185; ** = sodiated <i>m/z</i> 203 (glucose); AM = ammoniated carbohydrate products.	92
Figure 3.9	Product ion spectra from MS <sup>2</sup> experiments obtained for NH <sub>4</sub> Cl-doped bio-oils for <i>m/z</i> 180 present in positive ion spectra of (a) cellulose bio-oil, and (b) forest residue oil; <i>m/z</i> 342 in positive ion mode spectra of (c) cellulose bio-oil, and (d) forest residue oil; <i>m/z</i> 359 in negative ion mode spectra of (e) cellulose bio-oil, and (f) forest residue bio-oil.	93
Figure 3.10	Negative ion ESI-mass spectra of forest residue bio-oil fractions using SPE and lignin precipitation techniques.	95
Figure 3.11	Positive ion ESI- mass spectra of forest residue bio-oil fractions using SPE and lignin precipitation techniques.	96
Figure 4.1	Lab scale pyrolysis unit.	107
Figure 4.2	(a) Water content (% , wt/wt) for fresh and aged (at 80°C) bio-oil samples. (b) viscosity measurements (at 25 °C) for the fresh and aged bio-oil samples. Average of triplicate runs with %RSD between 5-8%.	113
Figure 4.3	TGA curves for the control and aged (at 80°C) bio-oil samples from ash and birch woods [sample code: AB=ash bio-oil, BB= birch bio-oil; -0,-1,-3,-7 present fresh, 1, 3 and 7 day aged bio-oils]. Curves represent average of duplicate runs.	113
Figure 4.4	GC/MS TIC for the fresh bio-oil samples. [Labeled peaks are identified in Table 4.2, AB-0: fresh ash bio-oil (control) and BB-0: fresh birch bio-oil (control)].	114
Figure 4.5	Relative peak area changes for identified compounds during accelerated aging (at 80°C) for bio-oil samples (see Table 4.2 for identification of numbered compounds in Figure 4.4). Bars represent average of duplicate runs; RSD < 5%.	118
Figure 4.6	Possible chemical reactions that may occur during bio-oil accelerated aging (at 80°C).	119

Figure 4.7	Py GC/MS TIC at 550 °C for residues from Py-GC/MS analysis at 270 °C [AB-0: fresh ash bio-oil (control), AB-7: 7-days aged ash bio-oil (at 80°C), BB-0: fresh Ash bio-oil (control) and BB-7: 7-days aged birch bio-oil (at 80°C)].	120
Figure 4.8	FTIR spectra of fresh and aged (at 80°C) bio-oil samples	122
Figure 4.9	<sup>13</sup> C NMR spectra for the fresh (AB-0) and 7-day aged (at 80°C) bio-oil (AB-7) sample from ash wood.	123
Figure 4.10	<sup>13</sup> C NMR spectra for the fresh (BB-0) and 7-days aged (at 80°C) bio-oil (BB-7) sample from birch wood.	124
Figure 4.11	Microscopic images (×10) for fresh and aged ash bio-oil (at 80°C).	125
Figure 4.12	Microscopic images (×10) for fresh and aged birch bio-oil (at 80°C).	126
Figure S3.1	Small-scale tube-furnace pyrolysis unit.	140
Figure S3.2	GC-MS: Individual products in bio-oils from a) cellulose, b) lignin and c) forest residue.	141

### List of Tables

Table 1.1	Organic components and ash in representative lignocellulosic biomass [ <i>Reprinted with permission from reference (10)</i> ].	7
Table 1.2	Classification of transportation-based biofuels [ <i>Reproduced with permission from reference (2)</i> ].	8
Table 1.3	Types of pyrolysis processes, processing conditions, and products obtained [ <i>Reproduced with permission from reference (2)</i> ].	11
Table 1.4	Variations of fast pyrolysis reactor systems [ <i>Reproduced with permission from references (2, 12-13)</i> ].	12
Table 1.5	Comparison of some properties of bio-oils produced by pyrolysis of wood and heavy fuel oil [ <i>Reproduced with permission from references (8-9)</i> ].	17
Table 1.6	Chemical composition of fast pyrolysis liquid [ <i>Reprinted with permission from reference (8)</i> ].	19
Table 1.7	Summary of methods for determining physical properties of bio-oil [ <i>Reprinted with permission from references (22-24)</i> ].	20
Table 1.8	Methods to slow down aging of bio-oils [ <i>Reprinted with permission from reference (42)</i> ].	27
Table 1.9	Major compounds and fractions recovered from bio-oil and their application (5, 13, 48).	29
Table 1.10	Bio-oil fractionation methods [ <i>Reprinted with permission from reference (15)</i> ].	31
Table 2.1	Bio-oil samples (Biomass feedstock, pyrolysis method and their sources).	44
Table 2.2	Development solvent system for TLC–FID analysis of bio-oil.	46
Table 2.3	Products detected in bio-oil samples and cracking fractions using Py-GC/MS and mass % of oil left in Py-cup.	51
Table 3.1	Model compounds.	77
Table 4.1	Initial bio-oil properties.	111
Table 4.2	Identified compounds in bio-oil samples from ash and birch wood.	117
Table S3.1	MS methods that have been used in characterization of bio-oils.	139
Table S3.2	Products identified in bio-oil samples shown in Figure S3.2.	142
Table S3.3	Model compounds: Positive ion mode ESI MS, with and without dopants.	142
Table S3.4	Model compounds: Negative ion mode ESI MS, with and without dopants.	145
Table S3.5	Tandem mass spectra in positive and negative modes for model compounds.	146
Table S3.6	Negative mode MS <sup>2</sup> product ions resulting from ESI-Ion Trap MS of selected ions from the mass spectra of cellulose-bio-oil.	148

Table S3.7	Positive mode MS <sup>2</sup> product ions resulting from ESI-Ion Trap MS of selected ions from the mass spectra of cellulose-bio-oil.	150
Table S3.8	Negative mode MS <sup>2</sup> product ions resulting from ESI-Ion Trap MS of selected ions from the mass spectra of lignin-bio-oil	152
Table S3.9	Positive mode MS <sup>2</sup> product ions resulting from ESI-Ion Trap MS of selected ions from the mass spectra of lignin-bio-oil.	154
Table S3.10	Negative mode MS <sup>2</sup> product ions resulting from ESI-Ion Trap MS of selected ions from the mass spectra of forest residue-bio-oil.	156
Table S3.11	Positive mode MS <sup>2</sup> product ions resulting from ESI-Ion Trap MS of selected ions from the mass spectra of forest residue-bio-oil.	157

## List of Abbreviations

APCI	Atmospheric pressure chemical ionization
APPI	Atmospheric pressure photoionization
Cbio	Cellobiose
DBE	Double-bond equivalents
DP	Degree of polymerization
EPC	Electronic pressure control
ESI	Electrospray ionization
FAB-MS	Fast atom bombardment mass spectrometry
FI-MS	Field ionization mass spectrometry
FID	Flame ionization detector
FT-ICR	Fourier transform ion cyclotron resonance
FTIR	Fourier transform infrared
G	Guaiacol
GPC	Gel permeation chromatography
Glu	D-glucose
HSQC	Heteronuclear single-quantum correlation
HHV	High heat value
HPTLC	High performance thin layer chromatography
HRMS	High-resolution mass spectrometry
LDI	Laser desorption ionization
LG	Levoglucosan
LC	Liquid chromatography

M.wt	Molecular weight
MALDI	Matrix-assisted laser desorption/ionization
MSD	Mass selective detector
MBMS	Molecular beam mass spectrometry
MS	Mass spectrometry
NMR	Nuclear magnetic resonance
Py-GC/MS	Pyrolysis-gas chromatography/mass spectrometry
Py-lignin	Pyrolytic lignin
Q-TOF	Quadruple-time-of-flight
RPA	Relative peak area
S	Syringol
SEC	Size exclusion chromatography
SPE	Solid phase extraction
TGA	Thermogravimetric analysis
TCD	Thermal-conductive detector
TLC-FID	Thin layer chromatography-flame ionization detector
TOF	Time-of-flight mass spectrometry
TIC	Total ion current
GC × GC	Two-dimensional gas chromatography
V	Vanillin



# **Chapter One**

## **Introduction**

## **1.1. Fuel from the renewable sources**

The major source for energy and fuel is from non-renewable fossil sources, i.e., crude oils, coals and natural gas. Currently, they have received considerable attention due to their depletion, rising cost, uncertainty of supply, and issues with safe storage and transportation. However, environmental concerns about fossil fuel have taken the center of stage in the last few decades because of global concern about climate change due to increasing greenhouse gas emissions from fossil fuel burning (i.e., CO<sub>2</sub>, SO<sub>2</sub>, and N<sub>2</sub>O) and air pollution in major cities (1-3). All these concerns about the use of fossil fuels have led to increasing research into alternative sources for fuels and chemicals, which are renewable, of which biomass as a feedstock has captured major attention.

Globally, biomass represents the fourth largest source of energy contributing to ca. 12% of the world's primary energy source, and 40-50% in many less-developed countries such as those in Africa (4-5). In 2006, 4.7 % of Canada's energy needs were from renewable biomass and waste, and this percentage is expected to increase to 6–9% in the next 20 years (6).

Biomass is defined as all living and dead biological materials, including forests, sawmill wastes, agricultural residues, micro-organisms, algae, and biological wastes (7). Biomass can be used directly as an energy source for heating and electricity, or used as feedstocks in conversion processes to make liquid, solid or gas fuels (7). Biomass can be environmentally friendly as most of biomass feedstock contains negligible amounts of sulfur, nitrogen, and ash (8). In addition, its combustion produces CO<sub>2</sub> that can be naturally recycled by the plants through photosynthesis (see Figure 1.1) (8). Living biomass (e.g., plants and trees), in turn, play a major role as a carbon sink through photosynthetic

conversion into carbon-rich compounds (e.g., cellulose and lignin) (2, 9). Thus unlike fossil fuels, biomass feedstock is a renewable resource so long as the selected living biomass is managed properly. The sustainability of biomass is a critical issue for a renewable feedstock as a source of energy. As such dedicated non food crops and various sources of waste, (i.e., forestry industry waste, agricultural residues, food-processing by-products) are primary candidates (4).

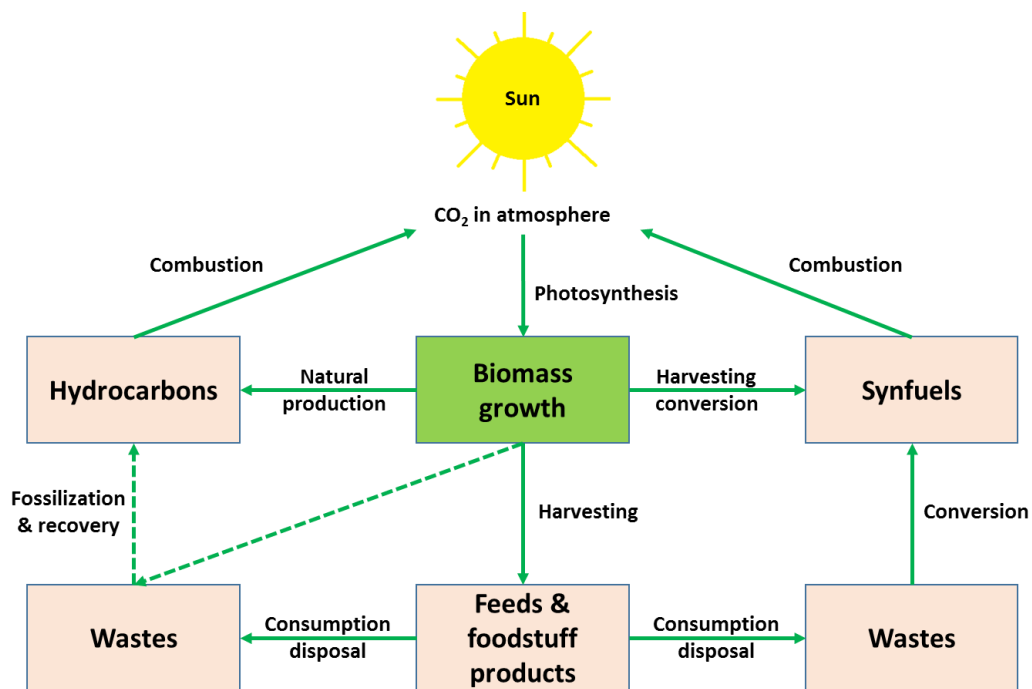


Figure 1.1. Main features of biomass energy technology [Reproduced with permission from reference (10)].

## 1.2. Woody feedstock main components

Biomass (typically, lignocellulosic biomass) is considered to be the major renewable source of energy and chemicals that will make a significant change in world-energy-use in the future (3, 11). The composition of lignocellulosic biomass is complex, mainly consisting of macromolecular (biopolymer) substances, such as hemicellulose,

cellulose and lignin, in addition to small amounts of low molecular weight substances, for example, extractives (tannins, fatty acids, and resins), and inorganic salts (10, 12). The three basic biopolymers are cellulose  $[C_6H_{10}O_5]_x$ , hemicelluloses such as xylan  $[C_5H_8O_4]_m$ , and lignin  $[C_9H_{10}O_3(OCH_3)_{0.9-1.7}]_n$  existing in varying amounts in all parts of the plant (8). Figure 1.2 illustrates the chemical structures of the major biopolymers found in lignocellulosic biomass, (11). In addition, Table 1.1 shows the percentage of organic components for representative biomass species as well as the corresponding ash contents (10). For the tree species the proportion of biopolymer wood components are different between hardwoods and softwoods. Hardwoods have a higher content of cellulose and hemicellulose compared to softwoods, whereas softwoods have a higher proportion in lignin (4, 8). Ash and protein contents in grass are higher than that for woody biomass.

Cellulose is the largest chemical component in biomass, representing 40–50% by weight of the wood samples (4, 10, 11). Cellulose is a high molecular-weight ( $10^6$  Da or more) linear homopolymer, composed of 5000-10000 glucopyranose units linked by  $\beta$ -1,4-glycosidic bonds (12-13). The main repeating unit within the cellulose polymer is a two glucose unit (“cellobiose”) (12). The macrostructure of cellulose is a superhelical shape (cellulose microfibrils) with a large H-bonding content between polymers (11). Therefore, cellulose microfibrils are strong, resistant to both chemical and biological attack, which provides wood its inherent strength (6, 8).

Unlike cellulose, hemicellulose is a heteropolymer composed of randomly, branched, amorphous, and short-chained polymers with a degree of polymerization of about 150 sugar units (1, 6). About 25–30% of dry wood samples is made of hemicellulose (4, 8), and consists of a mixture of hexoses (D-galactose, D-glucose, and D-mannose) and

pentoses (mainly L-arabinose and D-xylose) sugars and importantly varying degrees of acetyl groups (3). Because of its heterogeneous nature the hemicelluloses have little structural strength, and their chains are more easily decomposed into their monomeric units than cellulose chains (6).

In plant cells, lignin surrounds the cellulose microfibers and binds them together as well as protects the cellulosic fibers against microbial or fungal destruction (3, 13). It is found in 20-30% abundance in woody biomass (4) and is a heterogeneous aromatic polymer synthesized from phenyl propanoid precursors, i.e., guaiacyl (4-hydroxy-3-methoxyphenyl), syringyl (3,5-dimethoxy-4-hydroxyphenyl) and *p*-hydroxyphenyl units (see Figure 1.2) (3, 8, 14). Lignin structure is much more complicated than the carbohydrate polymers and its precise structure is highly variable (6). A hypothetical chemical structure for a formation of lignin shows it to be a highly branched and three-dimensional material, (Figure 1.2). Lignin has a higher thermal stability compared to cellulose and hemicellulose (1, 3, 8, 15). The composition of lignin differs among softwood, hardwood and grasses. Softwood lignin is mainly composed of guaiacyl units, while hardwood lignin is a guaiacyl-syringyl copolymer. The syringyl units fraction in hardwood is higher than that in softwood lignin (8, 13).

Extractives in biomass are chemicals that can be extracted from the dried milled sample with solvents (polar: water, alcohol, or non-polar: toluene, hexane) (13). The extractives found in wood are in small amounts compared to the amount of biopolymers. Extractives include fats, waxes, alkaloids, proteins, phenolics, simple sugars, pectins, mucilages, gums, resins, terpenes, starches, glycosides, saponins, and essential oils.

Generally, the extractives assist the plant metabolism, and serve as energy reserves and as defense compounds for a plant against microbial and insect attack (13).

The ash concentration in biomass depends on its origin, which can range from < 1% in softwoods to ca. 15% in herbaceous biomass and agricultural residues (14). The most abundant elements present in woody biomass are calcium and potassium (13-14). The presence of these elements is important in thermoconversion as they can catalyze biomass depolymerization and charring reactions (14). Sulfur, chlorine and heavy metals are present at trace levels in biomass (5).

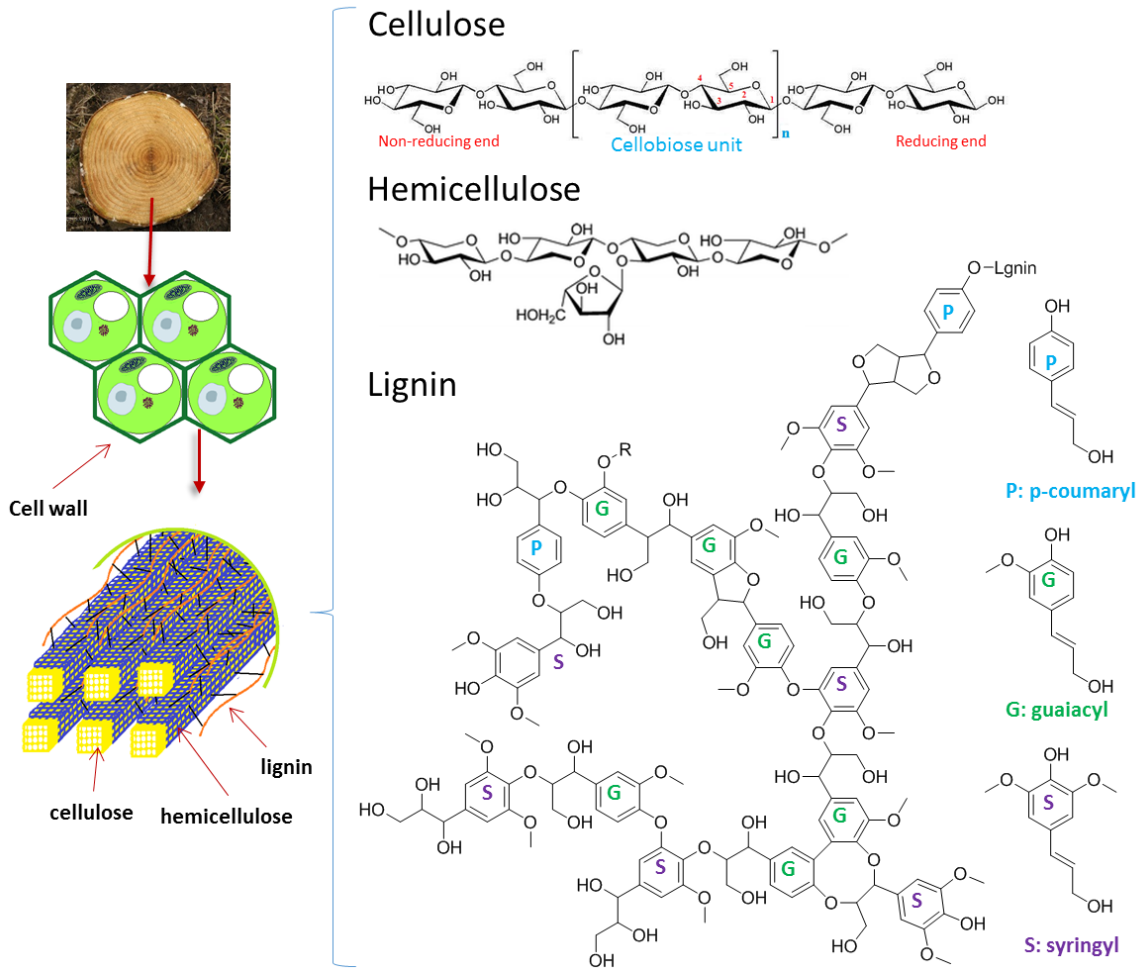


Figure 1.2. The schematic representation of the main biopolymer components in lignocellulosic biomass.

Table 1.1: Organic components and ash in representative lignocellulosic biomass  
 [Reprinted with permission from reference (10)].

<b>Biomass type</b>	<b>Herbaceous</b>	<b>Hardwood</b>	<b>Hardwood</b>	<b>Softwood</b>
Component (dry wt. %)	Bermuda grass	Poplar	Sycamore	Pine
Cellulose	31.7	41.3	44.7	40.4
Hemicellulose	40.2	32.9	29.4	24.9
Lignin	4.1	25.6	25.5	34.5
Crude protein	12.3	2.1	1.7	0.7
Ash	5.0	1.0	0.8	0.5
Total*	93.3	102.9	102.1	101.0

\* Sum of % recovered components from each biomass feedstock (Total = % cellulose + % hemicellulose + % lignin + % crude protein + % ash )

### 1.3. Biomass conversion methods

Energy produced from biomass is generally derived from wood and wood wastes (64%), followed by municipal solid waste (24%), agricultural waste (5%), and landfill gases (5%) (8). Different process-technologies can be used to convert biomass to different forms of energy and fuel, depending on the raw material and the form of energy that is wanted (9). The two major energy-conversion routes are biological such as fermentation and anaerobic digestion, and thermochemical such as combustion, gasification, and pyrolysis, and more recently through biotechnology and nanotechnology-based processes (2, 5, 7-8). Biological conversion is usually selective, producing a small number of products in high yields using biological catalysts, while thermal conversion produces complex mixtures of products within a very short reaction time (16). For example, lignin can be degraded easily by thermal methods, whereas it is considered to be very difficult to convert using fermentation (6). The biomass-conversion products can be used directly or they can

be upgraded to produce various energy forms such as biofuels, high energy density forms such as charcoal, liquid fuels (ethanol), and gaseous fuels (hydrogen, methane) (2).

Table 1.2 lists the four biofuel categories and their classification with representative examples (2). All biofuel are normally clean burning and renewable. The first generation bio-fuels are not preferred due to their competition with food and feed industry. However, the second-generation bio-fuels have an advantage in production cost and availability of their raw biomass feedstocks such as wood and agriculture wastes. As well, they do not have an influence on the food market like the first generation fuels. The third and fourth generation bio-fuels are also clean but they are considered expensive to be produced.

Table 1.2: Classification of transportation-based biofuels [*Reproduced with permission from reference (2)*].

<b>Type of biofuel</b>	<b>Sources of bio-fuel</b>	<b>Examples</b>
First-generation	Raw materials in competition with food and feed industry	<ul style="list-style-type: none"> <li>• Bioethanol from sugarcane</li> <li>• Biodiesel</li> </ul>
Second-generation	Non-food crops (energy crops), or waste residues	<ul style="list-style-type: none"> <li>• Biogas derived from waste and residues</li> <li>• Biofuels from lignocellulosic material</li> </ul>
Third-generation	Aquatic microorganisms like algae	<ul style="list-style-type: none"> <li>• Biodiesel produced from algae</li> <li>• Hydrogen derived from algal cultures</li> </ul>
Fourth-generation	Biofuels based on high solar efficiency cultivation	<ul style="list-style-type: none"> <li>• Carbon-negative technology</li> <li>• Technology of the future</li> </ul>

#### **1.4. Thermochemical conversion of biomass**

Thermochemical conversion methods for biomass include combustion, gasification, pyrolysis, and liquefaction. Figure 1.3 shows different types of products from these conversion methods (16). There are two general types: primary and secondary technologies (2). In primary conversion such as combustion, gasification, hydrothermal liquefaction, and



pyrolysis, the biomass is directly converted into products, while in secondary conversion; the products from primary conversion are used to produce desired energy, e.g., transportation fuel, electricity or chemicals (2).

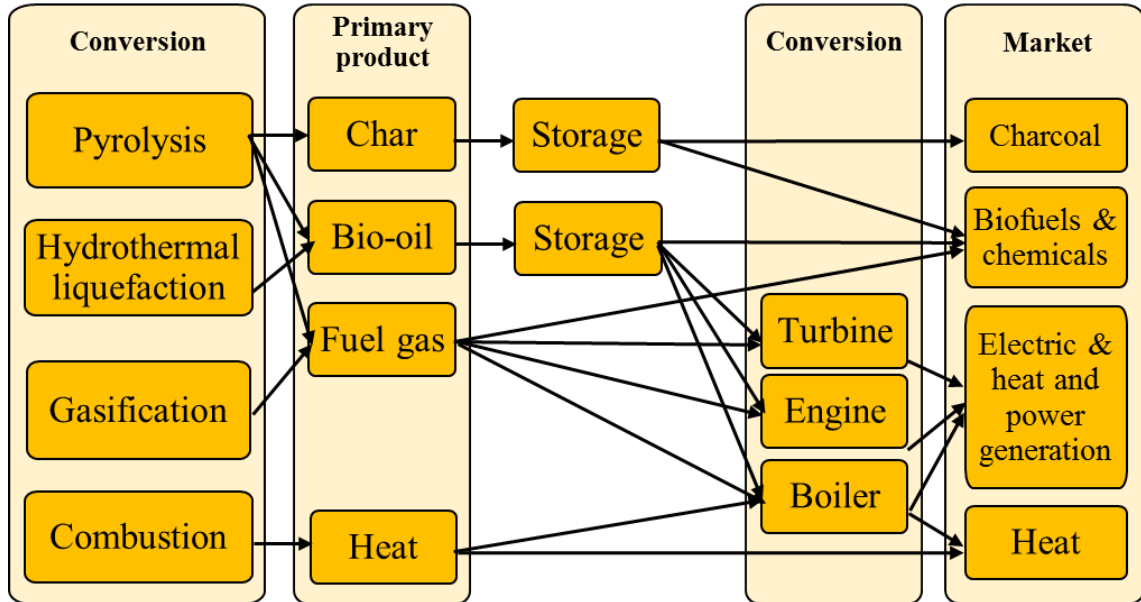


Figure 1.3. Products from thermal conversion of biomass [Reproduced with permission from references (6, 16)].

The stored energy within biomass can be simply released by combustion in the presence of an oxidant (6). As an alternative pyrolysis occurs when biomass undergoes thermal decomposition at high temperatures in the absence of air or oxygen to produce gas (e.g., synthesis gas (syngas)), liquid products (bio-oil), and a carbon-rich residue (bio-char). Gasification is similar to pyrolysis, but performed at higher temperature with partial oxidation. The gas, which is the major product here, consists of  $H_2$ ,  $CO$ ,  $CO_2$ , and  $H_2O$ . Gasification can also produce a larger portion of gaseous hydrocarbons when lower temperatures are used (13). Hydrothermal liquefaction of biomass involves a direct conversion of a biomass into bio-oil in the presence of water (with or without catalysts) at

low temperature (ca. 400 °C) and high pressure (2, 4). Liquefaction also yields solids and gases in this reducing environment (13).

### **1.5. Fast Pyrolysis**

Pyrolysis dates back to at least the time of the ancient Egyptians, when the pyrolysis product “tar” was used for caulking boats and as an embalming agent (8). Pyrolysis methods have been utilized over thousands of years for charcoal production. However, fast pyrolysis has become of interest to researchers only in the last 20 years (16). The products of pyrolysis include: gas products, liquid products, and carbonaceous solid (bio-char). The pyrolysis’ gaseous products (syngas) include CO, CO<sub>2</sub>, and CH<sub>4</sub>, while its liquid products (bio-oil) contain water and oils (6). All of these products are useable; the bio-oil can be used for heating, power generation, upgrading to transportation fuel, or manufacturing of suitable chemicals; the gaseous products and bio-char can be used for heating or soil amendment in case of char (Figure 1.3) (2). Many modes of pyrolysis have been developed and used with varying success, depending on their processing conditions, vapor residence times, and the yields of products (Table 1.3). Each method is selected based on the desired products. Fast pyrolysis primarily produces a liquid product while slow pyrolysis (torrefaction) produces primarily char and less gaseous product.

Among the pyrolysis methods, fast pyrolysis is the most favorable choice for bio-oil production because it quickly produces a high yield from bio-oil (60–75 %) and less from gaseous products (15–25 %) and char (10–20 %). Fast pyrolysis from a biomass can be done through high heat transfer, short reaction times and fast quenching of condensable oils with optimum process parameters (6, 12, 16). Many designed reactors have been used

to perform a fast pyrolysis with variation in their mechanism of heat transfer to biomass and ability to scale up. Table 1.4 lists some of the fast pyrolysis reactors with their specific features (2, 12-13). Some of these reactors have a low operational complexity such as the auger while ablative is considered to have a high operational complexity. Verma et al. (17) have reported full details of some of the fast pyrolysis reactors.

Table 1.3: Types of pyrolysis processes, processing conditions, and products obtained [Reproduced with permission from reference (2)].

<b>Mode/type of pyrolysis process</b>	<b>Residence time of vapor in pyrolysis zone</b>	<b>Rate of heating</b>	<b>Final temperature (°C)</b>	<b>Products (average %)</b>
Slow pyrolysis (Torrefaction)	ca. 30 min	Slow	ca. 290	Char, gas (80, 20 %) (vapors are burned)
Carbonization	Days	Slow	ca. 400	Char, liquid, gas (35, 30, 35 %)
Fast pyrolysis	< 2 s	High	ca. 500	Char, liquid, gas (13, 70, 17%,)

Table 1.4: Variations of fast pyrolysis reactor systems [*Reproduced with permission from references (2, 12-13)*].

<b>Reactor</b>	<b>Features</b>
1. Bubbling fluid bed reactor	<ul style="list-style-type: none"> <li>• Simple in construction and operation, good temperature control, efficient heat transfer, good control of vapor residence time.</li> <li>• Liquid yields of 70–75% obtained.</li> <li>• Rate of heating is the rate-limiting step therefore; small- (2–3 mm) sized biomass particles are required.</li> <li>• Requires a carrier gas.</li> </ul>
2. Ablative fast pyrolysis reactor	<ul style="list-style-type: none"> <li>• Heat transfer from hot reactor wall to “melt” wood that is in contact with it under pressure.</li> <li>• Molten wood vaporizes to product similar to that from 1.</li> <li>• Heat transfer not a rate limiting factor therefore large particles can be used.</li> <li>• Process limited to rate of heat supply to reactor, which can be more easily controlled and maintained.</li> <li>• No requirement of fluidizing gas therefore equipment is more compact and reaction system more efficient.</li> <li>• Absence of fluidizing gas increases partial pressure of condensable vapors, which increases vapor collection and subsequent condensation efficiency.</li> <li>• Process is surface area controlled therefore scaling is a more serious problem.</li> </ul>
3. Rotating cone reactor system	<ul style="list-style-type: none"> <li>• Similar to transported bed reactor system but transport affected by centrifugal forces in a rotating cone.</li> <li>• Recent development.</li> <li>• Carrier gas requirement but much less than that in 1.</li> <li>• Complex integrated operation required.</li> <li>• Liquid yields 60–70% on dry feed basis.</li> </ul>
4. Auger reactor system	<ul style="list-style-type: none"> <li>• Inside the reactor, pre-heated hot sand (or stainless-steel balls) and biomass are mixed.</li> <li>• Biomass is continuously pyrolyzed</li> <li>• The process requires hot circulation system for sand or steel balls.</li> <li>• Circulating heat transfer material reduces energy costs</li> <li>• Compact and does not require carrier gas.</li> <li>• Operates at lower process temperatures (400 °C) and particle size of biomass is not critical for operation as is the case for 1.</li> <li>• Suitable for the small scale pyrolysis process</li> <li>• Liquid yields 50-60 %</li> </ul>

## 1.6. Pyrolysis of lignocellulosic biomass

Pyrolysis of the main components of wood, shrubs and grasses (cellulose, hemicellulose and lignin) can be ordered, by their thermal degradation properties, from easy to difficult as follows (7):

*Hemicellulose > cellulose >>> lignin*

The degradation of cellulose occurs between 240 °C to 350 °C (13) and many researcher have suggested mechanisms for cellulose pyrolysis. A proposed pyrolysis model was suggested by Lin et al. (Figure 1.4) (18). In their model, the depolymerization of cellulose chains begins at a moderate temperature range of 100 °C to 150 °C and cellulose undergoes decomposition to produce oligosaccharides with relatively low molecular weight units. These oligosaccharides continue to degrade until monosaccharide units (anhydro-monosaccharides, i.e., levoglucosan-(LGA)) are obtained. Further dehydration and isomerization reactions of LGA can form other derivatives from anhydro-sugars such as 1,4:3,6-dianhydro- $\beta$ -D-glucofuranose (DGP), levoglucosenone (LGO), and 1,6-anhydro- $\beta$ -D-glucofuranose (AGF). It has been proposed that these anhydro-sugars can repolymerize to form anhydro-oligomers or undergo fragmentation/retro-aldol condensation, dehydration, decarbonylation, or decarboxylation to produce smaller compounds such as hydroxyacetaldehyde, hydroxyacetone, and glyceraldehyde. The small fragmented species can be formed directly from active cellulose. Further dehydration reactions can produce water and furanoses including furfural and hydroxymethylfurfural (5-HMF), etc., while decarbonylation and decarboxylation generates CO and CO<sub>2</sub>. All

products may additionally be transformed through condensation and polymerization reactions to produce char or decompose to light products (18).

Hemicelluloses are degraded at lower temperatures (200-260 °C) releasing more volatiles and less tars, and chars than cellulose (13). The hemicelluloses are responsible for yielding most of the acetic acid produced during lignocellulosic pyrolysis through a process of deacetylation of the hemicelluloses. Acetic acid is chiefly responsible for the high acidity of bio-oils (13).

Lignin is the toughest component in lignocellulosic materials against heat. Its pyrolysis process begins with thermal softening at ca. 200 °C followed by major decomposition at 280-500 °C (13). Decomposition may occur through homolytic cleavage of ether and carbon-carbon linkages (13) and from demethylation of methoxyl groups in guaiacyl and syringyl units at ca. 450 °C. In addition, lignin alkyl chains need high temperature (ca. 600 °C) to decompose (3). However, crosslinking and condensation reactions can also occur producing much higher char and lower bio-oil than the sugar components. The liquid product (known as pyroligneous acid) is composed of three groups of compounds; the monomeric phenolic compounds, the large molecular weight oligomers (pyrolytic lignins) and the light compounds (such as formaldehyde, acetaldehyde, methanol, acetone, acetic acid). Pyrolytic lignin is the major component and it represents 60-80% of the crude lignin-derived oil (3, 13). It has been found that pyrolytic lignin, separated from a bio-oil, has an average molecular weight between 650 and 1300 Da. It is mainly characterized as biphenyl, phenyl coumaran, diphenyl ether, stilbene and resinol structures (3).

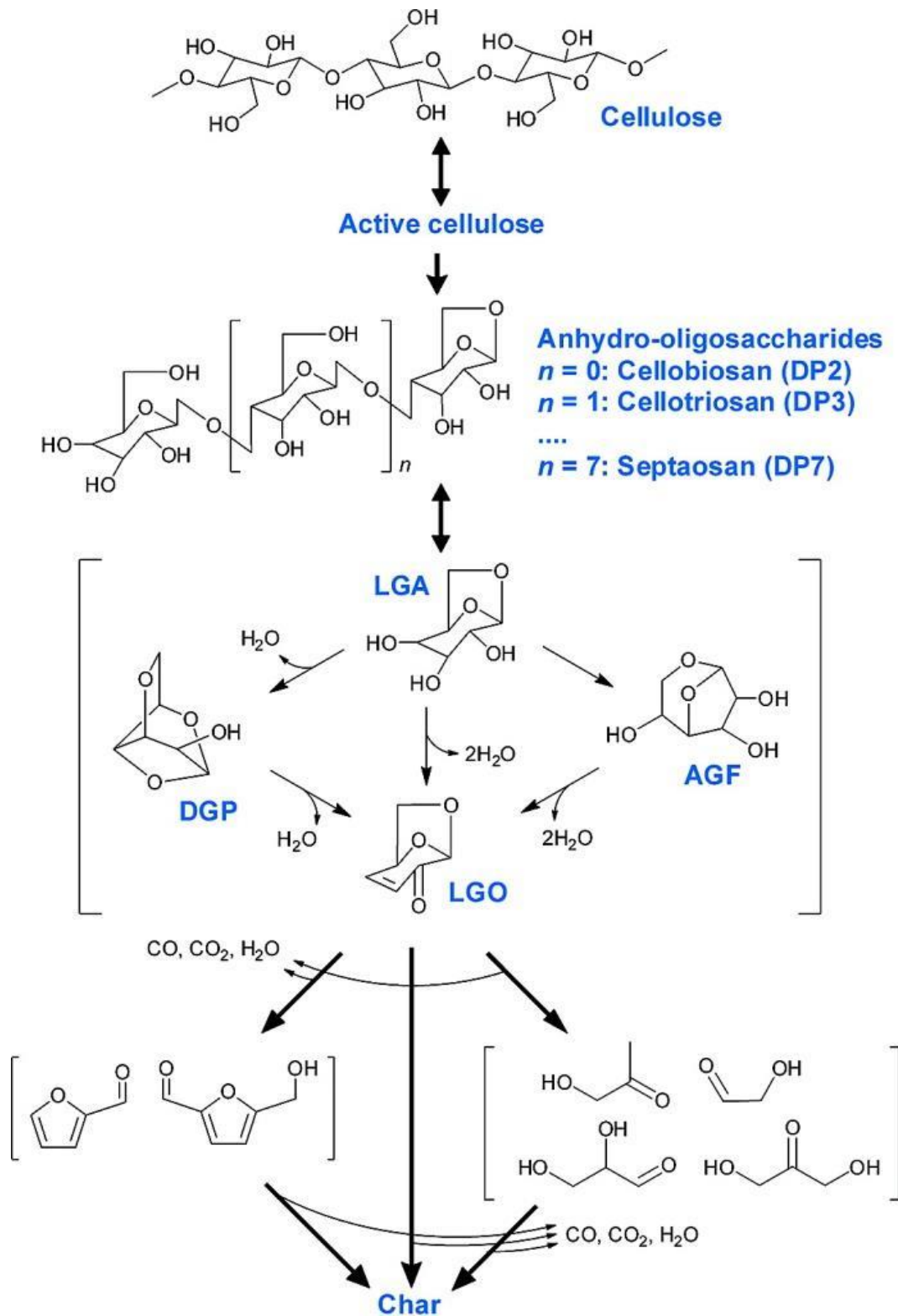


Figure 1.4. Proposed mechanism of cellulose pyrolysis (DP: degree of polymerization; compounds symbols can be found in text) [Adapted with permission from reference (18)].

## 1.7. Bio-oil

Bio-oils are commonly known as pyrolysis liquids, crude bio-oils, pyrolysis oils, or bio-crude oils (8, 12). The bio-oils are produced by fast pyrolysis followed by rapid quenching (condensing the hot vapors and trapping the oil in a trap so that these intermediate products will not participate in further thermal reactions). Many factors can affect the chemical nature of produced bio-oils, including the pyrolysis process (heating rate, residence time, and pressure), the feedstock pre-treatment (particle size and shape, moisture and ash content), vapor filtration and condensation steps (filter type, condensing method, medium, and cooling rate), and the type of biomass feedstock used (1, 13, 15). Table 1.5 shows a comparison of some basic properties between a bio-oil from wood and two petroleum fuels. Bio-oil has the advantage that it is a renewable and relatively clean fuel (15). Bio-oil has been shown to have little significance on health, environment, or have safety risks when being used (16). Finally, bio-oils from most of lignocellulosic biomass are a neutral CO<sub>2</sub> emission energy source, generating no SO<sub>x</sub> emissions and having 50% lower NO<sub>x</sub> emissions than diesel in gas turbines (13).

Physically, bio-oil is a dark brown, a homogeneous viscous liquid with an acrid or smoky odor (4). Bio-oils' colors may vary from almost nearly black through dark red-brown to dark green depending on the presence of small amounts of biochar and due to their chemical composition (16). The density of wood-derived pyrolysis liquid is typically 1.2 g/mL for a water content of 25% (8). Raw wood bio-oil has a low heating value, which is half of that of conventional heavy petroleum fuel oil. In addition, it has a higher specific gravity and viscosity (9). However, when compared with wood biomass, bio-oil has a



significantly higher energy density (ca. 8 times more than that of biomass) which makes pyrolysis attractive for energy densification (2).

Table 1.5: Comparison of some properties of bio-oils produced by pyrolysis of wood and heavy fuel oil [*Reproduced with permission from references (8-9)*].

<b>Properties</b>	<b>Pyrolysis bio-oil from wood</b>	<b>Heavy petroleum fuel</b>	<b>No 2. Diesel fuel</b>
Water content (wt. %)	15–30	0.1	-
pH	2.5	-	-
Specific gravity (g/mL)	1.2	0.94	0.85
Elemental composition (wt. %)	C	54–58	85
	H	5.5–7.0	11
	O	35–40	1
	N	0–0.2	0.3
	S	-	-
Ash	0–0.2	0.1	-
High Heat Value (MJ/kg)	16–19	40	44.7
Viscosity (at 50 °C) (cP)	40–100	180	< 2.39
Solids (wt. %)	0.2–1	1	-
Distillation residue (wt. %)	Up to 50	1	-

Bio-oil is a complex organic mixture that contains hundreds of highly oxygenated compounds include water, alcohols, carboxylic acids (e.g., acetic acid, and formic acid), aldehydes, ketones, pyrones, furans, phenols (e.g., syringols catechols, guaiacols, isoeugenol, and vanillin), furan carboxaldehydes, sugars (e.g., anhydrosugars) alkenes, aromatics, nitrogen compounds, miscellaneous oxygenates, and larger molecular weight oligomers (anhydro-oligosaccharides and lignin-derived oligomers) (3-4). Table 1.6 shows the chemical compositions of representative fast pyrolysis oil (8). The bio-oils have a high water concentration (20%–30%, wt/wt), and high contents of aldehydes, carboxylic acids and carbohydrates. Pyrolytic lignin “the water insoluble fraction on bio-oil” represents 15-30% (wt/wt) of the bio-oil. Most of this fraction are phenolic compounds including lignin-

derived oligomers. Bio-oil has a high oxygen content and a very low ash content similar to that for a biomass feedstock, as well as a relatively high acidity (9). Furthermore, bio-oils are immiscible with hydrocarbon liquids (16).

Bio-oil is basically a micro-emulsion mixture which is considered to be composed of a continuous phase from aqueous solution of sugar decomposition products (e.g., anhydrosugars) along with molecules from lignin decomposition (e.g., phenolic compounds) (5). This mixture can stabilize the discontinuous phase that is primarily composed of macromolecules of pyrolytic lignin by mechanisms such as hydrogen bonds and the presence of nanomicelles and micromicelles (5). The oligomeric compounds in the bio-oil are primarily formed from lignin, although some are formed from cellulose (13). Most of the oligomeric structures in the bio-oils are undetectable in gas chromatography (GC) however high pressure liquid chromatography-electrospray mass spectroscopy (HPLC-ESI MS) can be used to provide some separation and weight determination (13).

Water in the bio-oil has two sources; the first one is free water (original moisture) which vaporizes from biomass during pyrolysis, while the second source is the dehydration reactions that produce water as a byproduct during the pyrolysis (e.g., condensation reaction) (13, 19).

Based on the pyrolysis process, bio-oils are produced under non-equilibrium thermodynamic conditions. This can make some of its components tend to react with each other through several reaction mechanisms (e.g., polymerization, condensation, esterification, and etherification) at room or at higher temperatures. This results in the thermal and storage instability of bio-oil or “aging” (20). Bio-oil ages right after its

production, whereby its viscosity increases with time and phase separation may occur as a result of a breakdown of the microemulsion or via chemical reactions that occur in the oil with time (13).

Table 1.6: Chemical composition of fast pyrolysis liquid [*Reprinted with permission from reference (8)*].

<b>Major components</b>	<b>wt.%</b>
Water	20–30
Lignin fragments: insoluble pyrolytic lignin	15–30
Aldehydes: formaldehyde, acetaldehyde, hydroxacetaldehyde, glyoxal, methylglyoxal	10–20
Carboxylic acids: formic acid, propionic, butyric, pentanoic, hexanoic, glycolic (hydroxyacetic)	10–15
Carbohydrates: cellobiosan; levoglucosan, oligosaccharides, 1,6-anhydroglucofuranose	5–10
Phenols: phenol, cresols, guaiacols, syringols	2–5
Furfurals	1–4
Alcohols: methanol, ethanol	2–5
Ketones: acetol (1-hydroxy-2-propanone), cyclo pentanone	1–5

### 1.8. Bio-oil characterization

Full detailed analysis of bio-oils is a challenging task, and is impossible to accomplish using a single method. Therefore, more than one analytical technique is required for complete characterization of bio-oils (1, 21). A large number of analytical techniques has been used for bio-oil characterization. They are classified into two categories; physical properties and chemical properties. Some of these analytical techniques are reviewed in (1, 22). Most bio-oil characterization focuses on bulk measurements and particular chemical properties.

### 1.8.1. Physical characterization

The physical properties of the bio-oils vary depending on the pyrolysis process and the feedstock composition. Table 1.7 gives a summary of common methods that are recommended for bio-oil analyses as well as guidelines for each method (22-24). Most of these standard analyses have been exhaustively used and tested for assessing and evaluating the bio-oils (24).

Table 1.7: Summary of methods for determining physical properties of bio-oil [*Reprinted with permission from references (22-24)*].

No.	Physical Property	ASTM Standard	Method of determination
1	Density	D1298	Hydrometer method
		D4052	Digital density meter
2	Water content	D95	Distillation method
		E203	Karl Fisher reagent-volumetric method
3	Ash content	D482	Thermogravimetry method
		EN 7	Controlled evaporation of water to avoid foaming
4	Carbon residue	D189	Destructive distillation method of carbon residue determination
		D4530	Micro-method (gravimetric analysis at 500 °C under inert nitrogen atmosphere)
5	Viscosity	D88	Saybolt viscosity by viscometer method
		D445	Capillary method through viscometer
		D2170	Flow of liquid through calibrated glass capillary method
6	Flash point	D3828	Small scale cup test in which sample is placed and ignition spark is created
7	Heating value	D240	Heat of Combustion by Bomb Calorimeter method
8	Total acid value	D974	Color-Indicator titration
		D664	Potentiometric titration method
		D3339	Semi-micro color indicator titration
9	Elemental analysis	D5373	Estimation of CO <sub>2</sub> , H <sub>2</sub> O and NO <sub>x</sub> (oxidization of sample containing C, H and N)
		D5291	Determination of gases obtained after conversion from their respective elements
10	Solid content	D2276	Particulate contaminant in by line sampling (filtration through membrane)
		n.a	methanol/dichloromethane insolubles

n.a: not available

### 1.8.2. Chemical characterization

Several methods and techniques have been employed in order to analyze bio-oils' chemical composition including chromatographic techniques, mass spectrometry, and spectroscopic methods.

#### *Chromatographic techniques*

GC has been used successfully for decades for bio-oils' compositional analysis (1, 13, 21, 23, 25-26). But this technique is limited to the identification of volatile and thermally stable organic compounds, while a derivatization is required for more polar compounds' analyses (e.g., acids and poly-phenolics) (23, 26). Unfortunately, GC methods can analyze only 25-40% of bio-oil's compounds (13, 22). The detectors, which have been successfully used with GC, include flame ionization detector (FID), thermal-conductive detector (TCD) (for light gases) and mass spectrometry, specifically mass selective detection (22). FID is sensitive, reliable, and has a broad linear dynamic range and is widely used to quantify GC-amenable compounds (21). MS detection provides obvious mass spectral information and is one of the most popular detectors (4, 22). Hundreds of different bio-oil components have been identified using GC-MS and GC-FID (4, 22). Unfortunately, these chromatographic methods can not obtain complete information about the chemical composition of the volatile fraction for bio-oils due to insufficient chromatographic resolution in co-eluting peaks, unavailability of mass spectra of some bio-oil components in MS libraries, or standards for most of bio-oil compounds (1).

A comprehensive two-dimensional gas chromatography approach (GC × GC) has been used in the analysis of bio-oils (21). The GC × GC enhances the separation of bio-oils' compounds and allows for the detection of more compounds compared with

conventional GC (1). A detailed characterization of bio-oil can be obtained by employing time-of-flight mass spectrometry (TOF MS) with GC×GC. The obtained peak resolution by this method can help in better understanding the mechanisms that lead to formation of pyrolysis products (21). For example, GC×GC-TOF MS was used for the compositional characterization of two oil samples from flash pyrolysis of palm fruit bunch and pine wood chips (27). Analyses showed that major classes of compounds in the two bio-oil samples were ketones, cyclopentenones, furanones, furans, phenols, benzenediols, methoxy- and dimethoxy-phenols, and sugars. Each of the two bio-oils showed different chemical composition profiles depending on their biomass origin. Bio-oil from empty palm fruit bunch showed extra chemical classes including esters, aldehydes, and pyridines, while bio-oil from pine wood chips contained extra alcohols and cyclopentanediones (27). Staš et al. (1) listed 212 compounds they could detect and were able to examine mechanisms for the formation of certain key products.

Liquid chromatographic (LC) methods represent powerful tools to analyze bio-oils especially for polar, larger M.wt and nonvolatile compounds. Most of these compounds have oligomeric structures that are intractable to GC analysis (21). The LC methods can be used to analyze about 15 % (wt./wt.) of the bio-oils (1). Unfortunately, LC lacks the ability to analyze bio-oil's heavy fractions, as well as to quantitatively determine compounds without standards (1, 21). LC methods for bio-oil analysis include: (i) adsorption chromatography, (ii) gel permeation chromatography (GPC) (molecular weight distributions), and (iii) HPLC with UV, refractive index or MS detection (1, 13). The most common LC methods are those used to quantify water-soluble species or to obtain molecular weight distributions for the bio-oil samples (25). GPC, often called size

exclusion chromatography (SEC), is used to obtain molecular weight distributions for bio-oil samples (25, 28).

### *Mass spectrometric techniques*

MS techniques are powerful methods for molecular weight and structural identifications of bio-oil compounds (23, 26). GC-MS is the mass technique that has been most used for analyzing bio-oils. Identifications are based on a selective fragmentation of individual compounds by electron impact (EI) that can be assisted by mass libraries or by analysis of standards (1, 21). For detecting polar compounds, ESI-MS has been widely used through a direct-infusion or after HPLC separation (26). Other MS techniques have been utilized include LC–quadrupole time-of-flight mass spectrometry (LC–QTOF-MS), fast atom bombardment mass spectrometry (FAB-MS), field ionization mass spectrometry (FI-MS), time-of-flight mass spectrometry (TOF-MS), molecular beam mass spectrometry (MBMS), Fourier transform ion cyclotron resonance mass spectrometry (FTICR-MS), magnetic sector MS, laser desorption ionization-time of flight-mass spectrometry (LDI-TOF-MS), and matrix-assisted laser desorption/ ionization MS (MALDI-MS) (21). High-resolution mass spectrometry (HRMS) can provide accurate analysis of nonvolatile and high molecular weight components of bio-oils in addition to their volatile components. This approach can extend analysis by using the inherent mass accuracy data to obtain further information about bio-oil's component's molecular formula ( $C_cH_hO_o$ ) (1, 29-31). Many ionization techniques have been used to give HRMS data including; LDI, ESI, atmospheric pressure chemical ionization (APCI), and atmospheric pressure photoionization (APPI) (1). For example, Smith and Lee (29) have analyzed a bio-oil from loblolly pine using LDI-HRMS and identified over 100 compounds. Recently, bio-oils from fast pyrolysis of

different biomasses were analyzed by two types of HRMSs using ESI for ionization Q-TOF MS and FT-ICR MS (26). Unfortunately, there is no universal ionization technique that can be applied to all compounds in bio-oil samples. Some of the bio-oil components cannot be ionized using a single ionization technique. In this case, different ionization methods is required to provide complementary information about bio-oil's composition and its quantities (1).

#### *NMR and IR spectroscopic methods and TGA*

NMR spectroscopy has been utilized in bio-oil analysis due to its ability to provide detailed information about the entire sample including high molecular weight components (13, 21-22, 25, 28, 33-37). NMR has a number of attractive features including; comprehensive analysis and providing qualitative assessment of oxygen-containing functionalities in the sample (13, 22).  $^1\text{H}$  and  $^{13}\text{C}$  NMR are typically used for bio-oil analyses in order to determine carbon and hydrogen contents in bio-oil samples (aliphatic, olefinic, aromatic, methoxy/hydroxyl, carbonyl, etc.) (1, 25). In addition,  $^{31}\text{P}$  NMR has been used to measure quantities of hydroxyl (-OH) and carboxyl (-COOH) functional groups in bio-oils samples after they were selectively derivatized with a phosphorus group using reagents such as 2-chloro-4,4,5,5-tetramethyl-1,3,2-dioxaphospholane (21). Different bio-oil samples from switchgrass, alfalfa stems, corn stover, and guayule were analyzed by  $^1\text{H}$  and  $^{13}\text{C}$  NMR spectroscopy. The NMR spectra varied greatly among bio-oils depending on the percentage of carbon and hydrogen each of feedstock type (24). Ben and Raqauskas (33-35) have also investigated different NMR methods for bio-oil analysis from different feed stocks. They studied the accelerated aging of bio-oils using quantitative analysis  $^1\text{H}$ ,  $^{13}\text{C}$  NMR and heteronuclear single-quantum correlation (HSQC)-NMR



techniques. The results showed that the chemical structure of bio-oils clearly changed during aging (33).

FTIR analysis can provide useful information about various functional groups in a bio-oil sample (1, 13, 21, 25, 38-41). A large number of analyses has been accomplished by simple and direct interpretation of the spectra (23). FTIR has been used for characterization of carbonyl or any other oxygen-containing functional group. FTIR analysis results have shown a good correlation between the carbonyl absorption bands and the oxygen content as well as the carbon content in bio-oil samples (23). Lievens et al. (41) investigated the carbonyl groups in bio-oils from mallee wood, bark and leaves using FTIR spectroscopy where the 1490–1850  $\text{cm}^{-1}$  region in the bio-oils' FTIR spectra were deconvoluted with nine Gaussian bands. Each band represents a different type of carbonyl. The results showed that these carbonyl groups all had different concentrations in bio-oils based on the type of biomass feedstock.

TGA is one of the most commonly used methods for analyzing biomass and bio-oil samples. It is used to study the thermal behavior of a bio-oil or biomass feedstock and to obtain kinetic parameters for thermal reactions that take place during pyrolysis (21, 23). The loss of sample weight with temperature depends on volatility (or molar mass) of components in the bio-oil sample, and also their chemical nature and the overall bio-oil composition (14, 21-22).

Finally, all these chemical methods can participate together in obtaining valuable information about bio-oil composition and properties. However, most of the research focuses on bulk properties, especially those in the engineering fields. Much more work and

effort is necessary to obtain more rapid bio-oil analyses that would help in bio-oil utilization as a fuel and in chemical recovery.

## **1.9. Stability and chemical recovery from bio-oil**

### **1.9.1. Stability of bio-oil**

Bio-oil needs to be stable over a long period of time in order to maintain its initial physical properties during storage, shipping, and use. Different approaches have been used to minimize bio-oil aging. Table 1.8 lists a summary of some methods that have been used to enhance bio-oil stability (42).

Solvent addition has been used in several studies, in which a polar solvent (acetone, ethanol, ethyl acetate, furfural or a mixture of methyl isobutyl ketone and methanol) was added to bio-oil to reduce its viscosity and enhance its stability (42). For example, Hilton et al. (43) found that bio-oils from pine pellets and hull pellets can be stabilized with solvent-addition and stability of these bio-oils varied by solvent and feedstock type. Solvent addition can enhance desolation of some of the more complex compounds. In addition, it has useful effects on other properties such as acidity, heating value, miscibility with fossil fuels and delays in phase separation (44).

Baldwin et al. (45) reported that viscosity-increase (from accelerated aging at 80 °C) could be reduced 10-fold by hot gas filtration during the pyrolysis step and before bio-oil collection. Moreover, esterification with ethanol using a catalyst (acids,  $\text{SO}_4^{2-}/\text{M}_x\text{O}_y$ ) has been used to improve bio-oil stability, where the resulting product did not show viscosity increase after 3 months of aging (46). Emulsification of bio-oil with bio-diesel was used by Jiang et al. (47) where by the mixture (bio-oil/ bio-diesel) had no significant

change in its water content or viscosity after aging at 80 °C for 180 h compared to that for aged bio-oil alone.

Table 1.8: Methods to slow down aging of bio-oils [*Reprinted with permission from reference (42)*].

Method	Procedure	Mechanism
<b>Solvent addition</b>	<ul style="list-style-type: none"> <li>➤ Adding low-viscosity solvents, such as water, methanol, furfural, ethyl acetate, or acetone to combat increases in viscosity</li> <li>➤ Addition of low molecular weight alcohols to a mixture of high molecular weight hemiacetals, acetals, and esters</li> </ul>	<ul style="list-style-type: none"> <li>• Dilute the polymers</li> <li>• Phase stability of bio-oils during storage is increased</li> <li>• Shift the equilibrium composition to a mixture with a lower molecular weight and viscosity.</li> <li>• Reaction with bio-oil components:               <ul style="list-style-type: none"> <li>❖ Reducing the concentration of reactive aldehydes, by converting more of them to less reactive, relatively low to moderate molecular-weight hemiacetals and acetals:</li> <li>❖ Trans-acetalizing large hemiacetals and acetals to form lower molecular weight hemiacetals and acetals;</li> <li>❖ Converting organic acids to low molecular weight esters; and</li> <li>❖ Transesterifying large esters to form lower molecular weight esters</li> </ul> </li> </ul>
<b>Filtration</b>	<ul style="list-style-type: none"> <li>➤ Removing ash and char particulates from the pyrolysis oil vapors through filtration</li> <li>➤ Removing some salts like alkali metal sulfates and chlorides</li> </ul>	Reduce aging rates

Table 1.8 contd.

<b>Method</b>	<b>Procedure</b>	<b>Mechanism</b>
<b>Mild hydrogenation</b>	Mild hydrogenating (in presence a catalyst) of bio-oil to saturation (only the reactive aliphatics)	<ul style="list-style-type: none"> <li>• Viscosity increase reduced</li> <li>• Elimination of olefinic condensation</li> </ul>
<b>Limiting access to air and use of antioxidants</b>	Adding a small quantity of an antioxidant such as hydroquinone (e.g., hydroquinone is used as a free-radical trap to stabilize acrolein during storage and shipping)	<ul style="list-style-type: none"> <li>• Protect olefins from polymerizing by free-radical traps</li> <li>• Stop chain reaction of polymerization</li> </ul>
<b>Low temperature storage</b>	Store the bio-oils at low temperatures	Reduce aging rates

### 1.9.2. Chemicals recovery from bio-oil

Bio-oils produced through fast pyrolysis contain hundreds of compounds that are potentially commercially valuable. Some of these compounds that are in reasonable abundance are acetic acid, formic acid, formaldehyde, acetol, hydroxyacetaldehyde, furfural, 2,6-dimethoxyphenol, 4-methyl-2,6-dimethoxyphenol and 2-cyclopenten-1-one, and levoglucosan (5, 8). Bio-oils are therefore a promising renewable source for carbon-based compounds. Scientists have attempted to recover these chemicals or families of chemicals from bio-oils for use in the industrial field (48). As such, chemical production from bio-oils is potentially as valuable as their use as fuels. Chemicals/products that have been recovered are listed in Table 1.9 (5, 13, 48). Unfortunately, there are considerable hurdles to establishing markets for these chemicals including high cost, inefficient

separation and availability of suitable refining techniques. Currently, only practical marketable products are specialty food flavorings, such as liquid smokes (48). However, extraction and fractionation methods can be used to obtain more value-added components from bio-oils (20). Many of fractionation procedures have been used to separate bio-oil components, such as those shown in Table 1.10 (15).

Table 1.9: Major compounds and fractions recovered from bio-oil and their application (5, 13, 48).

<b>Compound/ fractions</b>	<b>Application</b>	<b>Recover method and modifying procedure</b>
Levoglucosan	<ul style="list-style-type: none"> <li>•Food additive (flavor compounds), pharmaceutical (antibiotics), pesticides, polymers, and surfactants</li> <li>•Levoglucosan can be fermented by microorganisms to produce citric and itaconic acids.</li> </ul>	Phase separation
Levoglucosenone	<ul style="list-style-type: none"> <li>•Pharmaceuticals (antibiotics)</li> <li>•Food additive (flavor compounds)</li> </ul>	Distillation
Furfural	<ul style="list-style-type: none"> <li>•Pharmaceutical, pesticide</li> </ul>	NA
Acetic acid	<ul style="list-style-type: none"> <li>•Specialty chemical</li> </ul>	NA
Formic acid	<ul style="list-style-type: none"> <li>•Preservative, antibacterial agent</li> </ul>	NA
Hydroxyacetaldehyde	<ul style="list-style-type: none"> <li>•Fragrance substances, pharmaceutical intermediates</li> </ul>	NA
Low-molecular-weight aldehydes (especially glycolaldehyde) e.g. liquid smoke®	<ul style="list-style-type: none"> <li>•Effective meat browning agents</li> </ul>	Aqueous extraction

Table 1.9 contd.

<b>Compound/ fractions</b>	<b>Application</b>	<b>Recover method and modifying procedure</b>
Glucoaldehyde, glyceraldehydes, privaldehyde, dihydroxyacetone, acetone, and diacetyl.	<ul style="list-style-type: none"> <li>•Food additive (smoke flavors, essences and browning agent)</li> <li>•A red-colored product can be used to brown and flavor sausages, bacon, fish, etc. (<a href="http://www.btgworld.com">http://www.btgworld.com</a>).</li> </ul>	1- Aqueous extract 2- Separation
All carboxylic acids and phenols e.g. BioLime®	<ul style="list-style-type: none"> <li>•Capturing SO<sub>x</sub> emissions from coal combustors,</li> <li>•Provides additional energy in the combustor</li> <li>•BioLime proved to be efficient in destroying nitrogen oxides</li> </ul>	React with lime to form calcium salts and phenates
Volatile organic acids, mostly formic, acetic, and propionic (also, aldehydes and esters)	<ul style="list-style-type: none"> <li>•Biodegradable de-icers, fertilizers</li> </ul>	1- Aqueous extract distilled off 2- React with lime
Whole bio-oil carbonyl groups	<ul style="list-style-type: none"> <li>•Biodegradable slow-release nitrogen fertilizer</li> <li>•A good soil conditioning material containing humic type matter (lignin)</li> </ul>	Reacting bio-oil with ammonia, urea,
Whole bio-oil	<ul style="list-style-type: none"> <li>•Alternative wood preservative that could replace creosote</li> </ul>	-
Water-soluble fraction	<ul style="list-style-type: none"> <li>•Environmentally friendly road deicers</li> </ul>	1- Aqueous extract 2- React with lime
Phenolic compounds	<ul style="list-style-type: none"> <li>•provide smoky flavors</li> </ul>	1- Solvent fractionation 2- Phase separation
Water-insoluble fraction (pyrolytic lignin)	<ul style="list-style-type: none"> <li>•Adhesives in plywood and particleboard manufacturing</li> <li>•Use as an extender within resin formulations</li> <li>•Phenol or polyphenols /formaldehyde resins</li> </ul>	1- Water insoluble fraction 2- Phenol-formaldehyde resins were synthesized

Table 1.10: Bio-oil fractionation methods [Reprinted with permission from reference (14)].

<b>Method</b>	<b>Solvents used</b>	<b>Mode of separation</b>	<b>Targeted chemicals</b>
Fractionation of vacuum-pyrolyzed birchwood-derived bio-oils	Pentane, toluene, water, ethyl acetate	Column separation	Syringol
bio-oil solvent method (NREL)	Ethyl acetate, sodium bicarbonate, phosphoric acid, sodium chloride, water	Solvent extraction	Lignin-rich fraction
Extraction of phenols from eucalyptus wood pyrolysis tar	Ethyl acetate, sodium hydroxide	Solvent extraction	Phenolic fraction
Bio-oil extraction procedure by Shriner et al.	Ether, sodium hydroxide	Solvent extraction	Acids and neutrals
Bio-oil extraction method of Christan et al.	Ethyl acetate, sodium hydroxide	Solvent extraction	Acids, neutrals, and phenols

### 1.10. Objectives of this study

Bio-oil is a complex mixture and many analytical methods have been used to obtain detailed information about its composition. The methods are numerous and range from simple to advanced, and each have their own advantages and disadvantages. Better techniques and approaches need to be developed, which can provide more rapid and useful compositional information that can be easily used by a cross-section of the research community to enhance knowledge about bio-oil formation mechanism/production factors and its upgrading, and end-use. As well, a more detailed approach to understanding the aging process of bio-oil will lead to better stabilization methods.

In this thesis, different “whole sample” analytical techniques using MS and TLC have been developed as well as a comprehensive study on bio-oil aging with detailed investigation into its causes.

Chapter 2, *Whole sample analysis of bio-oils and thermal cracking fractions by Py-GC/MS and TLC-FID*, demonstrates the usefulness of these techniques in characterizing different bio-oil samples and its fractions with whole sample analysis in mind. The advantages of using these techniques are their simplicity and the usefulness of chemical analysis on complex samples.

Chapter 3, *Direct Infusion Mass Spectrometric Analysis of Bio-oil Using ESI-Ion Trap MS*, illustrates the direct analysis of bio-oil samples by an ESI technique in combination with a low resolution mass spectrometer, i.e., Ion Trap MS and also with the use of the MS tandem capabilities. The MS<sup>n</sup> was not just used to rapidly measure molecular weight information but also deduce chemical structures with the power of MS<sup>2</sup>. The use of different dopants to form adducts was key to proper sample screening.

Chapter 4, *Accelerated Aging of Bio-oil from Fast Pyrolysis of Hardwood*, focuses on one of bio-oil’s major problems, sample instability. In order to study bio-oil aging in a proper time period, accelerated aging at 80 °C for different periods was performed. The changes in the bio-oil’s physicochemical properties were monitored by different analytical techniques and proposed mechanisms of bio-oil aging are presented.

### **1.11. Co-authorship statement**

The principal author of this thesis performed all the experimental work, and prepared all manuscripts’ drafts of manuscripts based on chapters two, three and four



under the supervision of the coauthor; Dr. Robert Helleur, who submitted the manuscript based on chapter 2 for publication. The manuscripts based on Chapter 3 and 4 were submitted to the journal by E. Alsbou. Both co-authors replied to the comments of the reviewers and editors.

## 1.2. References

1. Stas, M.; Kubicka, D.; Chudoba, J.; Pospisil, M. Overview of Analytical Methods Used for Chemical Characterization of Pyrolysis Bio-oil. *Energy Fuels* **2014**, *28*, 385-402.
2. Baskar, C.; Baskar, S.; Dhillon, R. S.; Editors Biomass Conversion: The Interface of Biotechnology, Chemistry and Materials Science. **2012**, 465.
3. Zhu, X.; Lu, Q. Production of chemicals from selective fast pyrolysis of biomass. *Biomass* **2010**, 147-164.
4. Demirbas, A. Current technologies for the thermo-conversion of biomass into fuels and chemicals. *Energy Sources* **2004**, *26*, 715-730.
5. Atadana, Frederick Williams, Catalytic Pyrolysis of Cellulose, Hemicellulose and Lignin Model Compounds, Master Thesis, **2009**, Biological Systems Engineering, Virginia Polytechnic Institute and State University, Blacksburg, VA, United States
6. Zhang, L.; Xu, C.; Champagne, P. Overview of recent advances in thermo-chemical conversion of biomass. *Energy Convers. Manage.* **2010**, *51*, 969-982.
7. Demirbas, A. Biomass resource facilities and biomass conversion processing for fuels and chemicals. *Energy Convers. Manage.* **2001**, *42*, 1357-1378.
8. Balat, M.; Balat, M.; Kirtay, E.; Balat, H. Main routes for the thermo-conversion of biomass into fuels and chemicals. Part 1: Pyrolysis systems. *Energy Convers. Manage.* **2009**, *50*, 3147-3157.
9. Xiu, S.; Shahbazi, A. Bio-oil production and upgrading research: A review. *Renewable Sustainable Energy Rev.* **2012**, *16*, 4406-4414.
10. Donald L. Klass, "Biomass for Renewable Energy and Fuels" Encyclopedia of Energy, Elsevier, [http://beraonline.org/yahoo\\_site\\_admin/assets/docs/cyclopediaofEnergy.35293015.pdf](http://beraonline.org/yahoo_site_admin/assets/docs/cyclopediaofEnergy.35293015.pdf), (2004).
11. Bridgwater, A. V. Review of fast pyrolysis of biomass and product upgrading. *Biomass Bioenergy* **2012**, *38*, 68-94.
12. Dekui Shen, Rui Xiao, Sai Gu and Huiyan Zhang, The Overview of Thermal Decomposition of Cellulose in Lignocellulosic Biomass "Cellulose - Biomass Conversion" Edited by Theo van de Ven and John Kadla, InTech, **2013**.
13. Isahak, W. N. R. W.; Hisham, M. W. M.; Yarmo, M. A.; Hin, T. Y. A review on bio-oil production from biomass by using pyrolysis method. *Renewable Sustainable Energy Rev.* **2012**, *16*, 5910-5923.

14. Mohan, D.; Pittman, C. U., Jr.; Steele, P. H. Pyrolysis of Wood/Biomass for Bio-oil: A Critical Review. *Energy Fuels* **2006**, *20*, 848-889.
15. Yaman, S. Pyrolysis of biomass to produce fuels and chemical feedstocks. *Energy Convers. Manage.* **2004**, *45*, 651-671.
16. Huber, G. W.; Iborra, S.; Corma, A. Synthesis of Transportation Fuels from Biomass: Chemistry, Catalysts, and Engineering. *Chem. Rev. (Washington, DC, U. S. )* **2006**, *106*, 4044-4098.
17. Verma, M.; Godbout, S.; Brar, S. K.; Solomatnikova, O.; Lemay, S. P.; Larouche, J. P. Biofuels production from biomass by thermochemical conversion technologies. *Int. J. Chem. Eng.* **2012**, 542426, 18.
18. Lin, Y.; Cho, J.; Tompsett, G. A.; Westmoreland, P. R.; Huber, G. W. Kinetics and Mechanism of Cellulose Pyrolysis. *J. Phys. Chem. C* **2009**, *113*, 20097-20107.
19. Czernik, S.; Bridgwater, A. V. Overview of Applications of Biomass Fast Pyrolysis Oil. *Energy Fuels* **2004**, *18*, 590-598.
20. Zhang, X.; Yang, G.; Jiang, H.; Liu, W.; Ding, H. Mass production of chemicals from biomass-derived oil by directly atmospheric distillation coupled with copyrolysis. *Sci. Rep.* **2013**, *3*, 1120, 7.
21. Bahng, M.; Mukarakate, C.; Robichaud, D. J.; Nimlos, M. R. Current technologies for analysis of biomass thermochemical processing: A review. *Anal. Chim. Acta* **2009**, *651*, 117-138.
22. Kanaujia, P. K.; Sharma, Y. K.; Agrawal, U. C.; Garg, M. O. Analytical approaches to characterizing pyrolysis oil from biomass. *TrAC, Trends Anal. Chem.* **2013**, *42*, 125-136.
23. Kanaujia, P. K.; Sharma, Y. K.; Garg, M. O.; Tripathi, D.; Singh, R. Review of analytical strategies in the production and upgrading of bio-oils derived from lignocellulosic biomass. *J. Anal. Appl. Pyrolysis* **2014**, *105*, 55-74.
24. Oasmaa, A.; Kuoppala, E.; Elliott, D. C. Development of the Basis for an Analytical Protocol for Feeds and Products of Bio-oil Hydrotreatment. *Energy Fuels* **2012**, *26*, 2454-2460.
25. Mullen, C. A.; Strahan, G. D.; Boateng, A. A. Characterization of Various Fast-Pyrolysis Bio-Oils by NMR Spectroscopy. *Energy Fuels* **2009**, *23*, 2707-2718.
26. Abdelnur, P. V.; Vaz, B. G.; Rocha, J. D.; de Almeida, M. B. B.; Teixeira, M. A. G.; Pereira, R. C. L. Characterization of Bio-oils from Different Pyrolysis Process Steps and Biomass Using High-Resolution Mass Spectrometry. *Energy Fuels* **2013**, *27*, 6646-6654.
27. Tessarolo, N. S.; dos Santos, L. R. M.; Silva, R. S. F.; Azevedo, D. A. Chemical characterization of bio-oils using comprehensive two-dimensional gas chromatography with time-of-flight mass spectrometry. *J. Chromatogr. A* **2013**, *1279*, 68-75.
28. Pan, S.; Pu, Y.; Foston, M.; Ragauskas, A. J. Compositional Characterization and Pyrolysis of Loblolly Pine and Douglas-fir Bark. *BioEnergy Res.* **2013**, *6*, 24-34.
29. Jarvis, J. M.; McKenna, A. M.; Hilten, R. N.; Das, K. C.; Rodgers, R. P.; Marshall, A. G. Characterization of Pine Pellet and Peanut Hull Pyrolysis Bio-oils by

- Negative-Ion Electrospray Ionization Fourier Transform Ion Cyclotron Resonance Mass Spectrometry. *Energy Fuels* **2012**, *26*, 3810-3815.
30. Liu, Y.; Shi, Q.; Zhang, Y.; He, Y.; Chung, K. H.; Zhao, S.; Xu, C. Characterization of Red Pine Pyrolysis Bio-oil by Gas Chromatography-Mass Spectrometry and Negative-Ion Electrospray Ionization Fourier Transform Ion Cyclotron Resonance Mass Spectrometry. *Energy Fuels* **2012**, *26*, 4532-4539.
  31. Smith, E. A.; Park, S.; Klein, A. T.; Lee, Y. J. Bio-oil Analysis Using Negative Electrospray Ionization: Comparative Study of High-Resolution Mass Spectrometers and Phenolic versus Sugarcic Components. *Energy Fuels* **2012**, *26*, 3796-3802.
  32. Smith, E. A.; Lee, Y. J. Petroleomic Analysis of Bio-oils from the Fast Pyrolysis of Biomass: Laser Desorption Ionization-Linear Ion Trap-Orbitrap Mass Spectrometry Approach. *Energy Fuels* **2010**, *24*, 5190-5198.
  33. Ben, H.; Ragauskas, A. J. In Situ NMR Characterization of Pyrolysis Oil during Accelerated Aging. *ChemSusChem* **2012**, *5*, 1687-1693.
  34. Ben, H.; Ragauskas, A. J. NMR Characterization of Pyrolysis Oils from Kraft Lignin. *Energy Fuels* **2011**, *25*, 2322-2332.
  35. Ben, H.; Ragauskas, A. J. Heteronuclear Single-Quantum Correlation-Nuclear Magnetic Resonance (HSQC-NMR) Fingerprint Analysis of Pyrolysis Oils. *Energy Fuels* **2011**, *25*, 5791-5801.
  36. Leonardis, I.; Chiaberge, S.; Fiorani, T.; Spera, S.; Battistel, E.; Bosetti, A.; Cesti, P.; Reale, S.; De Angelis, F. Characterization of Bio-oil from Hydrothermal Liquefaction of Organic Waste by NMR Spectroscopy and FTICR Mass Spectrometry. *ChemSusChem* **2013**, *6*, 160-167.
  37. Siengchum, T.; Isenberg, M.; Chuang, S. S. C. Fast pyrolysis of coconut biomass - An FTIR study. *Fuel* **2013**, *105*, 559-565.
  38. Gao, N.; Li, A.; Quan, C.; Du, L.; Duan, Y. TG-FTIR and Py-GC/MS analysis on pyrolysis and combustion of pine sawdust. *J. Anal. Appl. Pyrolysis* **2013**, *100*, 26-32.
  39. Gu, X.; Ma, X.; Li, L.; Liu, C.; Cheng, K.; Li, Z. Pyrolysis of poplar wood sawdust by TG-FTIR and Py-GC/MS. *J. Anal. Appl. Pyrolysis* **2013**, *102*, 16-23.
  40. Le Dreau, Y.; Dupuy, N.; Gaydou, V.; Joachim, J.; Kister, J. Study of jojoba oil aging by FTIR. *Anal. Chim. Acta* **2009**, *642*, 163-170.
  41. Leonardis, I.; Chiaberge, S.; Fiorani, T.; Spera, S.; Battistel, E.; Bosetti, A.; Cesti, P.; Reale, S.; De Angelis, F. Characterization of Bio-oil from Hydrothermal Liquefaction of Organic Waste by NMR Spectroscopy and FTICR Mass Spectrometry. *ChemSusChem* **2013**, *6*, 160-167.
  42. Diebold, J.P. (2002). A review of the chemical and physical mechanisms of the storage stability of fast pyrolysis bio-oils, in *Fast Pyrolysis of Biomass: A Handbook*, vol. 2 (ed. A.V. Bridgwater), CPL Press, Newbury, pp. 243-292.
  43. Hilten, R. N.; Das, K. C. Comparison of three accelerated aging procedures to assess bio-oil stability. *Fuel* **2010**, *89*, 2741-2749.
  44. Boucher, M. E.; Chaala, A.; Pakdel, H.; Roy, C. Bio-oils obtained by vacuum pyrolysis of softwood bark as a liquid fuel for gas turbines. Part II: Stability and

ageing of bio-oil and its blends with methanol and a pyrolytic aqueous phase. *Biomass Bioenergy* **2000**, *19*, 351-361.

45. Baldwin, R. M.; Feik, C. J. Bio-oil Stabilization and Upgrading by Hot Gas Filtration. *Energy Fuels* **2013**, *27*, 3224-3238.
46. Xu, J.; Jiang, J.; Sun, Y.; Lu, Y. Bio-oil upgrading by means of ethyl ester production in reactive distillation to remove water and to improve storage and fuel characteristics. *Biomass Bioenergy* **2008**, *32*, 1056-1061.
47. Jiang, X.; Ellis, N. Upgrading Bio-oil through Emulsification with Biodiesel: Thermal Stability. *Energy Fuels* **2010**, *24*, 2699-2706.
48. Bridgwater, A. V.; Meier, D.; Radlein, D. An overview of fast pyrolysis of biomass. *Org. Geochem.* **1999**, *30*, 1479-1493.

## Chapter 2

### Whole sample analysis of bio-oils and thermal cracking fractions by Py-GC/MS and TLC-FID<sup>1</sup>

---

<sup>1</sup> This chapter has been published; Alsbou, E.; Helleur, R. Whole sample analysis of bio-oils and thermal cracking fractions by Py-GC/MS and TLC-FID. *J. Anal. Appl. Pyrolysis* **2013**, *101*, 222-231.

## Summary

A combination of pyrolysis-GC/MS and TLC-FID techniques were used for whole sample analysis of bio-oil samples obtained from different lignocellulosic biomasses, (i.e., birch wood, pine wood, barley straw, and forest residue and its thermal-cracking fractions). Both techniques showed the ability to analyze the whole sample without cleanup or fractionation and to distinguish among the bio-oils based on their feedstock sources. The TLC-FID is a chromatographic method whereby the oil solution is spotted on a TLC rod, developed by a two solvent system and the chromatographic bands analyzed by flame ionization detection (FID). The Py-GC/MS instrument uses a sample cup and a vertical microfurnace to analysis bio-oils. The fraction of non-volatiles remaining in the cup were weighed after thermal evaporation-GC/MS. The hardwood birch bio-oil was shown to have syringol and its derivatives whereas pine wood and barley straw bio-oils were shown to have methoxyphenolic and non-methoxy-phenolic compounds, respectively. TLC-FID showed clear differences in the peak areas and shapes for the bio-oils fractions and were in agreement with the results obtained by Py-GC/MS. Furthermore, forest residue bio-oil and its thermal cracking fractions could be effectively characterized by TLC-FID (and Py-GC/MS) whereby the light fraction was composed of a wide range of lower polarity compounds while middle and heavy fractions had higher polarity compounds.

## 2.1. Introduction

### 2.1.1. Bio-oil

Pyrolysis is a promising thermal process for converting various biomasses and wastes (1-3) into high-energy-density fuels (i.e., biochar, bio-oil) while avoiding the high cost for transportation and technical difficulties that occur when biomass is used directly as fuel (3). Pyrolysis is a thermal decomposition (500–700 °C) that occurs in the absence of oxygen (1) and is classified as slow or fast depending on the heating rate, residence time and rate of product condensation (4-5). During pyrolysis, the biomass components are thermally depolymerised producing condensable vapors, incondensable gas, aerosol and char (1, 6, 7).

The liquid product, bio-oil is composed of a complex mixture of very polar to weakly-polar compounds (composed of C, H, O) and remains incompletely characterized (2, 8). It has been regularly reported that bio-oil is composed of approximately 35–40 wt.% oxygen, 55–60 wt.% carbon with high acidity (2–4 pH), density close to 12 g mL<sup>-1</sup>, and 15–45 wt.% water (9). The oxygenated compounds have been categorized as: pyrolytic lignin (15–20 wt.%), aldehydes (10–20 wt.%), organic acids (10–15 wt.%), anhydrosugars (5–10 wt.%) as well other compounds (1). Based on this composition, the bio-oil's components can be volatile (GC-amenable; 300 °C) and non-volatile compounds, and can also be oligomers. The complexity of bio-oil means it is extremely difficult to analyze and this leads to errors in measurements (5, 10). The amount of bio-oil produced and its composition can depend on the biomass source. The depolymerisation and fragmentation reactions for the main biomass compounds (cellulose, hemicellulose and lignin) produce various chemical products during pyrolysis (5, 9, 11-12). Moreover, the biomass feedstock

storage, pyrolysis method and product recovery play significant roles in the amount and composition of the bio-oil (9, 12-13).

Rapid whole sample analysis of bio-oil is important for a number of reasons. Bio-oil can be economically produced, but due to the product complexity, chemical instability and aging of bio-oil upon storage, it is not yet a proven commodity (2, 12, 14). These problems occur because bio-oil is not a product of thermodynamic equilibrium during pyrolysis and the chemical composition of the bio-oil tends to change toward thermodynamic equilibrium with time (8). This leads to instability during storage where the bio-oil undergoes phase separation and its viscosity increases because of highly reactive compounds that undergo esterification, condensation, polymerization or other reactions (5, 10). For example, the non-volatile compounds (i.e., sugars and lignin oligomers) have a tendency to polymerize or coke during the pyrolysis process (10). The acidity of bio-oil also can be a problem, since the bio-oil has a significant quantity of carboxylic acids. That acidity can cause corrosion problems if bio-oil is directly used and will require expensive upgrading (13-14).

Bio-oil usually contains small amounts of char (biochar) that can be a major problem due to its tendency to agglomerate and form large particles that can deposit and block the valves and injectors of engines and erode turbine blades if bio-oil is used as a fuel (13, 14). In many analyses the biochar needs to be completely removed when GC and HPLC columns are used.

Finally, rapid, whole sample analysis of upgraded bio-oil at various stages of the process would be very useful. Bio-oil upgrading has been used to enhance the quality and



stability of this mixture for use as a fuel using emulsification, hydrotreating, steam reforming and thermal and catalytic cracking (2, 8).

### 2.1.2. Analysis of bio-oil

The complete composition of bio-oil is not known because it is difficult to obtain if not impossible considering that bio-oil is composed of a wide range of groups of chemical compounds with different properties and each group has various compound polarities and molecular weights. Many researchers have chosen to fractionate bio-oil samples through multi-step extractions or column separations when analyzing or upgrading it (2). Various techniques have been used in attempts to overcome the problems encountered in characterizing bio-oil composition. Some of these techniques are: GC–FID (9-10, 13), GC–MS (1-2, 4-5, 15, 16), GC–TCD (7), HPSEC (17), GPC (6, 7), HPLC (1, 6), NMR (17-19), TGA (2, 4-5), FTIR (4, 17-19), elemental analyzer (7, 18, 19), TG–FTIR (11) and HPTLC (20). GC–MS and GC–FID have been used most often in characterization of bio-oil's volatile fraction and in online connection to pyrolysis (e.g., Py-GC/MS) (1-2, 4-7, 9-19). However GC can only account for 30–40 wt.% of the bio-oil composition (12, 21) due to the differences in volatility of different components. HPLC can provide some additional information but chemical structures are usually difficult to obtain (21) and normally it has been used to quantify some of the water-soluble components from bio-oil such as acetone, acetol and levoglucosan. The method of HPLC–UV was used to analyze aldehydes in bio-oil after derivatization with dinitrophenylhydrazine (1). FTIR was used in the determination of the functional group composition of bio-oil or its fractions (i.e., n-pentane soluble and insoluble “asphaltenes”) (10, 17-19). TGA is routinely used to observe the temperatures at

which thermo-conversions occur during pyrolysis (2, 4-6), and can be combined with FTIR to study the thermal stability of bio-oil during molecular distillation (11). GPC or SEC has been successfully applied to bio-oil to obtain molecular weight information (number average molecular weight, weight average molecular weight, and polydispersity) (6, 7, 17). The  $^1\text{H}$  NMR spectra of bio-oil have been used for compositional analysis in different studies (17-19). HPTLC has been applied to separation and quantification of sugars in bio-oil samples and their fractions including the anhydrosugars “levoglucosan and cellobiosan” in addition to glucose, arabinose, xylose and cellobiose (20).

TLC–FID is a technique that combines the feature of high resolution TLC separation on silica fused on quartz rods with the universal detection of a flame ionization detector (FID) similar to that used in gas chromatography (22-24). TLC–FID is especially suitable for the analysis of compounds that show no UV absorption or fluorescence, are unsuitable for GC analysis, and are difficult or impossible to show up by chemical reactions (23). The technique has been used in many scientific areas, and it has a wide range of applications including lipids, steroids, alkaloids, surfactants, stabilizers, lubricants, pesticides, cosmetics, polymers and amino acids (22-23). In addition, it has been used for both quantitative and qualitative determination of the different functional groups in tire-pyrolysis oil, vacuum gas oil and petroleum hydrocarbon (24-26). Also, it is commonly used for fast crude oil fractionation into saturated, aromatic, and polar compounds (25) and has been successfully used in the determination of wax in crude oils and bitumens involving two-step solvent development to obtain information on bitumen chemistry (27, 28).

Py-GC/MS has been commonly used for structural analysis of complex biopolymers including lignins, lignocellulosics and humic materials. Interestingly, the

technique and its resulting pyrolysis products show good agreement with the volatile pyrolysis products obtained from bench-scale off-line pyrolysis. This can make Py-GC/MS trustworthy for qualifying pyrolysis products expected from much larger pilot scale pyrolysis units and offers a useful technique for the study of the mechanisms of product formation (12). To further its usefulness, this study attempts, for the first time, to use a commercial Py-GC/MS to analyze bio-oil samples in their entirety without solvent addition or sample cleanup.

The objective of this study is to describe the characterization of “whole sample” bio-oil by two innovative approaches: (i) TLC–FID using a suitably developed solvent system and (ii) Py-GC/MS using a pyrolysis cup that is introduced to a heated vertical microfurnace unit. The investigation will examine the differences in the bio-oil profiles on both TLC chromarods and chromatograms for various bio-oils from different biomasses. Finally, it will study the profile of bio-oil fractions from the thermal-cracking of bio-oil obtained from forest residues.

## **2.2. Materials and methods**

Bio-oil samples and thermal-cracking fractions were kindly donated by a number of researchers as listed in Table 2.1, which describes the feedstock and general pyrolysis conditions. The water content of the samples was measured in duplicate via Karl-Fischer titrations. All samples were stored at 4 °C in airtight glass vials until analyzed. Vanillin, 1,6-anhydro- $\beta$ -d-glucose (levoglucosan) and glucose were all purchased from Sigma-Aldrich. All solvents and chemicals used were analytical grade.

Thermal-cracking was applied to bio-oil from softwood forest residue by using simple heating and distillation. The light fraction was collected during distillation and cut at 165 °C, middle distillate was cut at 345 °C (i.e., the fraction that boils between 165 and 345 °C) and a heavy fraction which remained in the reactor and was drained periodically during the cracking. To avoid bio-oil coking, polyethylene glycol, H-(O-C<sub>2</sub>H<sub>4</sub>)<sub>n</sub>-OH, (PEG; average mol. wt. 1450) was added to the reactor.

Table 2.1. Bio-oil samples (Biomass feedstock, pyrolysis method and their sources).

#	Biomass feedstock	Pyrolysis method	From
1	Barley straw	Fluidized-bed reactor	Dr. Mihalcik (Eastern Regional Research Center, Agricultural Research Service USDA)
2	Pine wood	Continuous-flow, bubbling fluid-bed	Dr. Elliott (Pacific Northwest National Laboratory, Washington state)
3	Birch wood	Fluidized bed reactor	Dr. Berruti, (ICFAR, Western University, Ontario)
4	Alcell lignin (mix hardwood)	Bubbling fluidised bed-fast	Dr. de Wild (Energy Research Centre of the Netherlands)
5	Forest residue	Fast pyrolysis	Dr. Ikura (CANMET Energy Technology Center, Ottawa, Ontario)
	Forest residue fractions (light, middle and heavy)	Thermal cracking	

The commercially available instrument for TLC–FID technique is known as Iatroscan®, and its TLC silica rods, called chromarods, that can be mounted in a rack designed for 10 rods. This makes it suitable for multiple samples compared with conventional TLC-techniques, and it is used for both chromatography and subsequent scanning (29). Figure 2.1 illustrates the TLC–FID design and its components. Separation

is achieved by a solvent development system for the extractable compounds spotted on the rods into resolved fractions. These fractions are then sequentially pyrolyzed off the rod by a controlled flame and the ions detected in the collector electrode. The FID signals are recorded as separated peaks for each fraction (29).

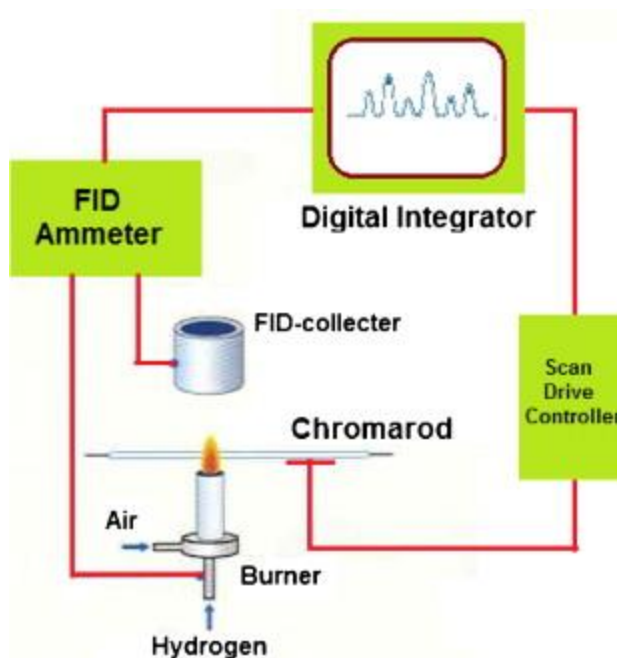


Figure 2.1. Iatroscan TLC-FID setup.

The TLC-FID Iatroscan<sup>®</sup> (MK-5, Iatron Labs, Tokyo, Japan) was used to separate bio-oil samples into several fractions on the silica SIII-chromarods (Mitsubishi Chemical Medience Co., Tokyo, Japan). The bio-oil solutions and standards were prepared in methanol. Each solution was prepared at 20 mg/mL, filtered through a micro-filter (0.45  $\mu\text{m}$ ) and stored in sealed glass vials until analysis. By using a 5  $\mu\text{L}$  disposable Hamilton syringe (Hamilton Co., USA), 1.0  $\mu\text{L}$  of the filtered bio-oil solution was spotted on the bottom of chromarods. The spots were focused at the origin point by developing twice with methanol. A rack of ten prepared chromarods was developed in solvents as given in Table 2.2. The chromarods were dried in a desiccator over anhydrous calcium chloride

for 5 min after each solvent development; the rods were scanned lengthwise under the air-hydrogen flame to detect the bio-oil fractions or standards. The hydrogen flow rate was 160 mL/min, the airflow rate 2000 mL/min and the scan rate 30 s per rod.

Table 2.2. Development solvent system for TLC–FID analysis of bio-oil.

<b>solvent</b>	<b>Time (min)</b>	<b>Distance (%)</b>	<b>Scan mode</b>
Solvent 1: (hexane:ethylacetate) (35:65, v:v)	25	95	PPS 20*
Solvent 2: (CH <sub>2</sub> Cl <sub>2</sub> :methanol:H <sub>2</sub> O) (85:14:1, v:v:v)	25	85	Normal

\* PPS 20: partial pyrolysis scan, 20% from chromarod length

Bio-oil sample analysis by Py-GC/MS was accomplished by weighing ca. 1 mg into a pyrolysis cup then introduced into a quartz tube vertical micro-furnace pyrolyzer PY-2020D (Frontier laboratories Ltd., Yoriyama, Japan), coupled to a HP 5890 II gas chromatograph/HP 5971A mass selective detector (MSD) (Hewlett Packard, Palo Alto, CA, USA) with a ChemStation Data system. The GC instrument was equipped with a split/splitless injector with an electronic pressure control (EPC). The MSD was operated under the following conditions: interface temperature, 250 °C; electron ionization energy, 70 eV; scan range,  $m/z$  40–550. Both the pyrolysis furnace and interface temperature were maintained at 250 °C. The GC injector temperature was set at 250 °C. A Zebron™ ZB-1701 GC capillary column (30 m × 0.25 mm i.d. × 0.25 μm film thickness) (Phenomenex, Inc., USA) was used. The temperature of the GC oven was held at 35 °C for 6 min to trap and focus the volatile components, then the temperature increased to 240 °C at 6 °C/min and held for 4 min. Helium was used as a carrier gas and the GC column was operated at a head pressure of 15 psi with a split flow of 40 mL/min (split ratio ca 1:10). The

identification of GC/MS peaks was mainly based on comparison with the spectra of the NIST spectrum library but also using mass spectra obtained from the literature (30).

## **2.3. Result and discussions**

### 2.3.1. Py-GC/MS

#### 2.3.1.1. Bio-oil samples

All of the bio-oil samples were subjected to volatilization at 250 °C via a pyrolysis cup/furnace interfaced to a GC/MS without solvent addition or filtration in order to account for all of the bio-oil components and to identify all GC-detectable compounds. Figure 2.2 shows a series of typical Py-GC/MS TIC obtained for different bio-oils derived from various lignocellulosic biomasses. These represent three classes of plants including hardwood (birch), softwood (pine) and straw (barley). It shows the ability of Py-GC/MS to suitably produce informative chromatograms with excellent peak separation when a polar column such as 1701 phase is used. Most of the abundant peaks are separated and the compounds identified from the analysis of bio-oil samples using normal solvent injection GC/MS or directly by on-line Py-GC/MS analysis of biomass samples (30). Abundant lignin pyrolysis products peaks were observed in the chromatograms, and cellulose and hemicellulose pyrolysis products were also detected but in lower abundance. The latter were represented by characteristic products such as acetic acid (**1**), acetol (**2**), and levoglucosan (**78**).

Use of a microfurnace pyrolyzer coupled to a GC/MS allows one to determine the non-volatile bio-oil residue after GC/MS analysis. The mass percent for residues left in the sample cup are listed in Table 2.3 and as shown in Figure 2.3. The water content plus

residue in the sample pyrolysis cup minus the sample weight can give us the GC-volatile fraction (by difference) and therefore a “whole bio-oil sample analysis”. Forest residue bio-oil had the highest water content followed by pine and birch woods bio-oils and the lowest was found in Alcell lignin bio-oil. The barley straw has the highest residue percentage at 28%, followed by pine wood and birch woods at 25% and 24%, respectively. This residue represents the non-volatile fraction from a bio-oil sample and can be used for further analysis on its composition. As a result of our measurements, Py-GC/MS was able to analyze 47–56% (wt/wt) of the bio-oil samples which exceeds the normally reported ~ 40% of sample literature reports states that GC is able to analyze. It must be noted that our measurement is only by weight difference and it is possible that some of the volatilized material in the microfurnace condenses in the GC injector port.

The Py-GC/MS of the different bio-oils (Figure 2.2 (a–c)) and the compounds identified (Table 2.3) illustrate clearly the difference in the chemical composition of the bio-oil samples based on their different feedstock. Acetic acid (**1**), the predominant carboxylic acid in bio-oil and acetol (**2**) were detected in all biomass-derived bio-oils, but were found in high abundance in the bio-oil from barley straw followed by wood bio-oils. Acetic acid is mostly produced through removal of acetyl groups in hemicelluloses (containing glucuronic acid and xylose as its main constituents) and to a minor extent from cellulose during its pyrolysis (12, 21, 31). Furaldehyde (**6**) in all bio-oils (except Alcell lignin bio-oil) showed a high abundance in bio-oil of birch wood, which is known to have high xylose content in hemicelluloses of hardwoods (12, 32). Levoglucosan (**78**) the primary product of the thermal degradation of cellulose, formed by depolymerisation reaction through transglycosylation (6, 12, 21, 32) was found in all bio-oils (except Alcell



lignin bio-oil). Its degradation further produces small amount of furans and acids such as acetic acid (**1**), propanoic acid (**4**), 2-furaldehyde (**6**), 1-(furan-2-yl)ethanone (**10**), dihydrofuran-2(*3H*)-one (**12**), (*5H*)-furan-2-one (**14**), 3-methylenedihydrofuran-2,5-dione (**16**), 3-methylfuran-2(*5H*)-one (**17**), 3,5-dimethylfuran-2(*5H*)-one (**20**), 3-hydroxydihydrofuran-2(*3H*)-one (**25**), 4-methylfuran-2(*5H*)-one (**30**), 3-methyldihydrofuran-2,5-dione (**33**), or undergoes more dehydration to produce 1,4:3,6-dianhydroglucopyranose (**45**) (detected only in birch wood and forest residue bio-oils) (*12*). The largest amounts of levoglucosan (**78**) were found in bio-oil from barley straw likely due to higher cellulose content in the barley straw (*31*).

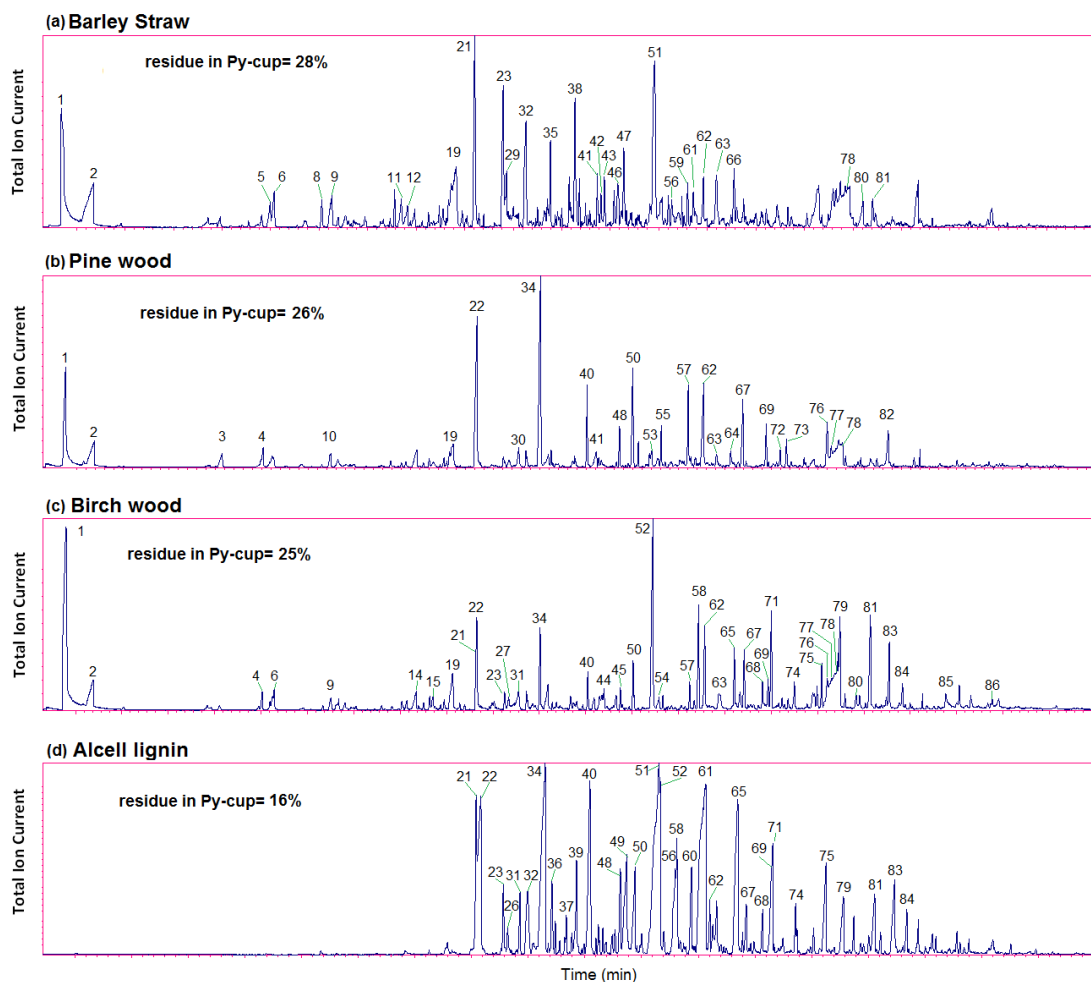


Figure 2.2. TIC of the volatile products of bio-oil obtained from (a) barley straw, (b) pine wood, (c) birch wood and (d) lignin.

Table 2.3. Products detected in bio-oil samples and cracking fractions using Py-GC/MS and mass % of oil left in Py-cup.

		Bio-oil feedstock				Forest residue bio-oil thermal cracking			
		Barley straw	Pine wood	Birch wood	Alcell lignin	Forest residue	Light	Middle	Heavy
% Water content (n = 2)		16	24	24	8	37	N/A	N/A	N/A
% Residue in Py-cup (average = 2)		28	26	25	16	16	N/A	N/A	N/A
% GC-detectable fraction		56	50	51	76	47	N/A	N/A	N/A
		Bio-oil feedstock				Forest residue bio-oil thermal cracking			
Peak no. <sup>a</sup>	Compound	Barley straw	Pine wood	Birch wood	Alcell lignin	Forest residue	Light	Middle	Heavy
1	Acetic acid	√√	√√	√√		√√	√√	√	
2	Hydroxy-acetaldehyde	√	√	√		√√	√√	√	
3	Hydroxypropanone		√						
4	Propanoic acid		√	√					
5	2-Cyclopentene-1-one	√							
6	2-Furaldehyde	√	√	√			√		
7	Ethadione						√	√	
8	2-Methyl-2-cyclopentene-1-one	√							
9	1-(Acetyloxy)-2-propanone,	√		√					
10	1-(Furan-2-yl)ethanone		√						
11	3-Methyl-2-cyclopentene-1-one	√							
12	Dihydrofuran-2(3 <i>H</i> )-one	√					√	√	
13	3-Methylcyclopent-2-enone						√		
14	(5 <i>H</i> )-Furan-2-one			√		√	√		
15	4-Methyl-5,6-dihydro-(2 <i>H</i> )-pyran-2-one			√					

Table 2.3 contd.

Peak no. <sup>a</sup>	Compound	Bio-oil feedstock				Forest residue bio-oil thermal cracking				
		Barley straw	Pine wood	Birch wood	Alcell lignin	Forest residue	Light	Middle	Heavy	
16	3-Methylenedihydrofuran-2,5-dione					√				
17	3-Methylfuran-2(5 <i>H</i> )-one						√			
18	2-Hydroxy-1-methyl-1-cyclopentene-3-one					√	√	√	√	
19	3-Methylcyclopentane-1,2-dione	√	√	√						
20	3,5-Dimethylfuran-2(5 <i>H</i> )-one						√	√		
21	Phenol	√√		√	√√	√	√	√	√	
22	Guaiacol		√√	√√	√√	√√	√√	√√	√√	
23	2-Methyl-phenol	√√		√	√		√			
24	3-Ethyl-2-hydroxycyclopent-2-enone							√		
25	3-Hydroxydihydrofuran-2(3 <i>H</i> )-one								√	
26	2-Hydroxy-5-methylbenzaldehyde				√					
27	3-Hydroxy-2-methyl-4 <i>H</i> -pyran-4-one			√			√	√		
28	3-Methylcyclopentane-1,2-diol					√	√	√		
29	2,6-dimethyl-phenol	√								
30	4-Methylfuran-2(5 <i>H</i> )-one		√							
31	3-Methyl-guaiacol			√	√					
32	4-Methyl-phenol	√√			√	√	√	√	√	
33	3-Methyldihydrofuran-2,5-dione					√				
34	4-Methyl-guaiacol		√√	√√	√√	√√	√√	√√	√√	
35	4,6-Dimethyl-phenol	√√								
36	4,5-Dimethyl-phenol				√					

Table 2.3 contd.

Peak no. <sup>a</sup>	Compound	Bio-oil feedstock				Forest residue bio-oil thermal cracking			
		Barley straw	Pine wood	Birch wood	Alcell lignin	Forest residue	Light	Middle	Heavy
37	2,6-Dimethoxy-toluene				√				
38	4-Ethyl-phenol	√√				√	√	√	
39	2,5-Dimethoxy-toluene				√√				
40	4-Ethyl-guaiacol		√√	√	√	√	√	√√	√
41	2-Ethyl-6-methyl-phenol	√	√						
42	2-Vinylbenzaldehyde	√							
43	2,3,4-Trimethyl-phenol	√							
44	3,4-Anhydro-d-galactosan			√		√		√	
45	1,4:3,6-Dianhydro- $\alpha$ -d-glucopyranose			√		√	√	√	√
46	2-Vinyl-phenol	√							
47	4-Vinyl-phenol	√							
48	4-Vinyl-guaiacol		√		√	√			
49	2-Methoxybenzene-1,4-diol				√				
50	4-Allyl-guaiacol		√√	√	√	√√	√	√√	√
51	1,2-Benzenediol	√√			√√	√√		√	
52	Syringol			√√	√√	√			
53	5-(Hydroxymethyl)-2-furaldehyde		√						
54	5-(Hydroxymethyl) dihydrofuran-2(3 <i>H</i> )-one			√		√		√	√
55	4-Propyl-guaiacol		√						
56	3-Methyl-1,2-benzenediol	√			√				
57	4-Propenyl-(cis)-Guaiacol		√√	√		√		√	
58	4-Methyl-Syringol			√√	√				
59	3-Hydroxy-benzaldehyde	√							
60	4-Propenyl-(trans)-Guaiacol				√	√		√	√
61	4-Methyl-1,2-benzenediol	√			√√				

Table 2.3 contd.

Peak no. <sup>a</sup>	Compound	Bio-oil feedstock				Forest residue bio-oil thermal cracking			
		Barley straw	Pine wood	Birch wood	Alcell lignin	Forest residue	Light	Middle	Heavy
62	Vanillin	√√	√	√√	√	√√		√	
63	Hydroquinone	√	√	√		√			
64	Homo-vanillin		√						
65	4-Ethyl-syringol			√	√√				
66	2-Methyl-hydroquinone	√√							
67	Acetoguaiacone		√	√	√	√		√	√
68	4-vinyl-syringol			√	√				
69	Guaiacyl acetone		√	√	√	√		√	√
70	1-(4-Hydroxyphenyl) ethanone					√√		√	√√
71	4-allyl-syringol			√√	√√				
72	Propioguaiacone		√						
73	Coniferyl alcohol		√						
74	(cis)-4-Propenyl-syringol			√	√				
75	(trans)-4-Propenyl-Syringol			√	√√				
76	Dihydro-coniferyl alcohol		√	√		√√			√√
77	Methyl-2-(4-hydroxy-3-methoxyphenyl)acetate		√	√					
78	Levoglucosan	√√	√	√		√√		√	√√
79	Syringaldehyde			√√	√				
80	1,6-Dianhydro- $\alpha$ -d-galactofuranose	√		√					
81	Acetosyringone	√		√√	√				
82	Coniferyl aldehyde		√						
83	Syringylacetone			√√	√√				
84	Propiosyringone			√	√				
85	Sinapyl alcohol			√					
86	Sinapinaldehyde			√					

√ = Present (low relative peak area), √√ = significant (high relative peak area)

a Peak # as observed in Figures 2.2 and 2.4

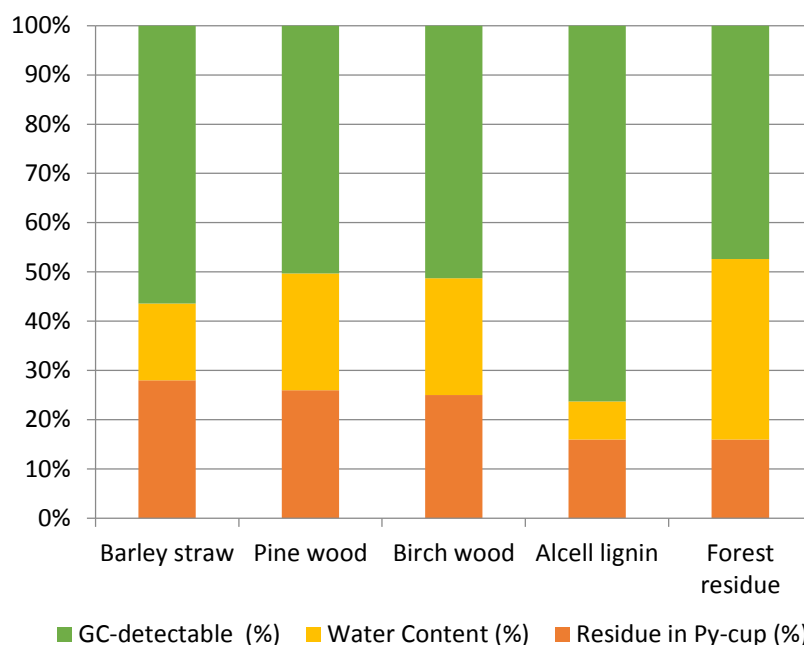


Figure 2.3. Mass % for residue in Py-cup, water content and GC-detectable in bio-oil obtained from barley straw, pine wood, birch wood lignin and forest residue.  $n=3$ ,  $RSD < 10\%$ .

Phenolic compounds of bio-oil are abundantly produced from the pyrolysis of the lignin (9, 12). Phenolic or lignin pyrolysis products such as nonmethoxy-phenols, guaiacols and syringols are all related to their lignin source from different plants. There were major differences in lignin-derived products observed in the Py-GC/MS due to the fact that the lignin composition differs strongly among hardwood, softwood or grassy plants (21). The difference is related to the lignin structures. Guaiacyl lignin is found mainly in softwoods produced through the polymerization of a higher fraction of coniferyl units (12) while guaiacyl–syringyl lignin is found in hardwoods produced from the copolymerization of both the coniferyl and sinapyl phenylpropane units.

The lignin and birch hardwood has similar proportions of syringol and guaiacol units, but as shown in birch bio-oil's Py-GC/MS (Figure 2.2(c)), the syringol-related products were found to be more significant (9,12). This is likely due to the *p*-sinapyl alcohol unit and its di-methoxy groups which likely degrade during pyrolysis to produce syringol derivatives (i.e., syringol (52), 4-methyl- (58), 4-ethyl- (65), 4-vinyl- (68), 4-allyl- (71), 4-(1-propenyl)- (74, 75), syringaldehyde (79), acetosyringone (81), syringlactone (83), propiosyringone (84), sinapyl alcohol (85) and sinapinaldehyde (86)) as listed in Table 2.3.

In pine wood bio-oil (Figure 2.2(b)) the most abundant peak was 4-methylguaiacol (34) followed by guaiacol (22), and its guaiacol-derivatives including: 4-methylguaiacol (34), 4-ethylguaiacol (40), 4-vinylguaiacol (48), 4-allylguaiacol (50), 4-propylguaiacol (55), (cis)-4-propenyl-guaiacol (57); vanillin (62); homovanillin (64); acetoguaiacone (67); guaiacylacetone (69); propioguaiacone (72); coniferyl alcohol (73); coniferyl alcohol (76) and coniferyl aldehyde (82). These products are related to the lignin monomers of softwood, which are mainly composed of guaiacol units and smaller amounts of syringol and *p*-hydroxyphenyl units (9, 12).

Phenol (21) and its derivatives (2-methyl- (23), 2,6-dimethyl- (29), 4-methyl- (32), 4,6-dimethyl- (35), 4-ethyl- (38), 2-ethyl-6-methyl- (41), trimethyl- (43), 2-vinyl- (46), and 4-vinyl- (47) were found in significant abundance in the bio-oil of barley straw. These compounds have been previously reported in high concentration in bio-oil from barley straw (6) and are related to the major monomeric units in straw i.e. *p*-coumaryl alcohol, which is found almost exclusively in grasses and straw (30, 32). The other types of lignin monomers are found in grasses but in lower quantities and their pyrolysis products were also detected.



The presence of catechols found in barley straw (Figure 2.2(a)), are likely lignin-derived products since sinapyl alcohol monomeric units have been found in grassy crops such as in switchgrass but not in pine wood (32). Alcell lignin bio-oils (Figure 2.2(d)) also contain catechols, particularly, 1,2-dihydroxybenzene (**51**) followed by 1,2-dihydroxy-3-methylbenzene (**56**), 1,2-dihydroxy-4-methylbenzene (**61**), hydroquinone (**63**) and 2-methylhydroquinone (**66**).

Finally, the bio-oil from Alcell lignin (Figure 2.2(d)) is comparable with lignin-derived products from hardwood and therefore similar bio-oil lignin products from birch wood (Figure 2.2(c) and Table 2.3) were expected. It had almost no peaks related to cellulose or hemicellulose pyrolysis, and lignin pyrolysis products related to phenols, guaiacols, and syringols were dominant.

#### 2.3.1.2. Forest residue bio-oil and its thermal cracking fractions

To determine the usefulness of TLC–FID and Py-GC/MS for analysis of bio-oil upgrading, simple thermal cracking was performed on the bio-oil obtained from forest residue to produce three fractions (light, middle and heavy fraction). In order to understand the bio-oil fractionation through this process, Py-GC/MS was used to analyze of bio-oil produced from forest residue and the thermal fractions are illustrated in Figure 2.4 and the products identified in Table 2.3. First, there are differences in the chemical composition of forest residue bio-oil (Figure 2.4(a)) from the other wood derived bio-oils (Figure 2.2(b and d)) (13). The guaiacols (**22**, **34**, **50**, and **70**) are predominant in the GC/MS of forest residue bio-oil as shown in Figure 2.4(a). The cellulose derived product levoglucosan (**78**) shows a very large abundance. Acetic acid (**1**) and acetol (**2**) were abundant and peaks were as

large as in the birch wood bio-oils. In addition, new pyrolysis products were also detected such as compounds (7, 13, 16–18, 20, 24–25, 28, 33 and 70). The differences are likely because forest residue includes the needles and bark which contain more extractives and tannins.

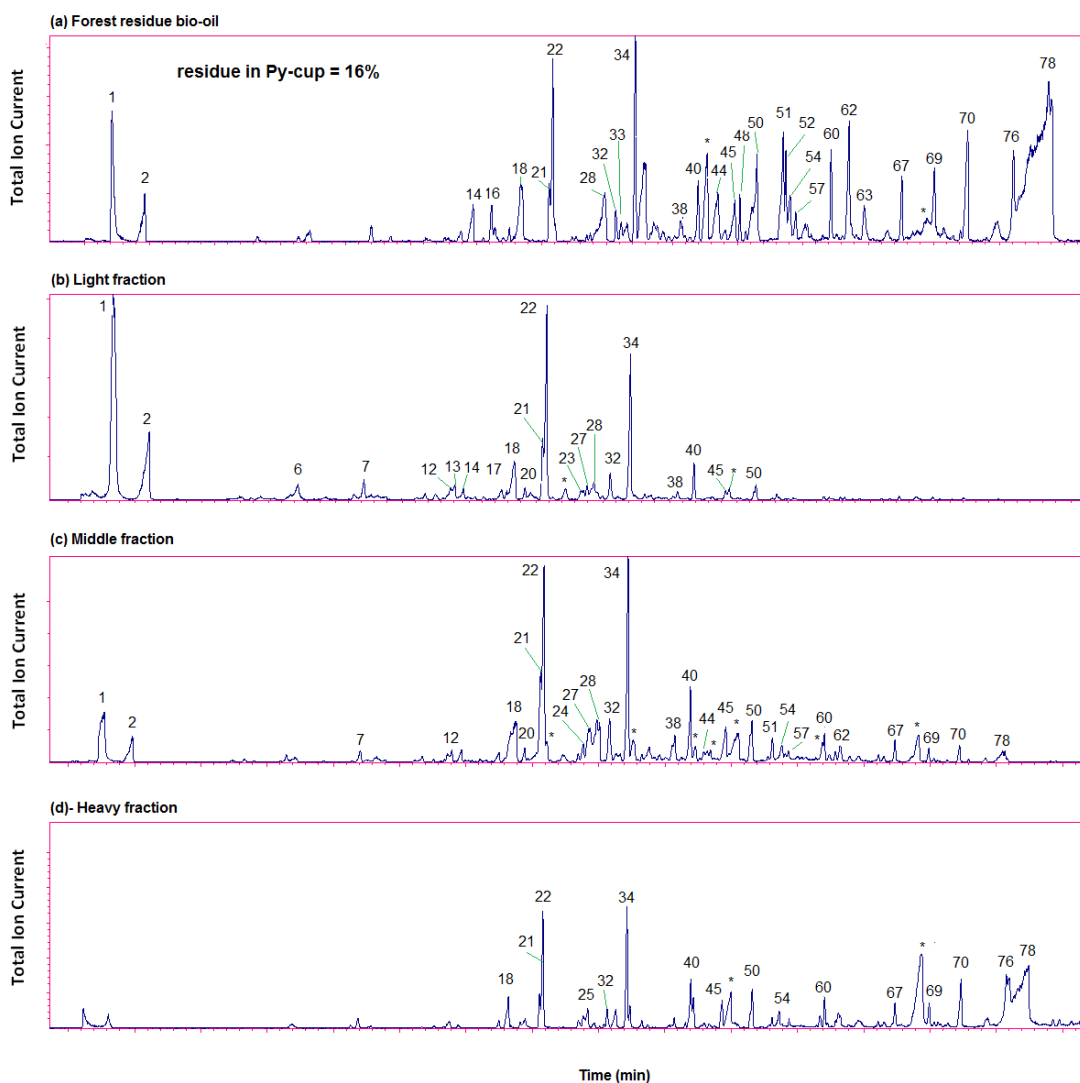


Figure 2.4. TIC of the volatile products of forest residue bio-oil and its thermal cracking fractions in presence of 30% PEG. (a) Forest residue bio-oil, (b) light fraction, (c) middle fraction and (d) heavy fraction. (\* PEG degradation products).

The thermal cracking of forest residue bio-oil was undertaken at three cracking stages and 30% polyethylene glycol (PEG) was added to suppress bio-oil coking. The PEG

was compatible (soluble in) with bio-oil and stable at high temperatures. PEG keeps bio-oil molecules separated thereby inhibiting coke formation. Note that PEG's degradation products can be observed in the fraction's GC/MS as peaks marked by an asterisk. The light fraction (Figure 2.4(b), 165 °C) can be considered as a mixture of lower polarity compounds in bio-oil. The TIC shows high amounts for acetic acid (**1**) and acetol (**2**), in addition to other small pyrolysis products. The middle fraction (Figure 2.4(c), 345 °C) shows some carry-over of the small components but also shows peaks of higher polarity compounds along with some levoglucosan (**78**). This fraction can be considered as a fraction that represents the medium polarity compounds in the bio-oil. The heavy fraction (residue left in reactor) should be mainly composed of the highest polarity compounds as observed in Figure 2.4(d) along with non-GC able components. (i.e., char) or products formed probably through subsequent polymerization of smaller components during thermal cracking. However, the TIC clearly shows compounds of medium polarity that are less intense. The levoglucosan (**78**) peak is of considerable abundance, and separates with the last fraction and is notably stable even after high thermal cracking conditions.

### **2.3.2. TLC–FID analysis**

#### **2.3.2.1. Bio-oil samples**

TLC–FID is a liquid-solid chromatographic technique and, as such, is able to separate and detect both polar volatile and non-volatile compounds. TLC–FID can separate bio-oil into three polarity zones (fractions) on chromarods. In Figure 2.5(a–e), the FID response is shown vs. chromarod scan time inversely, representing relative mobility of bio-oil fractions during development after two solvent systems (Table 2.2). The peak at the

origin is thought to represent high molecular weight compounds or the condensed polymerization fraction of bio-oil. Biochar may also be present, however the study samples were carefully filtered (0.45  $\mu\text{m}$ ).

The TLC–FID chromatograms show three general areas representing zones of component polarity that can be classified into: (i) least polar fraction which is resolved within scan time 1–4 min, (ii) medium polarity fraction between 11 and 14 min in the second development, and (iii) higher polar/condensed fraction that is stacked at the origin on the rods. The observed broadening of peaks in the chromatogram relates to the range of compounds with different polarities. As shown in Figure 2.5(a), standards (representative of bio-oil fractions) travel along the chromarod depending on their polarity with separation of vanillin, levoglucosan and glucose. Vanillin represents a group of pyrolysis products (i.e., phenol, 2,6-methyl-phenol, guaiacol, 4-hydroxy cinnamic acid, 4-hydroxy-methyl furaldehyde and syringic acid). The more polar standards levoglucosan and glucose separate by the second development solvent (Figure 2.5(b)).

All three bio-oil samples (Figure 2.5(c), (d), (e)) and Figure 2.6(b) showed a broad first development peak with their maximum intensity close to the vanillin standard. Lignin bio-oil (Figure 2.5(b)) revealed a very high abundance of phenolic compounds moving with the first development solvent and very little in the second. In the second development, scans showed a significant peak corresponding to anhydrosugars that were also observed in all bio-oil GC/MS chromatograms. Interestingly, free sugars have been thought to be present in some bio-oils (33) especially those that are aged. No band peaks related to reducing sugars were observed (20, 33). Glucose was observed in bio-oil in a recent study using HPTLC (20). There is a significant stationary peak at the origin for all bio-oil samples, but

barley straw and forest residue bio-oil showed by far the largest peak. This may be explained by the presence of large amounts of polar extractives in the forest residue bio-oil and due to bio-oil aging (barley bio-oil was 2 years old).

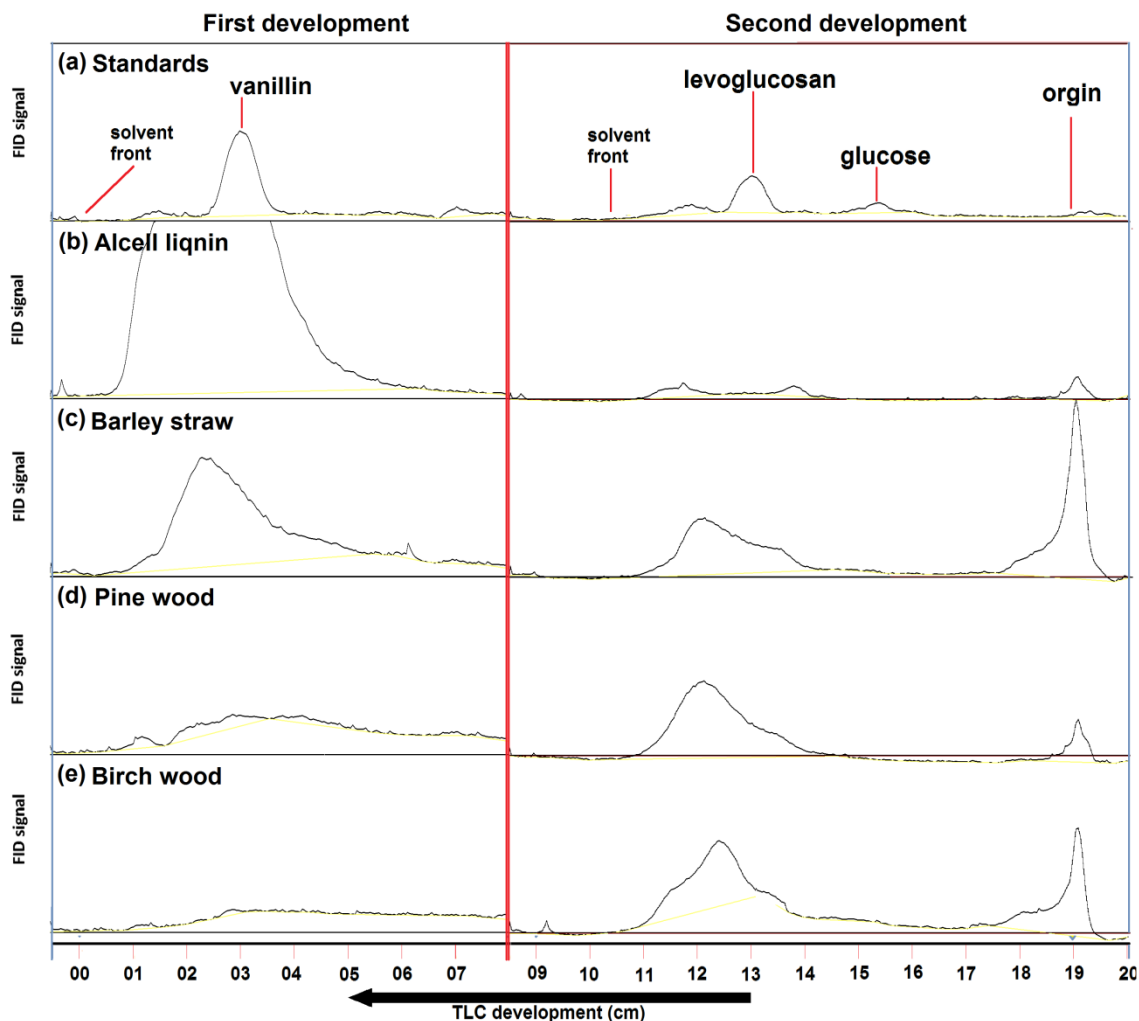


Figure 2.5. TLC–FID chromatograms of (a) standards, (b) lignin bio-oil, (c) barley straw bio-oil, (d) pine wood bio-oil, and (e) birch wood bio-oil.

The bio-oil from barley straw showed the largest first development peak (lignin products) followed by pine then birch wood. There is a similar trend that could be identified by looking at their bio-oil's lignin product peaks by Py-GC/MS (Figure 2.2). The

explanation may be the different lignin types in each. Straw would have more nonmethoxy-phenolic residues compared to the more highly substituted phenolic moieties of wood lignins. It is expected that more lignin-derived pyrolysis products would come from less substituted phenolic lignin compared with samples with higher methoxy-phenolic lignin of softwood followed by hardwood. The higher polarity fraction (second development) represents anhydrosugars and other carbohydrate products, and some minor from lignin pyrolysis products (as observed in Alcell lignin profile).

Finally, although the TLC–FID peaks of bio-oil mixtures are broad in nature, the integrated peaks associated with the first and second development and those at the origin can be used to represent the sum of lignin-related, carbohydrate-related and polymeric-derived products, respectively (Figure 2.7). The relative peak areas give a quick pictorial capture of the quantity of each polarity fraction in a sample. For example, the Alcell lignin bio-oil shows the highest peak area for the lowest polarity fraction among the bio-oils followed by barley and pine wood bio-oils. Birch bio-oil had nearly same amount of low and medium polarity fractions. More experimental work is needed to confirm the identification of the compounds present in each fraction; however, TLC–FID can be very useful for rapid screening of bio-oil chemical groups.

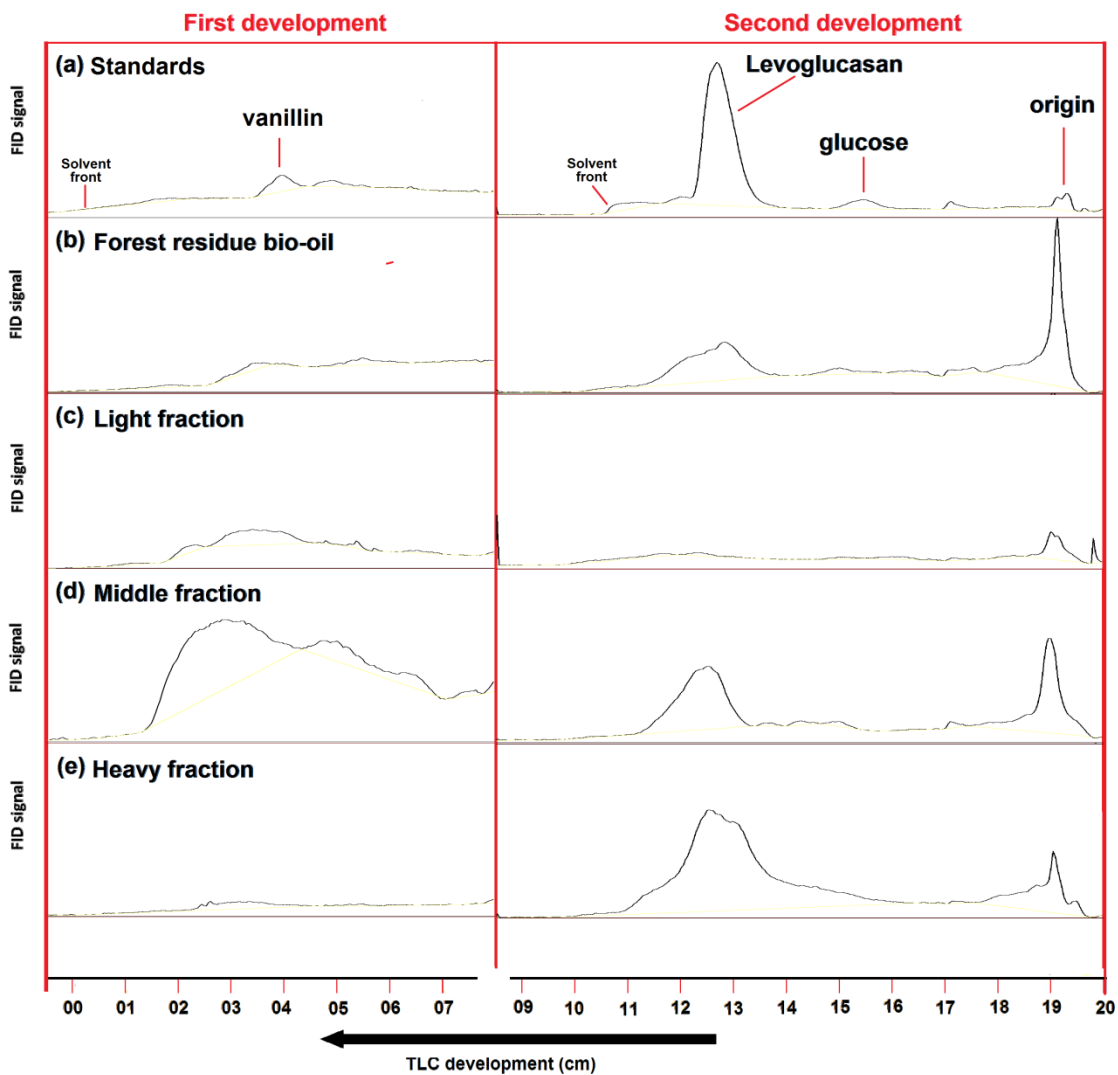


Figure 2.6. TLC–FID chromatograms of forest residue bio-oil and its thermal cracking fractions. (a) Standards, (b) forest residue bio-oil, (c) light fraction, (d) middle fraction, and (e) heavy fraction.

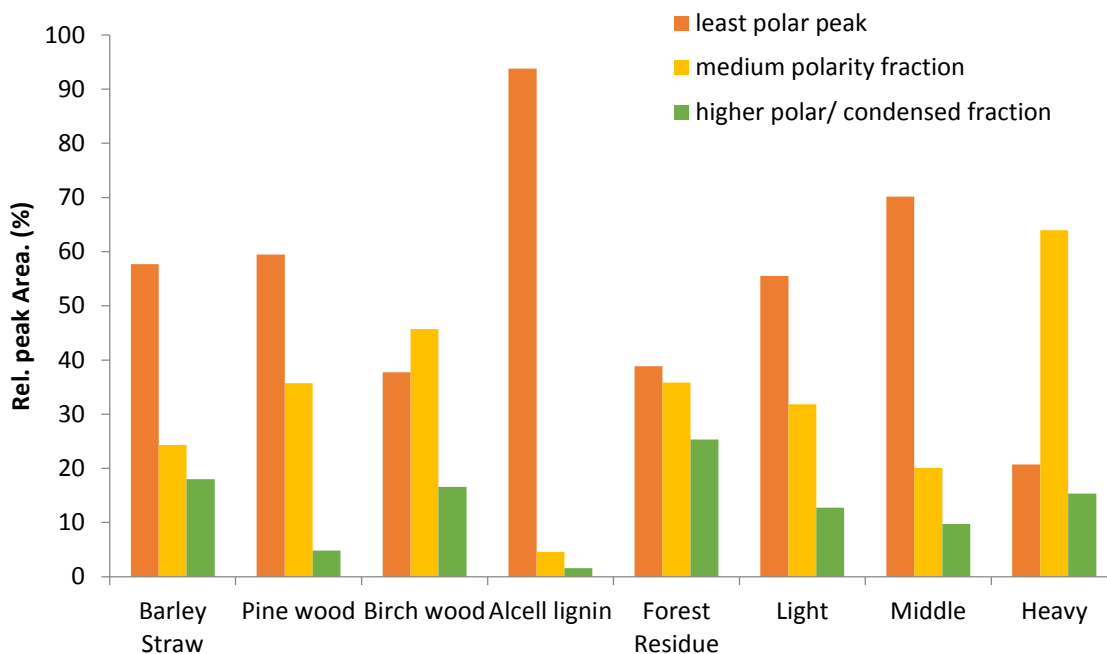


Figure 2.7. Relative peak area for polarity zones on TLC chromatograms obtained for bio-oil from barley straw, pine wood, birch wood, lignin and forest residue.  $n=3$ , %RSD < 10%.

### 2.3.2.2. Forest residue bio-oil and its thermal cracking fraction

This study also examined bio-oil of forest residue and its potential upgrading by thermal cracking. The profile of this bio-oil and its thermal cracking fractions (light, middle, and heavy) are shown in Figure 2.6. The bio-oil has a similar profile to that of birch and pine bio-oil (Figure 2.5(e)) but with a larger peak in the origin. This is likely due to the fact that the forest residue contains other types of woody material (more bark, leaves, etc.) and therefore more extractives and higher nitrogen content (13). The light fraction (Figure 2.6(c); 165 °C) shows a small but significant peak in the first development and little in second development with an insignificant peak at the origin. The profile can be explained by the presence of lower molecular weight compounds that are also detected in its Py-



GC/MS (Figure 2.4(b)). The middle fraction (Figure 2.6(d); 345 °C) has a much larger contribution to the 1<sup>st</sup> development band and a significant carbohydrate band in the second development. This is confirmed by the detection of polar components observed by Py-GC/MS (Figure 2.4(c)) such as 3,4-anhydro-galactosan (**44**), 1,4:3,6-dianhydroglucopyranose (**45**) and levoglucosan (**78**). The heavy fraction (residue remaining) (Figure 6(e)) shows components mainly in the second development. The second development scan gave two overlapping broad peaks; one being levoglucosan. Finally the peaks at the origin in both middle and heavy fractions are likely very highly polar components or condensed/polymerized products that remain after filtration through a 0.45 µm filter. Of the thermal cracking fractions the heavy fraction had the largest peak area (Figure 2.7) for medium polarity components (ca. 70%).

## 2.4. Conclusion

Py-GC-MS and TLC-FID can be used together to rapidly profile whole bio-oil samples with minimal sample preparation. TLC-FID analysis, for the first time, was carefully controlled (solvent system, sample size, scan conditions) for a rapid, two solvent development, analysis of bio-oil. Both techniques can distinguish general and specific differences between bio-oil samples based on their feedstock. TLC-FID showed striking band (compound group) differences among hardwood, softwood and straw bio-oils, and further, among the thermal cracking fractions of forest residue bio-oil. The technique was shown to be complimentary to the Py-GC/MS method for bio-oil analysis. It was shown that the Py-GC/MS unit (with sample cup) can be adopted for whole sample bio-oil

characterization and that the non-volatile fraction of the sample can be accurately measured after GC/MS analysis.

## 2.5. References

1. Tessini, C.; Mueller, N.; Mardones, C.; Meier, D.; Berg, A.; von Baer, D. Chromatographic approaches for determination of low-molecular mass aldehydes in bio-oil. *J. Chromatogr. A* **2012**, *1219*, 154-160.
2. Yang, C.; Zhang, B.; Moen, J.; Hennessy, K.; Liu, Y.; Lin, X.; Wan, Y.; Lei, H.; Chen, P.; Ruan, R. Fractionation and characterization of bio-oil from microwave-assisted pyrolysis of corn stover. *Int. J. Agric. Biol. Eng.* **2010**, *3*, 54-61.
3. Abdullah, H.; Wu, H. Bioslurry as a fuel. 4. preparation of bioslurry fuels from biochar and the bio-oil-rich fractions after bio-oil/biodiesel extraction. *Energy Fuels* **2011**, *25*, 1759-1771.
4. Gercel, H. F. Bio-oil production from *Onopordum acanthium* L. by slow pyrolysis. *J. Anal. Appl. Pyrolysis* **2011**, *92*, 233-238.
5. Ortega, J. V.; Renehan, A. M.; Liberatore, M. W.; Herring, A. M. Physical and chemical characteristics of aging pyrolysis oils produced from hardwood and softwood feedstocks. *J. Anal. Appl. Pyrolysis* **2011**, *91*, 190-198.
6. Mullen, C. A.; Boateng, A. A.; Hicks, K. B.; Goldberg, N. M.; Moreau, R. A. Analysis and comparison of bio-oil produced by fast pyrolysis from three barley biomass/byproduct streams. *Energy Fuels* **2010**, *24*, 699-706.
7. Pattiya, A. Bio-oil production via fast pyrolysis of biomass residues from cassava plants in a fluidised-bed reactor. *Bioresour. Technol.* **2011**, *102*, 1959-1967.
8. Zhang, Q.; Chang, J.; Wang, T.; Xu, Y. Review of biomass pyrolysis oil properties and upgrading research. *Energy Convers. Manage.* **2006**, *48*, 87-92.
9. Zhang, L.; Kong, S. Multicomponent vaporization modeling of bio-oil and its mixtures with other fuels. *Fuel* **2012**, *95*, 471-480.
10. Pollard, A. S.; Rover, M. R.; Brown, R. C. Characterization of bio-oil recovered as stage fractions with unique chemical and physical properties. *J. Anal. Appl. Pyrolysis* **2012**, *93*, 129-138.
11. Guo, X.; Wang, S.; Wang, Q.; Guo, Z.; Luo, Z. Properties of bio-oil from fast pyrolysis of rice husk. *Chin. J. Chem. Eng.* **2011**, *19*, 116-121.
12. Azeez, A. M.; Meier, D.; Odermatt, J.; Willner, T. Fast Pyrolysis of African and European Lignocellulosic Biomasses Using Py-GC/MS and Fluidized Bed Reactor. *Energy Fuels* **2010**, *24*, 2078-2085.
13. Oasmaa, A.; Kuoppala, E.; Solantausta, Y. Fast Pyrolysis of Forestry Residue. 2. Physicochemical Composition of Product Liquid. *Energy Fuels* **2003**, *17*, 433-443.
14. Javaid, A.; Ryan, T.; Berg, G.; Pan, X.; Vispute, T.; Bhatia, S. R.; Huber, G. W.; Ford, D. M. Removal of char particles from fast pyrolysis bio-oil by microfiltration. *J. Membr. Sci.* **2010**, *363*, 120-127.

15. Galletti, G. C.; Reeves, J. B.,III; Bocchini, P.; Muscarella, C. I. Compositional Differentiation of Maize Hybrid Stovers Using Analytical Pyrolysis and High-Performance Liquid Chromatography. *J. Agric. Food Chem.* **1997**, *45*, 1715-1719.
16. Thangalazhy-Gopakumar, S.; Adhikari, S.; Ravindran, H.; Gupta, R. B.; Fasina, O.; Tu, M.; Fernando, S. D. Physicochemical properties of bio-oil produced at various temperatures from pine wood using an auger reactor. *Bioresour. Technol.* **2010**, *101*, 8389-8395.
17. Putu, A. E.; Ozcan, A.; Putu, E. Pyrolysis of hazelnut shells in a fixed-bed tubular reactor: yields and structural analysis of bio-oil. *J. Anal. Appl. Pyrolysis* **1999**, *52*, 33-49.
18. Acikgoz, C.; Kockar, O. M. Characterization of slow pyrolysis oil obtained from linseed (*Linum usitatissimum* L.). *J. Anal. Appl. Pyrolysis* **2009**, *85*, 151-154.
19. Sensoz, S.; Can, M. Pyrolysis of pine (*Pinus Brutia* Ten.) chips: 2. Structural analysis of bio-oil. *Energy Sources* **2002**, *24*, 357-364.
20. Tessini, C.; Vega, M.; Mueller, N.; Bustamante, L.; von Baer, D.; Berg, A.; Mardones, C. High performance thin layer chromatography determination of cellobiosan and levoglucosan in bio-oil obtained by fast pyrolysis of sawdust. *J. Chromatogr. A* **2011**, *1218*, 3811-3815.
21. Mohan, D.; Pittman, C. U., Jr.; Steele, P. H. Pyrolysis of Wood/Biomass for Bio-oil: A Critical Review. *Energy Fuels* **2006**, *20*, 848-889.
22. Relffova, K.; Orinak, A.; Nemcova, R.; Vreva, F. The possibility of TLC-FID detection in oligosaccharide analysis. *JPC J. Planar Chromatogr. - Mod. TLC* **2003**, *16*, 192-195.
23. Demirci, F. Applied Thin-Layer Chromatography-Best Practice and Avoidance of Mistakes. 2nd ed. By E. Hahn-Deinstrop. Translated by R. G. Leach. Wiley-VCH, Weinheim. 2007. (e-book). *J. Nat. Prod.* **2008**, *71*, 1661.
24. Barman, B. N. In *In Application of thin-layer chromatography with flame-ionization detection to heavy oil processing: Feeds, products and effects of process variables.* **2002**; *Prepr. Pap. - Am. Chem. Soc., Div. Fuel Chem.* **2002**, *47*, pp. 649-651.
25. Mastral, A. M.; Murillo, R.; Callen, M. S.; Garcia, T.; Snape, C. E. Influence of Process Variables on Oils from Tire Pyrolysis and Hydropyrolysis in a Swept Fixed Bed Reactor. *Energy Fuels* **2000**, *14*, 739-744.
26. Wang, S.; Guo, G.; Yan, Z.; Lu, G.; Wang, Q.; Li, F. The development of a method for the qualitative and quantitative determination of petroleum hydrocarbon components using thin-layer chromatography with flame ionization detection. *J. Chromatogr. A* **2010**, *1217*, 368-374.
27. Lu, X.; Kalman, B.; Redelius, P. A new test method for determination of wax content in crude oils, residues and bitumens. *Fuel* **2008**, *87*, 1543-1551.
28. Le Guern, M.; Chailleux, E.; Farcas, F.; Dreessen, S.; Mabile, I. Physico-chemical analysis of five hard bitumens: Identification of chemical species and molecular organization before and after artificial aging. *Fuel* **2010**, *89*, 3330-3339.
29. Adlard, E. R. Asphaltenes and Asphalts. I. Developments in Petroleum Science 40A by T. F. Yen, G. V. Chilingarian. *Chromatographia* **1996**, *42*, 235.
30. Ralph, J.; Hatfield, R.D. Pyrolysis-GC-MS characterization of forage materials J. *Agric. Food. Chem.* **1991**, *39*, 1426-1437.

31. Sun, R.; Sun, X. F.; Liu, G. Q.; Fowler, P.; Tomkinson, J. Structural and physicochemical characterization of hemicelluloses isolated by alkaline peroxide from barley straw. *Polym. Int.* **2002**, *51*, 117-124.
32. Thangalazhy-Gopakumar, S.; Adhikari, S.; Gupta, R. B.; Fernando, S. D. Influence of Pyrolysis Operating Conditions on Bio-Oil Components: A Microscale Study in a Pyroprobe. *Energy Fuels* **2011**, *25*, 1191-1199.
33. Lian, J.; Chen, S.; Zhou, S.; Wang, Z.; O'Fallon, J.; Li, C.; Garcia-Perez, M. Separation, hydrolysis and fermentation of pyrolytic sugars to produce ethanol and lipids. *Bioresour. Technol.* **2010**, *101*, 9688-9699.

## Chapter 3

### **Direct infusion mass spectrometric analysis of bio-oil using ESI-Ion Trap MS<sup>2</sup>**

---

<sup>2</sup> This chapter has been published; Alsbou, E.; Helleur, B. Direct Infusion Mass Spectrometric Analysis of Bio-oil Using ESI-Ion Trap MS. *Energy Fuels* **2013**, *28*, 578-590.

## Summary

Direct infusion-electrospray ionization (ESI)-Ion Trap MS and ESI-Ion Trap MS<sup>2</sup> were used for direct analysis of bio-oil from forest residue and reference bio-oils from cellulose and hardwood lignin. It was found that the bio-oil concentration and mode of MS analysis are important parameters in obtaining reproducible and structurally informative data. In order to study sensitivity and selectivity with ESI-Ion Trap MS, a selection of model compounds was studied with and without dopants. Dopants included NaCl, formic acid and NH<sub>4</sub>Cl in positive ion mode and NaOH and NH<sub>4</sub>Cl in negative ion mode. NH<sub>4</sub>Cl addition can be used to distinguish carbohydrate-derived products from other bio-oil components. NaOH and NaCl additives produced the highest peak intensities in negative ion mode as deprotonated adducts and in positive mode as sodiated adducts, respectively. ESI-MS<sup>2</sup> was used successfully for confirmation of individual target ions such as levoglucosan and cellobiosan, as well as for some structural products of lignin. Simple bio-oil fractionation into hydrophilic and hydrophobic components provided less complex and more interpretive ion spectra.

### 3.1. Introduction

The thermoconversion of biomass feedstocks such as forest and crop residues is widely considered a viable approach to produce biofuels and chemicals. Fast pyrolysis is the most common conversion method that produces liquid fuels. It is performed via fast heating of dried biomass to high temperatures (400–600 °C) in the absence of oxygen with short reaction times (<2 s) (1,2). Under optimized conditions, the feedstock can be converted into 60–75% (wt./wt.) liquid (bio-oil), depending on the type of feedstock and the remainder is a carbon-rich biochar and noncondensable gaseous product (3-5).

Bio-oil is a dark brown, free-flowing or viscous liquid. It is also a very complex mixture of organic compounds from thermal depolymerization and dehydration of components such as cellulose, hemicellulose, and lignin, which are common components of biomass (2, 4, 5). Moreover, bio-oils contain a large amount of water with high acidity. The compounds are mostly oxygenated, with a wide variety of different functional groups such as alcohols, esters, ethers, aldehydes, ketones, acids, olefins, aromatics, phenols, carbohydrates, and other derivatives (1, 3). The average molecular weight (M.wt) of bio-oil can vary depending on the biomass feedstock and pyrolysis temperature and normally within a range from 300 to 700 Da (6, 8).

Analyzing the chemical composition of bio-oil can help researchers in understanding the chemistry of pyrolysis (for optimizing the pyrolysis process to produce useful fuels and valuable chemicals) and eventually, to improve the chemical stability of the bio-oil (3). Unfortunately, there is no one particular characterization method for bio-oil samples. Many of the methods are based on bulk property measurements such as pH, water-content, acidity, density, viscosity, and heating value (7). Other measurements are obtained

by chemical methods, including GC-FID, GC-MS, FTIR (2, 4, 9), NMR (9), SEC/GPC (2, 6), and TGA (2, 4). For example, a combination of FTIR and NMR has been used for measuring the functional groups in bio-oils (5). GC-FID and GC-MS are very effective in identifying and measuring volatile compounds including some of the higher boiling products. GPC is used for oligomer analysis by measuring the oil's average M.wt (2). Nevertheless, GPC does not provide structural information on higher M.wt components that play an important role in the stability and usefulness of the bio-oil product. Finally, any chromatographic method requires significant analysis time and does not provide a very thorough chemical profiling in one analysis (5).

Mass spectrometry (MS) has frequently been adopted by researchers to analyze bio-oil due to its advantages of speed, specificity, and sensitivity. MS can be a powerful method for molecular weight and structural identification for a wide range of compounds. In combination with GC, it is the most common method utilized to identify volatile components in bio-oils (5). However, it is challenging to analyze the less volatile fraction due to the high M.wt and polarity of its components. A table summarizing the MS methods that have been used to characterize bio-oils and their related components can be found in the *Supporting Information* (Table S3.1-Appendix). Field ionization (FI) method is a soft ionization technique used for ionization of nonvolatile compounds. For example, Py-FI-MS has been used to analyze thermally ejected components from pyrolytic-lignin (6). The mass spectra clearly showed fragmented monomers and dimers related to lignin-derived compounds (6). In other studies (10, 11), FI-MS was applied to analyze bio-oil from chicken manure. Schnitzer et al. (10) reported that Py-FI MS and pyrolysis-field desorption



MS (Py-FD-MS) can produce a high M.wt range of mass ions, which is significantly higher than what Py-GC MS can produce.

Matrix-assisted laser desorption/ionization (MALDI) is a soft ionization technique, allowing for the study of larger molecules. MALDI has been used for analysis of molar mass distribution of pyrolytic-lignin (6). In the spectra, a series of peak maxima at  $m/z$  170–200 intervals were detected as lignin repeating units. Another spectral feature was the presence of repeating intervals between peak maxima of 14–16 Da (6). However, when using MALDI, matrix ions in the low molar mass region (150–300 Da) can interfere with observing analyte ions. For this reason, laser desorption/ionization (LDI) was used because no matrix is needed. Such a “matrix free ion” spectrum can be obtained within the region of low mass range (<300 Da). Smith et al. (5) has used LDI with high-resolution mass spectrometry (HRMS) to analyze bio-oil and termed this analysis “Petroleomic”. They reported over 100 compounds identified in loblolly pine bio-oil. Most of these components contained 3–6 oxygen atoms with 9–17 double-bond equivalents (DBE). The compounds containing 4 oxygen atoms and 9–13 DBE were the most abundant. It is apparent that LDI-HRMS is suitable for analyzing dimers and trimers of depolymerized lignin (6, 7). However, the work failed to report the presence of ions less than  $m/z < 250$  or to obtain useful data for carbohydrate-derived products (5).

Electrospray ionization (ESI) is a soft ionization technique that is easily used in both positive and negative ion modes and can give M.wt information. Positive ion mode ESI is used to detect polar compounds containing N-, O-, or S-containing heterocyclics, amines, ethoxylate, and esters while negative ion mode is suitable for phenols, carboxylic acids, sulfonates, and phosphonates (7, 12-14). Nonpolar hydrocarbons, such as paraffin

and aromatics, are difficult to ionize. Based on the above selectivity and because of the inherent high polarity of components in bio-oil, ESI-MS can be a useful tool for rapid analysis of bio-oil components that are not amenable to GC analysis. ESI-HRMS has been used in many studies for the characterization of bio-oils (2, 3, 7, 9, 11, 12, 15). Three HRMS instruments (FT-ICR, orbitrap and Q-TOF) interfaced with ESI in negative ion mode have been used to validate the methodology and investigate the difference in mass discrimination and resolution for the analysis of bio-oil samples (12). It was found that FT-ICR is best suited but with limitations in low mass discrimination. The method allowed for characterization of 800 chemicals compared to 40 by GC-MS. The negative ion mode spectra were dominated by low mass compounds ( $m/z$  100–250). In another study, bio-oil from pine pellets and peanut hulls was analyzed by negative ion mode ESI-FTICR MS and results showed an ability to characterize thousands of compounds due to the inherent high resolution of the FTICR (3). Spectra confirmed that the bio-oils from red pine were dominated by highly oxygenated species where  $O_2$ – $O_7$  species with 1–22 of DBE and  $C_4$ – $C_{39}$  were the predominant components (2, 3, 12). Hundreds of compounds present in chicken manure bio-oil have been characterized by negative ion mode ESI triple-quadrupole MS (9). The majority of these compounds were fatty acids, N-heterocyclics, phenols, sterols, diols, and alkyl benzenes. Tandem MS was used for structural confirmation of the N-heterocyclic compounds (11). The water/methanol extract of bio-oil from a biochar was analyzed using ESI MS to determine molar mass distribution (7). The average mass was  $m/z$  320 with the range  $m/z$  100–1100, in agreement to SEC data. ESI-MS was used to study model oligosaccharides and lignin degradation products (13, 14). The lignin products were analyzed in both positive and negative ion modes after being doped

with NaCl and NaOH, respectively (14). The NaCl dopant forms abundant sodiated adduct,  $[M+Na]^+$ , while NaOH assists in the formation of anions from deprotonation. It was noted that some of the lignin products fragmented during ESI and that care must be taken in interpreting spectra. In another study, negative ion mode ESI and APCI were used for analysis of oligosaccharide products such as chloride adducts ( $[M+Cl]^-$ ) (13). Sugars can be readily identified by the chlorine isotope pattern with no fragmentation. With tandem  $MS^n$  experiments, structural information on di- and oligosaccharides present in bio-oil mixtures may be obtained.

In the present study, direct injection ESI Ion Trap MS analysis of forest residue bio-oil (as a test sample) along with bio-oils from cellulose and lignin pyrolysis were investigated. The Ion Trap MS was chosen because of its availability and simplicity to researchers as well as for its capability for structural elucidation by  $MS^n$ . Sample preparation and instrumental parameters were optimized using model pyrolysis products and the bio-oils from lignin and cellulose. GC/MS was used to verify some of the target analytes present. The study utilized selected dopants in MS analysis as a means of increasing selectivity and sensitivity to differentiate between lignin and cellulose-derived ions. Finally, simple fractionation of forest residue bio-oil before MS analysis was examined to deal with the complexity of the mass spectra.

## 3.2. Materials and Methods

### 3.2.1 Samples and Materials

Bio-oil from hardwood forest residue and hardwood Alcell lignin produced by fast pyrolysis was kindly provided by Dr. Ikura (CANMET Energy Technology Center, Ottawa, Ontario) and Dr. de Wild (Energy Research Centre of The Netherlands), respectively. Cellulose bio-oil was produced using a home-built small scale tube-furnace pyrolysis unit (3 g sample) at 500 °C with N<sub>2</sub>-gas flow (300 mL min<sup>-1</sup>). Figure S3.1 in *Supporting Information* (Appendix) shows the assembled pyrolyzer unit. The bio-oil vapors were collected using a water-cooled condenser and followed by a liquid-N<sub>2</sub> trap. All samples were placed in airtight glass vials and stored at 4 °C until analyzed. Model compounds of lignocellulose bio-oil, levoglucosan (LG), guaiacol (G), vanillin (V), syringol (S), glucose (Glu), and cellobiose (Cbio), were analyzed. Their structures are shown in Table 3.1. All were purchased from Sigma-Aldrich. Solvents used were HPLC-grade (Sigma-Aldrich).

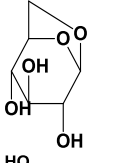
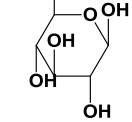
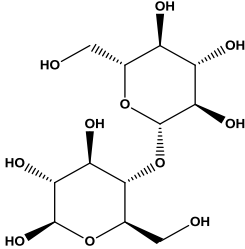
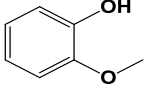
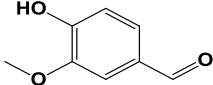
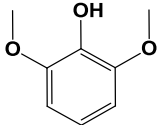
### 3.2.2 Py-GC-MS

This technique was described in chapter 2 (16). Approximately 1 mg of bio-oil was weighed inside a pyrolysis cup then introduced into a quartz tube vertical microfurnace pyrolyzer PY-2020D (Frontier laboratories Ltd., Yoriyama, Japan), coupled to a HP 5890 II gas chromatograph/HP 5971A mass selective detector (MSD) (Agilent, CA, U.S.A.). The MSD was operated under the following conditions: interface temperature, 270 °C; electron ionization energy, 70 eV; and scan range,  $m/z$  40–550. The pyrolysis furnace, interface temperature, and GC injector port were maintained at 270 °C. Helium carrier gas flow rate was 2 mL/min and the split flow of 40 mL min<sup>-1</sup>. A GC capillary column (Zebron ZB-

1701, 30 m × 0.25 mm i.d. × 0.25 μm film thickness, Phenomenex, Inc., U.S.A.) was used.

The GC oven was held at 50 °C for 6 min to trap and focus the volatile components and then the temperature was increased to 260 °C at 5 °C/min and held for 4 min.

Table 3.1. Model compounds.

Name	Code	M.wt (Da)	Structure
Levoglucozan (1,6-Anhydro-β-D-Glucose, 99%)	LG	162	
Glucose (D-(+)-Glucose, ≥99.5%)	Glu	180	
Cellobiose (D-(+)-Cellobiose, ≥98%)	Cbio	342	
Guaiacol (2-Methoxyphenol, ≥98%)	G	124	
Vanillin (4-Hydroxy-3-methoxybenzaldehyde, ≥97%)	V	152	
Syringol (2,6-Dimethoxyphenol, ≥98%)	S	154	

### 3.2.3 ESI-Ion Trap MS

The model compounds and bio-oil samples were dissolved in the solvent (methanol/water, 1:1, v:v) at 10 mg mL<sup>-1</sup>. To examine analyte concentration dependence on MS results samples were diluted to 2, 1, 0.2, 0.1, and 0.01 mg mL<sup>-1</sup>. A 1 mL Hamilton syringe loaded onto a syringe pump was used to infuse diluted samples directly into the ESI chamber at a rate of 0.01 mL min<sup>-1</sup>. The instrument used was an ESI Ion Trap mass spectrometer (Agilent 1100 series SL LC/MSD (Trap) CA, USA). The ESI MS analysis was accomplished in Smart mode using drying temperature of 350 °C, high purity N<sub>2</sub> at 8 L min<sup>-1</sup> and N<sub>2</sub>-nebulizer pressure of 15 psi. Full scan mass spectra were acquired over the range *m/z* 50–1000. For MS<sup>n</sup> experiments, helium gas was used as a collision gas with a fragmentation amplitude voltage of 1 V and the mass window was 1.5 Da. Optimization experiments of ESI-MS and ESI-MS<sup>2</sup> conditions were carried using model compounds listed in Table 3.1, as well as for bio-oils produced from cellulose and hardwood lignin.

### 3.2.4 Bio-oil fractionation

Two methods were used to fractionate the forest residue bio-oil into hydrophilic and hydrophobic components for further MS analysis, that is, lignin precipitation and solid phase extraction (SPE). For lignin precipitation, ca. 2 g of bio-oil was first mixed with ice/water at a ratio of 1:1 (v/v) by high-speed stirring (2500 rpm) for 2 h, then centrifuged for 5 min at 5000 rpm to separate the water-soluble from the solid water-insoluble fraction (Py-lignin). The Py-lignin was then washed twice with cold water and air-dried.

In SPE, a reversed-phase (C-18) cartridge (6 ml, Sigma Aldrich, USA) was first conditioned with MeOH followed by nanopure water. The forest residue bio-oil (15 mg)

was dissolved in 100  $\mu\text{L}$  methanol then loaded onto the top of the cartridge. The water-soluble fraction was eluted by  $8 \times 250 \mu\text{L}$  water under suction (vacuum manifold, Sigma-Aldrich) providing a flow rate of ca. 5 mL/min. The water-insoluble fraction was then eluted by  $8 \times 250 \mu\text{L}$  methanol. Further elution with MeOH showed little bio-oil sample remaining on the cartridge. Each fraction (250  $\mu\text{L}$ ) was collected in 20 mL vials for ease of dilution and stored at 4  $^{\circ}\text{C}$  until analyzed by ESI-MS.

### **3.3. Results and Discussion**

#### **3.3.1 Py-GC/MS**

The medium polar GC-column (Zebron ZB-1701) was installed with the microfurnace (Py)-GC/MS. Figure 3.1 shows the GC/MS TIC for bio-oils derived from cellulose, lignin, and forest residue. The chromatograms clearly reveal the compositional differences between cellulose and lignin bio-oils as well as showing that the forest residue bio-oil is a mixture of the two other bio-oils. Figure 3.1 also labels some of the model compounds used in this study. More details on peak identity can be found in Figure S3.2 and Table S3.2 (*Supporting Information-Appendix*).

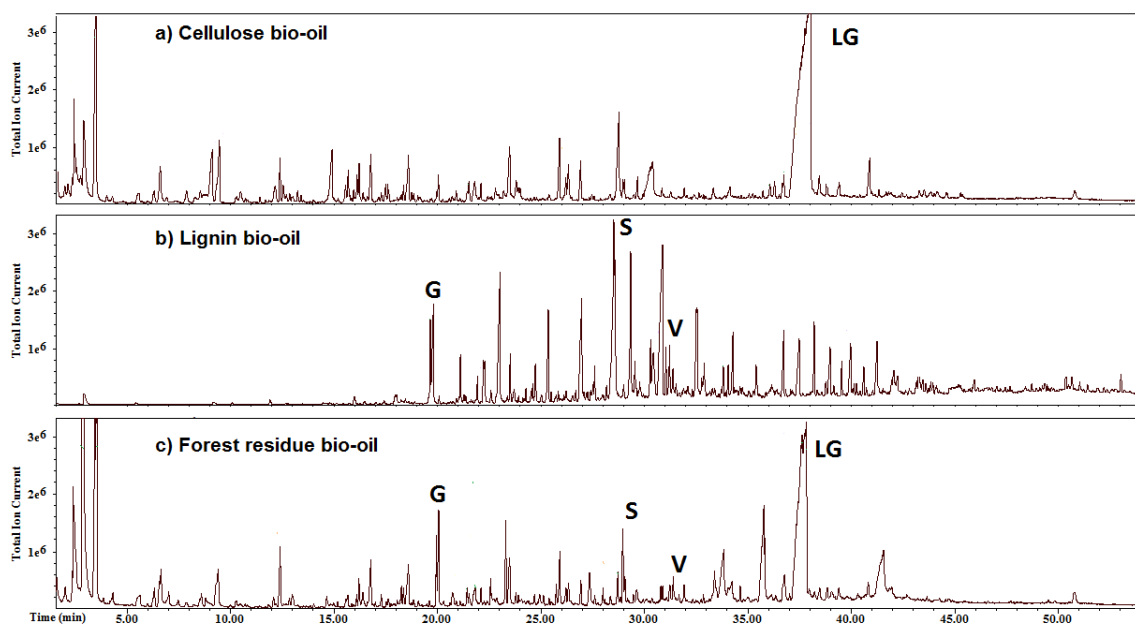


Figure 3.1. GC/MS TIC of bio-oils from a) cellulose, b) lignin and c) forest residue. [LG: levoglucosan, G: guaiacol, S: syringol, and V: vanillin].

### 3.3.2 ESI Ion Trap MS

This MS instrument was used to analyze bio-oils as a low mass resolution mass analyzer compared with high mass resolution mass analyzers (2, 3, 7, 9, 12-15). MS experiments were run in both polarity modes, with and without dopants. When tandem MS experiments were performed, conditions were first optimized using model compounds.

#### 3.3.2.1 Model Compounds

##### *Without Dopant*

The model compounds were analyzed under ESI conditions in both negative and positive ion modes (detailed spectral data are given in *Supporting Information* (Appendix), Tables S3.3 and S3.4). Results clearly show that the sodiated adducts were dominant ions. The carbohydrate compounds all showed strong sodiated adduct signals, that is, 70–80% of total ions. This is possible due to trace amounts of  $\text{Na}^+$  ions present in the solvent. It has



been shown that HPLC grade solvents have significant amounts of  $\text{Na}^+$  (14). The model compound “Cbio” showed significant fragment ions with the loss of water  $[\text{M}-\text{H}_2\text{O}+\text{H}]^+$ . The lignin model compounds formed sodiated adducts (100%-base peak) along with protonated ions (5–20%; from the base peak). In negative ion mode, all model compounds formed deprotonated ions (80% LG, 100% Glu, 95% Cbio, 100% G, 70% S, and 100% V). LG, Glu, and S formed small amounts of deprotonated dimers, while Cbio resulted in some fragmentation. In contrast with positive ion mode results, the deprotonated ions are less intense making subsequent tandem MS more difficult. In general, most model compounds in negative ion mode gave molecular ions with little fragmentation, which makes this approach suitable for M.wt analysis of bio-oil components.

#### *With Dopants*

The model compounds were analyzed by ESI with small amounts of dopants including formic acid,  $\text{NH}_4\text{Cl}$ , and  $\text{NaCl}$  in positive ion mode and  $\text{NaOH}$ , and  $\text{NH}_4\text{Cl}$  in negative ion mode (more detailed spectra in *Supporting Information* (Appendix), Tables S3.3 and S3.4). The final concentrations of the dopants were 0.1 mg/mL formic acid, 0.5 mg/mL  $\text{NH}_4\text{Cl}$ , 0.5 mg/mL  $\text{NaCl}$ , and 1 mg/mL  $\text{NaOH}$ . These dopants were used to study their effects on sensitivity and selectivity enhancement in MS analysis and to compare the results with those obtained in other studies (13, 14).

In positive ion mode ESI, formic acid was used to enhance protonated-ion formation. Unfortunately, the results were not as expected and the results were mixed. LG and Glu formed only sodiated ions with almost the same results as no dopant. Cbio did show a protonated ion; however, it fragmented easily with loss of water  $[\text{M}-\text{H}_2\text{O}+\text{H}]^+$ . Lignin compounds had mixed results, some showed strong protonated ions, while others

mainly sodiated ions. As predicted, the addition of NaCl resulted in sodiated ions with higher peak intensities for all model compounds. Thus, NaCl is good dopant for analysis of bio-oil compounds and M.wt analysis. In the case of NH<sub>4</sub>Cl addition, carbohydrates showed an ability to form strong NH<sub>4</sub><sup>+</sup>-adducts, while the lignin compounds remained as protonated or sodiated ions. There was some fragmentation observed with the carbohydrates NH<sub>4</sub><sup>+</sup>-adduct ions, but their intensities were weak. The NH<sub>4</sub><sup>+</sup>-adduct formation was evidenced by the presence of even numbered *m/z* due to the addition of 18 Da. Also, tandem MS<sup>2</sup> results show -17 Da loss (NH<sub>3</sub>) leaving protonated ions [M+H]<sup>+</sup>, as illustrated in Figure 3.2 for carbohydrates model compounds.

In negative ion mode ESI, the NaOH-doped model compounds readily formed deprotonated ions. However, Cbio underwent fragmentation with the loss of water. Also LG and Glu formed deprotonated dimers. According to Hauptert et al. (14), the NaOH dopant is beneficial for the analysis of lignin-derived products. Finally, in the case of the NH<sub>4</sub>Cl dopant, carbohydrate compounds readily formed Cl<sup>-</sup>-adducts with strong peak intensities. The Cl<sup>-</sup>-adducts can be easily confirmed by chlorine's isotopic pattern and by MS<sup>2</sup>. The results for carbohydrate analysis were the same as those of Vinueza et al. (13). The usefulness of tandem MS in carbohydrate analysis can be illustrated by the MS<sup>2</sup> spectra of the carbohydrate Cl<sup>-</sup>-adducts shown in Figure 3.2 with the loss of HCl.

Tandem MS studies of different adduct ions of model compounds is important when analyzing complex bio-oil samples that contain many uncharacterized carbohydrate and lignin analytes. Additional MS<sup>2</sup> results for sodiated and deprotonated ions of model compounds are given in Table S3.5 in *Supporting Information* (Appendix). Results showed

that the lignin model compounds fragmented by losing methyl groups, while carbohydrates fragmented with losses of water ( $-\text{H}_2\text{O}$ ) and formaldehyde ( $-\text{CH}_2\text{O}$ ).

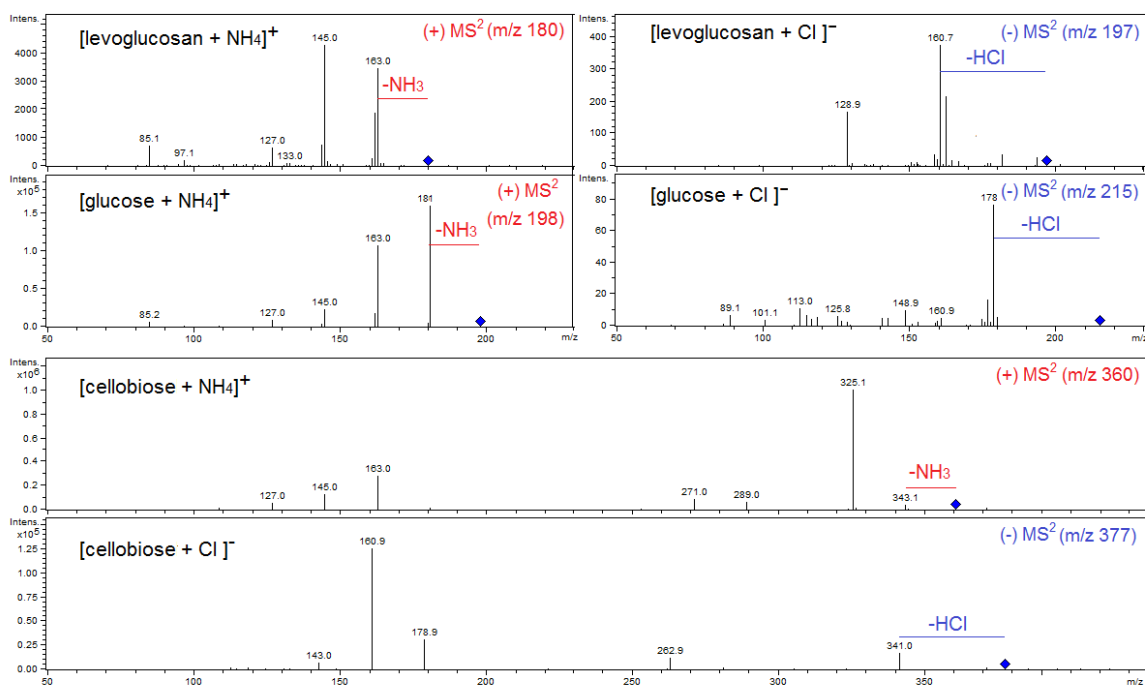


Figure 3.2. Product ion spectra from the  $\text{MS}^2$  analysis for  $\text{NH}_4^+$  and  $\text{Cl}^-$  adducts of model carbohydrates.

### 3.3.2.2 Bio-oil Samples

Bio-oil is a complex mixture containing a very large number of polar compounds with a wide range of M.wt. The use of positive and negative ion modes in ESI-MS was attempted along with different dopants (based on the results of the model compounds) in order to enhance the sensitivity and selectivity of analysis. The mass resolution in the Ion Trap MS is not sufficient to resolve all compounds in a bio-oil mixture. However, all mass peaks obtained by ESI-MS without a N-containing dopant, are single charged with mass intervals of 2 Da as described in the literature (2, 3, 7, 9, 11-14). Low M.wt compounds (<500 Da) dominate in bio-oils. Optimized ESI conditions for bio-oil analysis required

solutions to be at low concentrations ( $0.1 \text{ mg mL}^{-1}$ ) to obtain good peak intensity with low background.

### *Without Dopant*

The ESI-MS ion spectra in negative and positive ion modes of three bio-oils (cellulose, lignin, and forest residue) are shown in Figures 3.3 and 3.4. The mass spectrum for forest residue showed at least 400 significant peaks related to pyrolysis-derived compounds. The high mass ion distribution was noted to be lower in positive ion mode than in negative ion mode for all bio-oils, the most abundant ions being observed in the  $m/z$  150–400 region. A number of significant ions were investigated using tandem MS experiments (Tables S3.6–S3.11 in *Supporting Information-Appendix*). A selected number of the  $\text{MS}^2$  results are further discussed below.

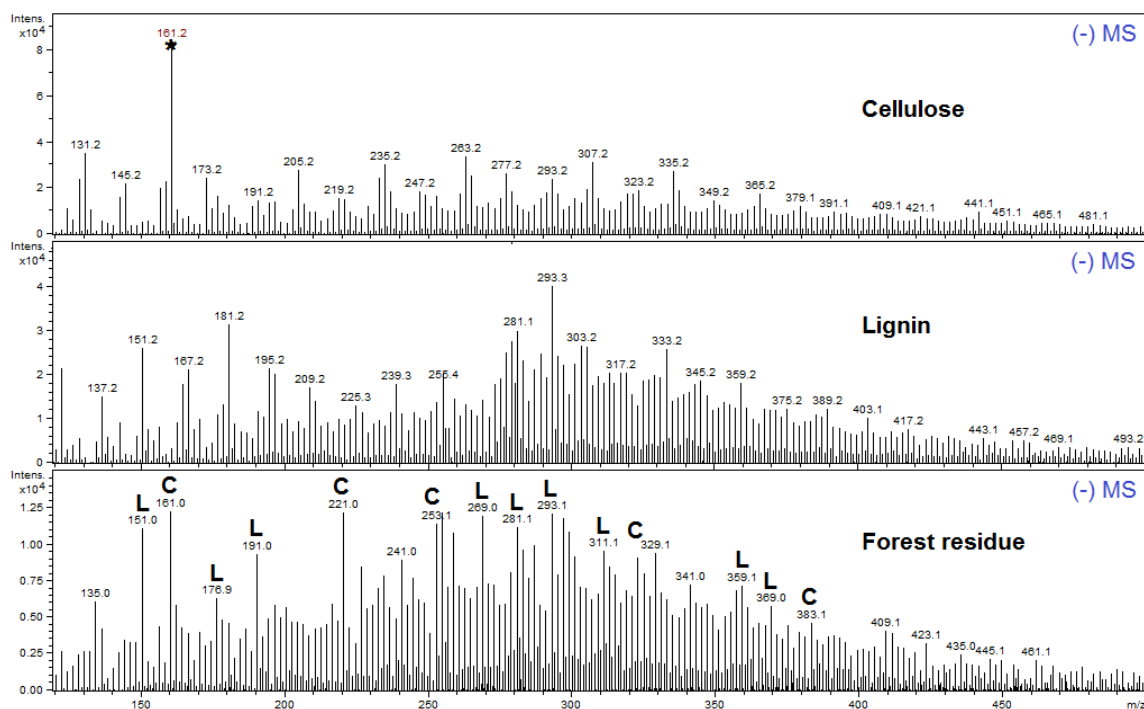


Figure 3.3. Negative ion ESI-Ion Trap mass spectra of bio-oils. \*= deprotonated LG; C= carbohydrate-derived; L= lignin-derived.

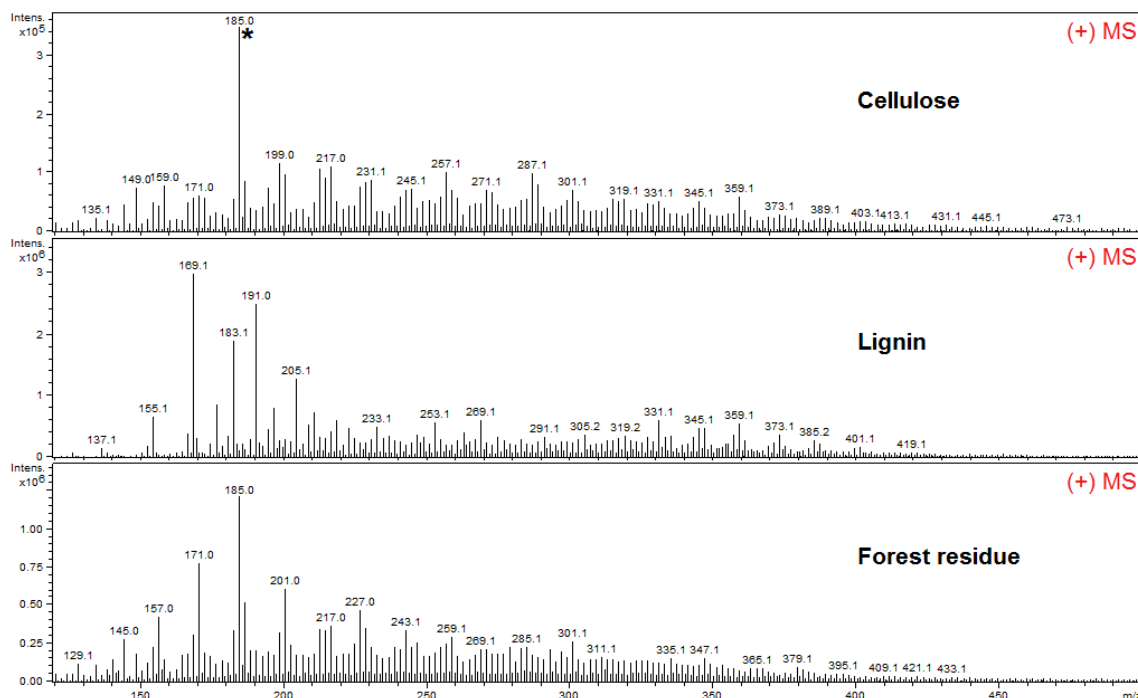


Figure 3.4. Positive ion ESI-Ion Trap mass spectra of different bio-oils. \* = sodiated LG.

The cellulose bio-oil spectrum (Figure 3.3) is made up of deprotonated ions ( $[M-H]^-$ ) in negative ion mode. The presence of LG ( $m/z$  161), a major pyrolysis product of cellulose, in bio-oils, was confirmed by GC-MS (Figure 3.1). There is also evidence for the presence of small amounts of cellobiosan ( $m/z$  323), another cellulose pyrolysis product and a dimer of Glu and LG.(12) Other deprotonated ions including  $m/z$  173, 205, 219, 235, 247, 263, 277, 293, 335, 349, and 365 were observed. All of these compounds corresponding peaks in the positive ion mode ESI MS spectra (Figure 3.4) can be accounted for as sodiated carbohydrate ions. These spectra also shows significant abundance of protonated species such as LG ( $[M+H]^+$ , 163  $m/z$ ). In general, the ion intensities were greater in positive ion mode with low background. LG ( $[M+Na]^+$ , 185  $m/z$ ) was the dominant peak in positive ion spectra, in addition to other significant-carbohydrate ions

(maxima peaks), as shown in Figure 3.4. The product ion spectra from MS<sup>2</sup> experiments for all significant ions including LG and cellobiosan, showed carbohydrate-related fragments by the neutral loss of water (-H<sub>2</sub>O) and formaldehyde (-CH<sub>2</sub>O), as observed with the model carbohydrate compound's spectra (Table S3.6 and S3.7 in *Supporting Information- Appendix*). These fragmentations can also be seen in Figure 3.5, the MS<sup>2</sup> of parent ions *m/z* 161 and 323 in negative ion mode and *m/z* 185 in positive ion mode. The spectra show clear evidence that *m/z* 161 and *m/z* 185 observed in cellulose and forest residue bio-oils were LG based on their similarity with the MS<sup>2</sup> spectra of LG standard. The evidence that *m/z* 323 (negative ion mode spectra) of forest residue bio-oil is cellobiosan is supported by MS<sup>2</sup> data (Figure 3.5 h). Finally, there were no significant ions related to the presence of glucose in any of the bio-oils.

Alcell lignin bio-oil is composed mainly of lignin pyrolysis products from hardwood. Its negative ion mode ESI Ion Trap MS spectrum revealed many deprotonated ions ([M-H]<sup>-</sup>) (Figure 3.3). As expected from results of model lignin compounds, its mass spectra (positive mode) showed ions that were mostly all sodiated. For lignin bio-oil, there were two distinct ion regions in its MS spectrum in both polarity modes; one low M.wt (*m/z* 100–250) representing monomers with another region representing dimers and some trimers (*m/z* 250–450). Many ion maxima were separated by 14 or 2 Da representing CH<sub>2</sub>-mass differences and saturation/unsaturation of the lignin bio-oil components, respectively.

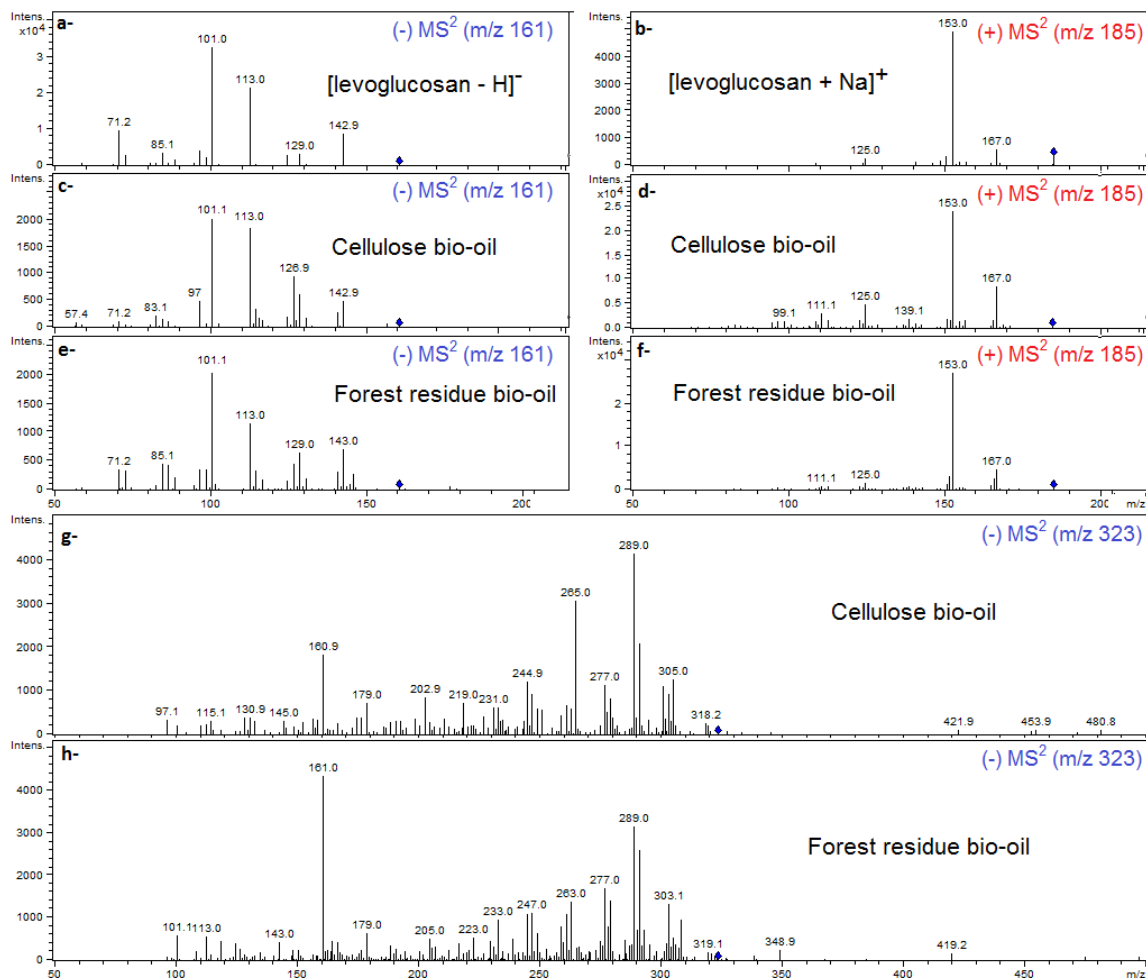


Figure 3.5. Product ion spectra from MS<sup>2</sup> experiments for LG standard in negative ion (a) and positive ion (b); for cellulose's  $m/z$  161 in negative ion (c) and for  $m/z$  185 in positive ion (d) forest residue's  $m/z$  161 in negative ion (e) and  $m/z$  185 positive ion (f) and for cellulose (g) and forest residue bio-oil's (h)  $m/z$  323 in negative ion.

MS<sup>2</sup> experiments have also been used extensively for the structural analysis of major lignin pyrolysis products (Table S3.8 and S3.9 in *Supporting Information-Appendix*). It was observed that most product ion spectra (negative ion) showed fragmentation patterns related to methoxy-substituted phenolic compounds. Fragmentations include the loss of -CH<sub>3</sub> and -H<sub>2</sub>O, in addition to other neutral losses such as monoxide (-CO), carbon dioxide (-CO<sub>2</sub>), formaldehyde (-CH<sub>2</sub>O), and methanol

( $-\text{CH}_3\text{OH}$ ) as shown in the  $\text{MS}^2$  spectra for the negatively charged ions  $m/z$  151 and  $m/z$  317 in Figure 3.6. A major ion in both lignin and forest residue bio-oils was  $m/z$  151 which underwent fragmentation to lose a neutral methyl radical indicating a methoxy group bound to an aromatic ring. Loss of CO suggested that the product is vanillin, which was further confirmed by the  $\text{MS}^2$  analysis of vanillin standard and by literature data (17). Similarly, the parent ion spectra of  $m/z$  317 showed loss of  $\text{CH}_3$  radical, as well as ions formed from the loss of  $\text{H}_2$ -radicals. Further  $\text{MS}^3$  experiments on the lower masses  $m/z$  163 and 191 fragmentations of  $m/z$  317 were done. Both showed a loss of  $\text{CH}_3$  as illustrated in Figure 3.6 d and e. These simple examples illustrate the usefulness of  $\text{MS}^n$  to characterize the structure of lignin pyrolysis products.

Further investigation of ESI-MS spectra of forest residue bio-oil gave the following results. In negative ion mode spectra (Figure 3.3), the major ion was  $m/z$  161 the LG product based on  $\text{MS}^2$  experiments. Based on results of ESI-MS of cellulose and lignin bio-oils in negative ion mode, and selected  $\text{MS}^2$  experiments, the following ions can be tentatively assigned as carbohydrate-derived, that is,  $m/z$  221, 253, 323, and 383. As well, ions  $m/z$  151 (vanillin), 177, 191, 269, 281, 293, 311, 241, 359, and 369 were tentatively assigned as lignin-derived products (Table S3.10 and S3.11 in *Supporting Information- Appendix*).

Based on the results obtained by  $\text{MS}^2$  analysis, the negative ion mode provided more interpretable results allowing the distinction between carbohydrate and lignin components. However, some of the resulting  $\text{MS}^2$  spectra were complicated due to the low resolving power of the Ion Trap MS.



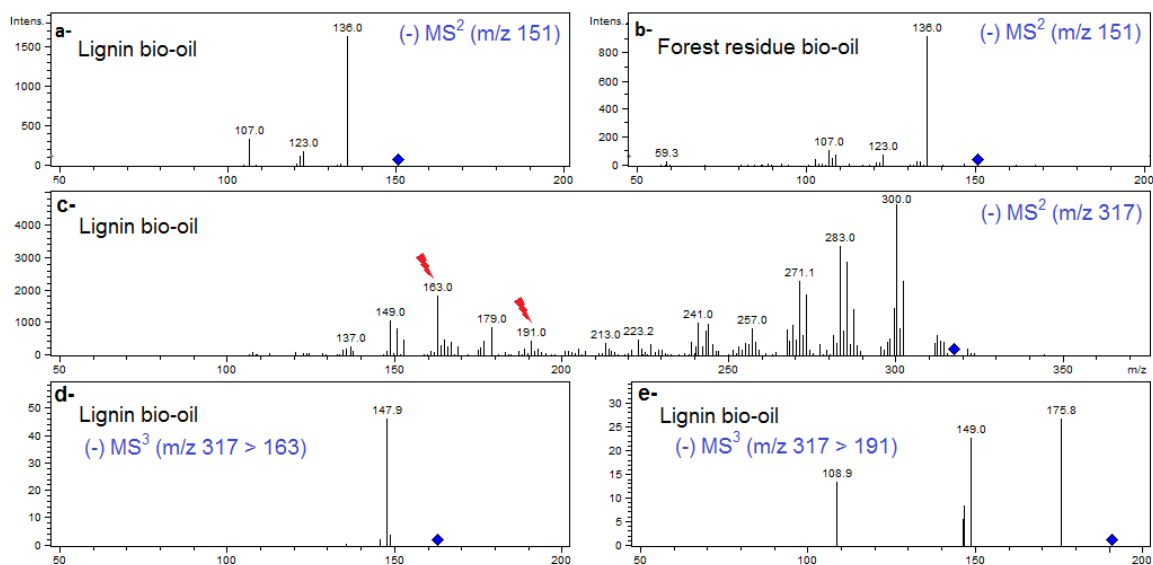


Figure 3.6. Product ion spectra from negative ion MS<sup>n</sup> experiments. MS<sup>2</sup> of *m/z* 151 from (a) lignin bio-oil and (b) forest residue bio-oil and (c) *m/z* 317 and MS<sup>3</sup> of *m/z* 163 (d) and *m/z* 191 (e) from lignin bio-oil's parent ion *m/z* 317.

### *With Dopants*

In order to enhance the ionization selectivity between lignin and cellulose pyrolysis products and increase ionization efficiency by ESI-MS, the dopants that showed promise with model compounds (section 3.2.1) were used. NaOH dopant showed little enhancement in negative ion mode. Other dopants did not significantly improve the ESI-MS spectra of lignin bio-oil. As no NH<sub>4</sub><sup>+</sup>- or Cl<sup>-</sup>-adducts were observed with lignin's phenolic products, the use of NH<sub>4</sub>Cl dopant for selectively ionizing carbohydrate products was investigated.

NaCl-doped samples provided improved positive ion mode mass spectra with much higher ion intensities for the bio-oils (Figure 3.7 and 3.8) when compared to nondoped oils (Figure 3.4), except for the lignin bio-oil sample (it is possible there is a high Na-content in this bio-oil). More promising results were obtained from the use of NH<sub>4</sub>Cl dopant. As was found with model compounds, NH<sub>4</sub><sup>+</sup> can readily form adducts with cellulose products

but not with lignin products. Many ions in the cellulose and forest residue oils spectra were detected as  $\text{NH}_4^+$ -adducts. This can be distinguished by their even numbered  $m/z$  as marked in the spectra as AM in Figures 3.7 and 3.8. The proof for the presence of this adduct was shown by loss of ammonia (17 Da) by  $\text{MS}^2$  analysis (Figure 3.9 a and b) such as for LG  $[\text{M}+\text{NH}_4]^+$  at  $m/z$  180. Unfortunately, the  $\text{Na}^+$  and protonated adducts were comparatively intense along with the  $\text{NH}_4^+$ -adducts. However, better results were obtained for chloride adducts using  $\text{NH}_4\text{Cl}$  addition. As shown in Figures 3.7 and 3.8, lines are used to connect the deprotonated ions with their corresponding  $\text{Cl}^-$ -adducts present in cellulose and forest residue bio-oils. The mass difference between them is the chloride ion. Hence LG and cellobiosan were detected in cellulose and forest residue bio-oil as  $\text{Cl}^-$ -adducts at  $m/z$  197 and 359, respectively. The  $\text{Cl}^-$ -adduct of  $m/z$  359 was confirmed by the loss of  $\text{HCl}$  (36 Da) under  $\text{MS}^2$ , as shown in Figure 3.9e and f. Other  $\text{Cl}^-$ -adduct ions were investigated by  $\text{MS}^2$ , and it can be tentatively suggested that some of the larger carbohydrate products are linked to a levoglucosan moiety.

Based on  $\text{ESI-MS}^n$  data, the  $\text{NH}_4\text{Cl}$  dopant can be used to identify the carbohydrate components in bio-oil samples by their  $\text{Cl}^-$ -adducts readily identified by the  $\text{Cl}$ -isotope pattern and peak intensity enhancement in negative ion mode. In positive ion mode, the even number  $m/z$  signature of  $\text{NH}_4^+$ -adducts also plays a role in assigning carbohydrate compounds in bio-oil MS spectra.

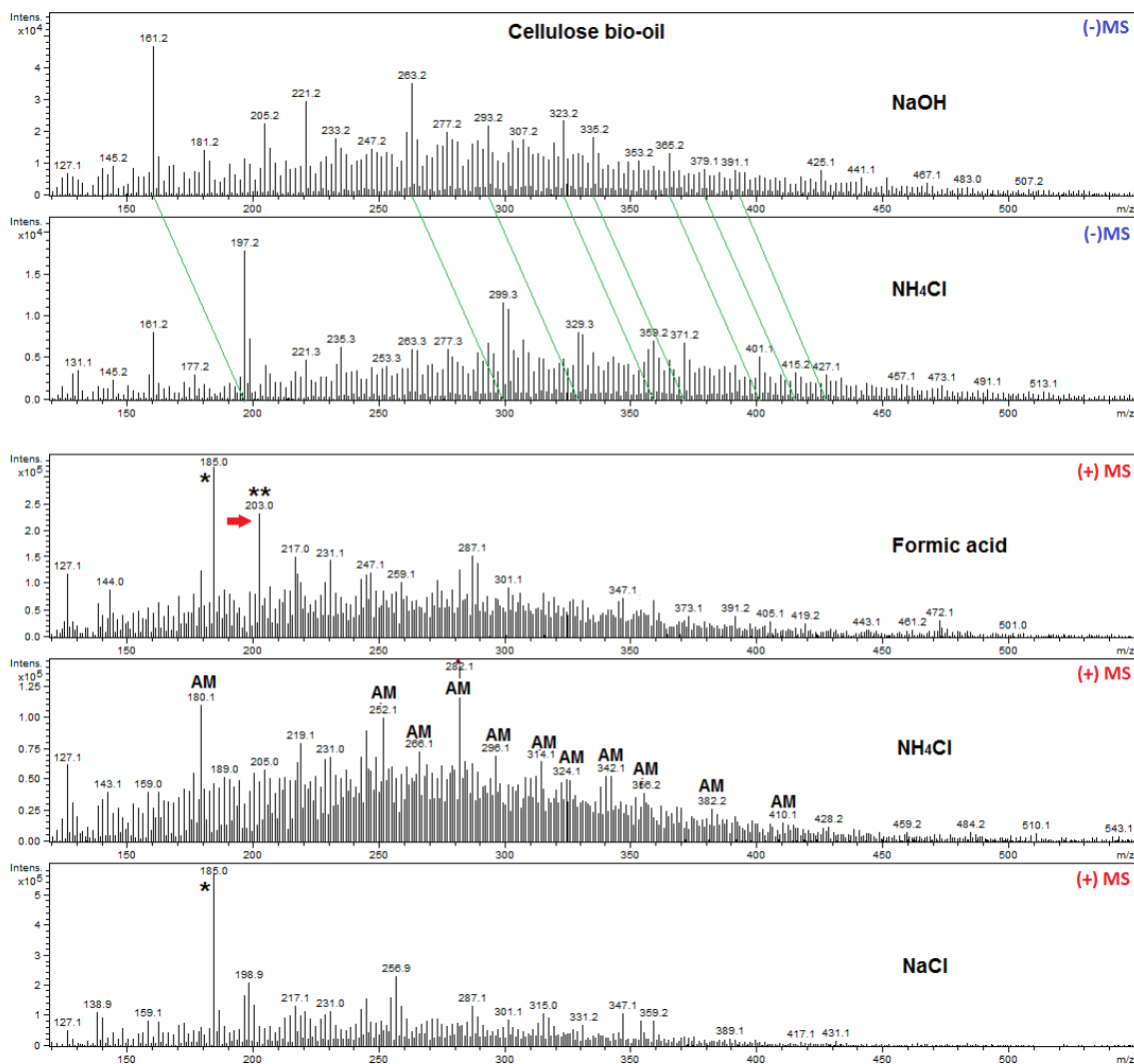


Figure 3.7. Negative and positive ion ESI mass spectra of the various doped cellulose bio-oil samples. \* = sodiated levoglucosan  $m/z$  185; \*\* = sodiated  $m/z$  203 (glucose); AM = ammoniated carbohydrate products.

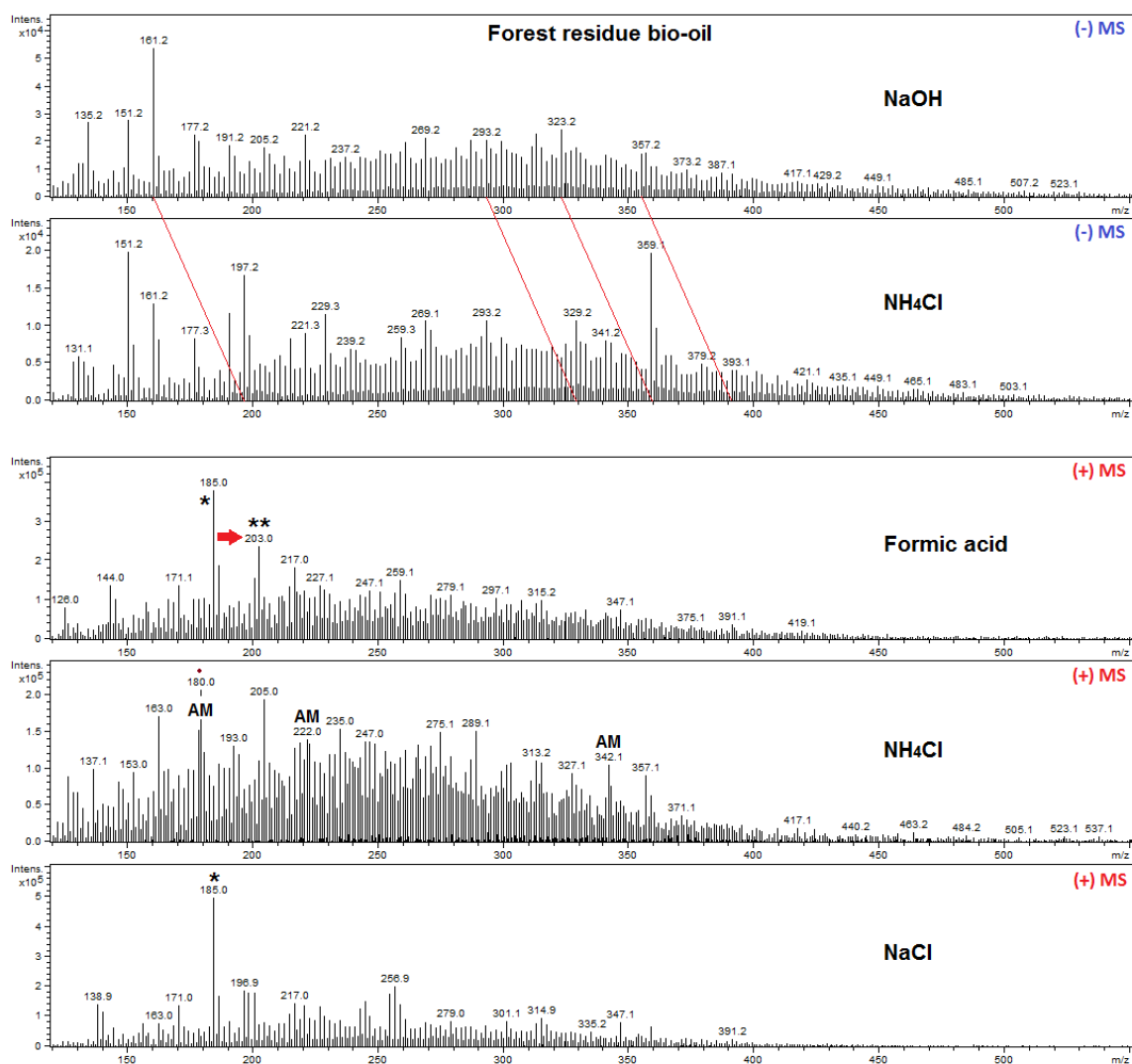


Figure 3.8. Negative and positive ion ESI MS spectra of various doped forest residue bio-oil samples. \* = sodiated levoglucosan  $m/z$  185; \*\* = sodiated  $m/z$  203 (glucose); AM = ammoniated carbohydrate products.

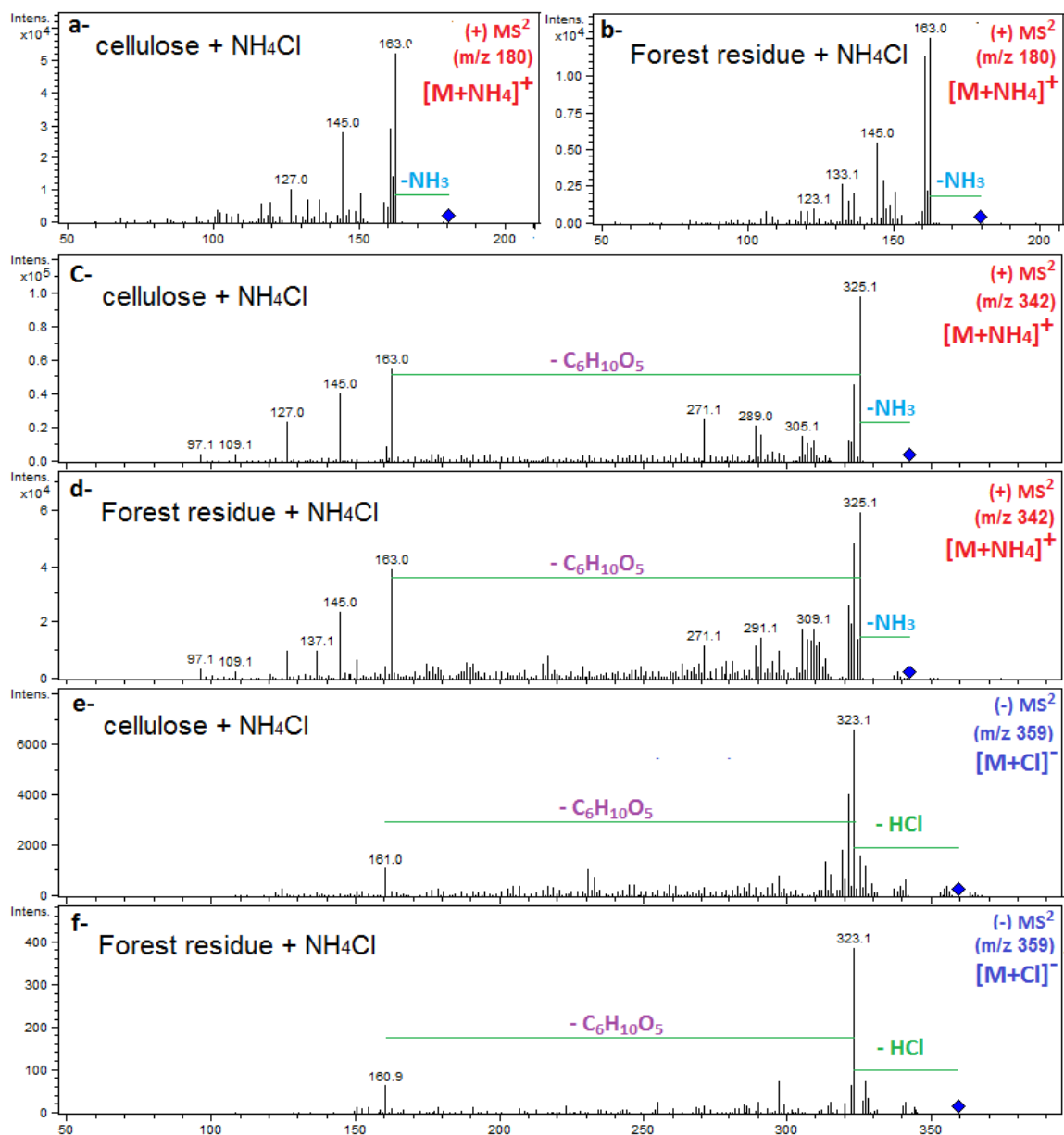


Figure 3.9. Product ion spectra from MS<sup>2</sup> experiments obtained for NH<sub>4</sub>Cl-doped bio-oils for m/z 180 present in positive ion spectra of (a) cellulose bio-oil, and (b) forest residue oil; m/z 342 in positive ion mode spectra of (c) cellulose bio-oil, and (d) forest residue oil; m/z 359 in negative ion mode spectra of (e) cellulose bio-oil, and (f) forest residue bio-oil.

### 3.3.2.3 Bio-oil fractionation

Bio-oil fractionation (hydrophilic and hydrophobic fractions) was used to simplify the ESI-mass spectra of the forest residue bio-oil sample. One method used solid phase extraction C-18 (SPE), a simple and efficient extraction/separation method using a reverse phase C-18 resin-packed column (18). After the bio-oil was loaded the hydrophilic fraction (chiefly water-soluble carbohydrates) was eluted with water (SPE-water) followed by MeOH (SPE-methanol), which elutes lignin products. The second fractionation method was lignin precipitation, a commonly used method to subdivide bio-oil into water-soluble (low M.wt products and water-soluble carbohydrates) and water-insoluble (mainly pyrolytic lignin, particularly higher M.wt oligomers of partially depolymerized lignin) components (2, 6, 19, 20).

The ESI MS spectra are given for all four fractions (SPE and lignin precipitation) under negative (Figure 3.10) and positive (Figure 3.11) ion modes. Comparison of the spectra of SPE and lignin precipitation fractions, i.e, the two hydrophilic and two hydrophobic, are similar in their ion masses observed. SPE-water fraction (water-soluble fraction) is known to contain compounds including acids, alcohols, aldehydes, ketones, and sugars.(20) These compounds are mainly derived from decomposition of cellulose and hemicellulose. Both positive and negative ion mode spectra of this water-soluble fraction showed strong signals for LG and cellobiosan. A significant outcome of bio-oil fractionation was the observation of a higher oligosaccharide at  $m/z$  485, possibly cellotriosan. MS<sup>2</sup> experiments confirmed their presence in the bio-oil based on characteristic fragmentation pattern of carbohydrates, as discussed previously. Further confirmation was made by using the NH<sub>4</sub>Cl dopant and the clear observations of strong Cl<sup>-</sup>

-adducts with these anhydrosugars targets were detected. These results were further confirmed when the SPE-water fraction was analyzed in positive ion mode, and the resulting spectra showed even mass  $m/z$  appearing at LG  $m/z$  180 and cellobiosan  $m/z$  342. Among the two fractionation methods, SPE provides a simple and effective way to obtain good ESI-MS spectra of the carbohydrate-derived products.

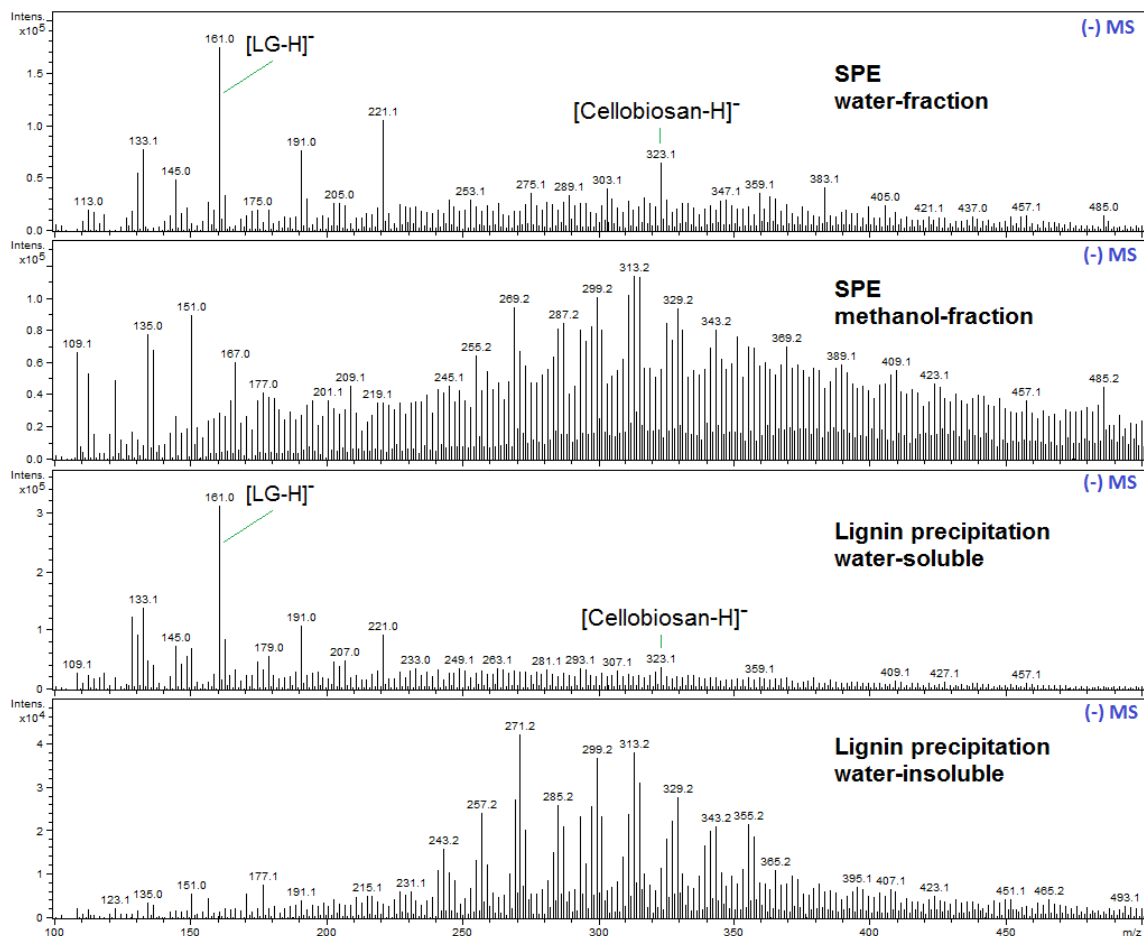


Figure 3.10. Negative ion ESI-mass spectra of forest residue bio-oil fractions using SPE and lignin precipitation techniques.

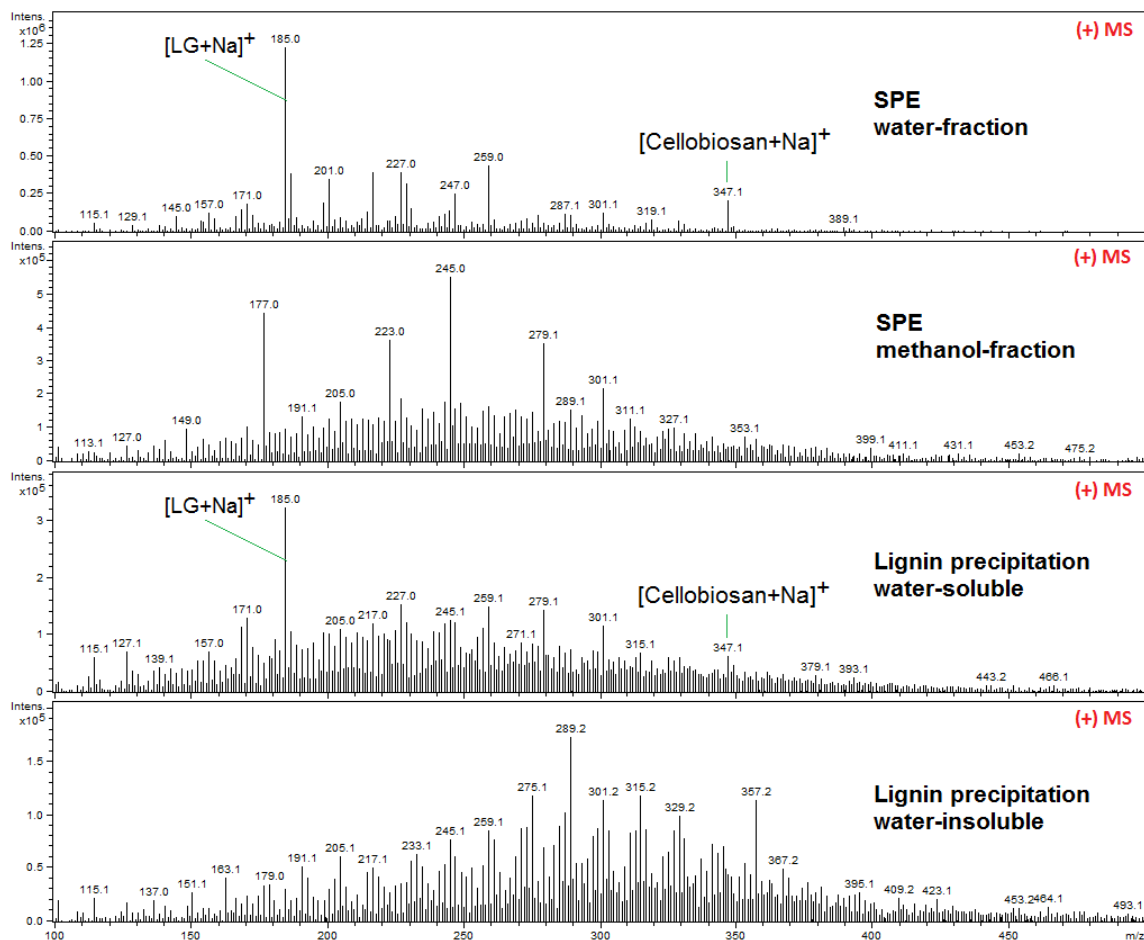


Figure 3.11. Positive ion ESI- mass spectra of forest residue bio-oil fractions using SPE and lignin precipitation techniques.

In contrast, the mass spectra (nondoped) of SPE-methanol and lignin precipitated (water-insoluble) fractions showed no or little carbohydrate-related ions. As expected, the negative ion mode spectra revealed mostly deprotonated ions ( $[M-H]^-$ ), while in positive ion mode ions were sodiated ( $[M+Na]^+$ ). The ion abundance was highest (positive ion mode) for  $m/z$  250–350, representing the dimer region of lignin products. As in all other mass spectra containing lignin products, the major ions are separated by 14 and 2 Da. The product ion spectra results of  $MS^n$  experiments for major ions showed fragment patterns related to methoxy phenolic compounds similar to that discussed previously. In summary,



fractionation of bio-oil by the lignin precipitation helps to simplify the spectra of lignin-derived products and also to allow the researcher to perform MS<sup>n</sup> experiments with an Ion Trap MS.

### **3.4. Conclusion**

ESI-Ion Trap MS and ESI-Ion Trap MS<sup>2</sup> have been successful in analyzing bio-oil components and in distinguishing between carbohydrate and lignin-derived products. Doped bio-oil samples with NH<sub>4</sub>Cl, NaCl, and NaOH results in higher sensitivity with higher peak intensity obtained in positive ion compared to negative ion mode. Negative ion mode provides more interpretable ESI MS<sup>n</sup> results for analysis of bio-oil samples. NaOH-doped samples showed more intense peaks for deprotonated ions, especially for lignin products. Promising results were obtained from NH<sub>4</sub>Cl-doped samples, as it was found that carbohydrate products readily formed ammonium adducts in positive ion mode and chloride adducts in negative ion mode, while no ammonium or chloride adduct formation was observed for lignin-derived products. Fractionation of bio-oil was successfully applied to provide fractions giving less complex spectra leading to more useful MS<sup>2</sup> analysis. SPE provided the best results for the water fraction (carbohydrate), while the lignin fraction is best obtained from the lignin precipitation method. This study provides a basis for other studies to expand on the analysis of bio-oil by ESI-MS using low resolution MS with different modes and dopants or with higher resolving power instruments, such as FT-ICR MS.

### 3.5. References

1. Xu, F.; Xu, Y.; Yin, H.; Zhu, X.; Guo, Q. Analysis of Bio-oil Obtained by Biomass Fast Pyrolysis Using Low-Energy Electron-Impact Mass Spectrometry. *Energy Fuels* **2009**, *23*, 1775-1777.
2. Liu, Y.; Shi, Q.; Zhang, Y.; He, Y.; Chung, K. H.; Zhao, S.; Xu, C. Characterization of Red Pine Pyrolysis Bio-oil by Gas Chromatography-Mass Spectrometry and Negative-Ion Electrospray Ionization Fourier Transform Ion Cyclotron Resonance Mass Spectrometry. *Energy Fuels* **2012**, *26*, 4532-4539.
3. Jarvis, J. M.; McKenna, A. M.; Hilten, R. N.; Das, K. C.; Rodgers, R. P.; Marshall, A. G. Characterization of Pine Pellet and Peanut Hull Pyrolysis Bio-oils by Negative-Ion Electrospray Ionization Fourier Transform Ion Cyclotron Resonance Mass Spectrometry. *Energy Fuels* **2012**, *26*, 3810-3815.
4. Moraes, M. S. A.; Georges, F.; Almeida, S. R.; Damasceno, F. C.; MacIel, G. P. D. S.; Zini, C. A.; Jacques, R. A.; Caramão, E. B. Analysis of products from pyrolysis of Brazilian sugar cane straw. *Fuel Process Technol* **2012**, *101*, 35-43.
5. Smith, E. A.; Lee, Y. J. Petroleomic Analysis of Bio-oils from the Fast Pyrolysis of Biomass: Laser Desorption Ionization-Linear Ion Trap-Orbitrap Mass Spectrometry Approach. *Energy Fuels* **2010**, *24*, 5190-5198.
6. Bayerbach, R.; Nguyen, V. D.; Schurr, U.; Meier, D. Characterization of the water-insoluble fraction from fast pyrolysis liquids (pyrolytic lignin). Part III. Molar mass characteristics by SEC, MALDI-TOF-MS, LDI-TOF-MS, and Py-FIMS. *J. Anal. Appl. Pyrolysis* **2006**, *77*, 95-101.
7. Cole, D. P.; Smith, E. A.; Lee, Y. J. High-Resolution Mass Spectrometric Characterization of Molecules on Biochar from Pyrolysis and Gasification of Switchgrass. *Energy Fuels* **2012**, *26*, 3803-3809.
8. Hassan, E. M.; Yu, F.; Ingram, L.; Steele, P. The potential use of whole-tree biomass for bio-oil fuels. *Energy Sources, Part A* **2009**, *31*, 1829-1839.
9. Das, D. D.; Schnitzer, M. I.; Monreal, C. M.; Mayer, P. Chemical composition of acid-base fractions separated from biooil derived by fast pyrolysis of chicken manure. *Bioresour. Technol.* **2009**, *100*, 6524-6532.
10. Schnitzer, M. I.; Monreal, C. M.; Jandl, G. The conversion of chicken manure to bio-oil by fast pyrolysis. III. Analyses of chicken manure, bio-oils and char by Py-FIMS and Py-FDMS. *J. Environ. Sci. Health, Part B* **2008**, *43*, 81-95.
11. Kazi, Z. H.; Schnitzer, M. I.; Monreal, C. M.; Mayer, P. Separation and identification of heterocyclic nitrogen compounds in biooil derived by fast pyrolysis of chicken manure. *J. Environ. Sci. Health, Part B* **2011**, *46*, 51-61.
12. Smith, E. A.; Park, S.; Klein, A. T.; Lee, Y. J. Bio-oil Analysis Using Negative Electrospray Ionization: Comparative Study of High-Resolution Mass Spectrometers and Phenolic versus Sugaric Components. *Energy Fuels* **2012**, *26*, 3796-3802.
13. Vinueza, N. R.; Gallardo, V. A.; Klimek, J. F.; Carpita, N. C.; Kenttämaa, H. I. Analysis of carbohydrates by atmospheric pressure chloride anion attachment tandem mass spectrometry. *Fuel* **2013**, *105*, 235-246.
14. Hauptert, L. J.; Owen, B. C.; Marcum, C. L.; Jarrell, T. M.; Pulliam, C. J.; Amundson, L. M.; Narra, P.; Aqueel, M. S.; Parsell, T. H.; Abu-Omar, M. M.; Kenttämaa, H. I.

- Characterization of model compounds of processed lignin and the lignome by using atmospheric pressure ionization tandem mass spectrometry. *Fuel* **2012**, *95*, 634-641.
15. Gellerstedt, G.; Li, J.; Eide, I.; Kleinert, M.; Barth, T. Chemical Structures Present in Biofuel Obtained from Lignin. *Energy Fuels* **2008**, *22*, 4240-4244.
  16. Alsbou, E.; Helleur, R. Whole sample analysis of bio-oils and thermal cracking fractions by Py-GC/MS and TLC-FID. *J. Anal. Appl. Pyrolysis* **2013**, *101*, 222-231.
  17. Owen, B. C.; Hauptert, L. J.; Jarrell, T. M.; Marcum, C. L.; Parsell, T. H.; Abu-Omar, M. M.; Bozell, J. J.; Black, S. K.; Kenttamaa, H. I. High-Performance Liquid Chromatography/High-Resolution Multiple Stage Tandem Mass Spectrometry Using Negative-Ion-Mode Hydroxide-Doped Electrospray Ionization for the Characterization of Lignin Degradation Products. *Anal. Chem. (Washington, DC, U. S. )* **2012**, *84*, 6000-6007.
  18. Kanaujia, P. K.; Sharma, Y. K.; Agrawal, U. C.; Garg, M. O. Analytical approaches to characterizing pyrolysis oil from biomass. *TrAC, Trends Anal. Chem.* **2013**, *42*, 125-136.
  19. Oasmaa, A.; Kuoppala, E.; Solantausta, Y. Fast Pyrolysis of Forestry Residue. 2. Physicochemical Composition of Product Liquid. *Energy Fuels* **2003**, *17*, 433-443.
  20. Mullen, C. A.; Boateng, A. A. Chemical Composition of Bio-oils Produced by Fast Pyrolysis of Two Energy Crops. *Energy Fuels* **2008**, *22*, 2104-2109.

## Chapter 4

### Accelerated Aging of Bio-oil from Fast Pyrolysis of Hardwood<sup>3</sup>

---

<sup>3</sup> This chapter has been published; Alsbou, E.; Helleur, B. Accelerated Aging of Bio-oil from Fast Pyrolysis of Hardwood. *Energy Fuels*, **2014**, 28, 3224–3235.

## Summary

Bio-oil is chemically and thermally unstable during storage and transportation. For that reason, it is necessary to evaluate the changes in properties (chemical and physical) of bio-oil during storage to understand its chemical instability, which will further assist researchers in stabilization strategies. This chapter describes the evaluation of an accelerated aging process on the physical and chemical properties of bio-oil from fast pyrolysis of ash and birch woods using two different pyrolyzers, a pilot-scale (auger) and lab-scale (tube furnace), respectively. The produced oils (freshly made) were aged at 80 °C over different periods (1, 3, and 7-days) in sealed, nitrogen-purged Nalgene vessels. Fresh oil was analyzed alongside aged-oils. Fresh oil was analyzed alongside aged oils. Bio-oils were characterized by viscometer, Karl Fischer titration (H<sub>2</sub>O), pyrolysis–gas chromatography/mass spectrometry (GC/MS), thermogravimetric analysis (TGA), photo-microscopy, <sup>13</sup>C nuclear magnetic resonance (NMR), and Fourier transform infrared spectroscopy (FTIR). The water content, viscosity, decomposition temperature (TGA), and ash content levels in bio-oil samples all increased as the aging period lengthened. GC/MS analysis showed a major reduction in GC-analyzable components (indicating an overall decrease in volatility). The mass of residue remaining after pyrolysis-GC/MS increased and the structures of pyrolysis products of this non-volatile residue along with NMR and FTIR data suggests the following aging processes; some of the reactive compounds undergo polymerization or reaction with other compounds including olefins, alcohols and aldehydes. Some possible reaction mechanisms are given. The oils remained a single phase throughout the initial study period; however, on day 7, a clear phase separation was observed by photo-microscopy.

#### 4.1. Introduction:

Bio-oil is a complex mixture of condensed-volatiles usually produced from the fast pyrolysis of biomass feedstock when a sample is rapidly heated to 400–600 °C in a non-oxidizing environment within a short residence time (< 2 s). During the pyrolysis, the biomass constituents (cellulose, hemicellulose and lignin) thermo-chemically decompose into smaller organic and carbon-based products (1-2). The main products are condensable volatiles (bio-oil), bio-char, and non-condensable gases (syngas, e.g., CO, CH<sub>4</sub>, and H<sub>2</sub>). Physically, the bio-oils are dark brown with a smoky odor, and notable high viscosity and water content (20-30%) (1-3). Chemically, the bio-oil is acidic (pH ~2-4), and composed of carbon (44-47%), oxygen (46-48%) and hydrogen (6-7%) and a small amount of nitrogen (0-0.2%), and sulfur (<0.01%) (1,3-4). As a thermochemical product of lignocellulosic material, it contains a large and complex number of highly oxygenated polar components (e.g. alcohols, aldehydes, carboxylic acids, esters, ethers, ketones, phenols, sugars) (2-3,5).

Bio-oil is a promising alternative and sustainable energy source because it can be easily transported, and can be used as a fuel in modified gas turbines and heating applications, or as a feedstock to produce chemicals, or it can be upgraded to transportation fuels (4,6-7).

However, the use of bio-oil is found to be limited because of several shortcomings. One is its chemical and thermal instability during storage. This is due to its volatility, high reactive oxygen content, high acidity, and chemical complexity (1-2,5-10). By itself, the bio-oils undergo chemical and physical changes likely because several reactions, including oxidation, condensation, and polymerization (6, 8, 10-11). Diebold (12) reported the

possibility of ten major reactions that can occur after bio-oil production and during storage. Polymerization can include reactions between species with double bonds, esterification, and etherification (1, 13). These reactions continued after bio-oil production because the reaction has not reached thermodynamic equilibrium after the rapid quenching (an important step for fast pyrolysis) of pyrolysis volatiles. The products continue to react during storage until stability (equilibrium) is reached (9-10, 12). Because of some losses of volatile components produced upon further degradation, and in-situ polymerization reaction, the bio-oil on aging achieves increased average molecular weight (M.wt), viscosity, degree of phase separation, and water content (4-6, 12-14).

The term “aging” of bio-oil has been used to describe the change in viscosity of bio-oil over time, particularly when it is heated (1, 13-14). Elevated temperatures increase the rate of the aging reactions, forming higher M.wt compounds. This can also lead to two layer phase separation. The bottom layer contains less hydrophilic components mainly derived from the pyrolytic lignin. The upper layer is a less viscous aqueous fraction (5, 7-8, 11, 14). The phase separation can occur because of increased water content (a byproduct from condensation and esterification reactions) and the partial removal of lower M.wt compounds caused by partial volatility and reactivity of the carboxylic, alcoholic or other polar functional groups (1, 13). If the temperature of the bio-oil is raised above 200 °C, gummy-like and finally char-like materials are formed by polymerization (14). It has been found that the pyrolytic-lignin is a major contributor to bio-oil instability (7, 10), because some phenolic compounds are still reactive and can polymerize to produce higher M.wt compounds. These new compounds can reach a weight of 1000 Da or more over time (1, 4, 7). The aging of bio-oil makes its handling, transport, storage, and use as a fuel difficult

(2, 5, 11). One issue is coke formation or crystallization and precipitation during distillation when bio-oil is heated (2, 13). Ash and other solids, such as small amounts of biochar in bio-oil could increase the corrosion and gumming problems in engine valves, clog the fuel system and nozzle, and block filters. In addition, the higher viscosity causes a higher pressure drop, while increased water content lowers the heating value and causes ignition delay (13). Phase separation of the oil leads to even more problems when trying to identify uses (4, 12).

Accelerated aging experiments have been investigated by storing the bio-oil at elevated temperature for a short period of time (e.g., storage at 80-90 °C for a specific length of time, typically from a few hours up to a several days) (1-12). These experiments have been developed so that the aging rate is equivalent to a particular period if the bio-oil had been stored at room temperature (10). Accordingly, accelerated aging experiments have been used as a normal method for demonstrating the aging processes and properties of bio-oil samples (1, 4, 12). Aging processes at higher temperature occur faster because of the tendency for chemical reactions to show higher reaction rates at higher temperatures (2, 10). To reduce the aging process, bio-oils can be placed in a freezer to minimize or stop the reactions and allow for comprehensive characterization (10).

Nolte and Liberatore (1) showed increases in viscosity of 57, 300 and 720 % when a bio-oil from oak was aged in a hermetically sealed concentric cylinder rheometer with shear at 90 °C for 8, 16, and 24 h, respectively. Their results were close to the results in the current study in terms of using a standard quiescent aging method. Boucher et al. (8) used different temperatures (room temperature, 40, 50 and 80 °C) to accelerate the bio-oil aging for 7.75 days. They found that the viscosity increased significantly during the first 65 days



of storage at room temperature, while when bio-oils were aged at 40, 50 and 80 °C for same period of time, the bio-oil properties were significantly changed at 80 °C compared to that at 40 or 50 °C, which were not critical. In addition, it was found the M.wt increase after storage of bio-oil at 80 °C for 1 week was equivalent to that after storage for one year at room temperature (8, 11). Trinh et al. (4), were reported that aged bio-oils by heating in an oven for 24 h at 80 °C using tightly closed containers and this accelerated process was found to be equivalent to aging of bio-oil at room temperature for approximately one year (4). “Round robin studies” were set up to study the repeatability of accelerated aging of the same bio-oil with respect to changes in viscosity over a range of temperatures of periods (14). The study revealed that increase in viscosity at room temperature for 6 months was equivalent to that of an accelerated aging test at 80 °C for 24 h. In addition, it was shown that the viscosity change for unfiltered bio-oil was higher compared to filtered bio-oil in most cases.

There are some factors that can affect the rate of aging (defined as an increase in viscosity over time), which includes high concentration of reactive species, such as aldehydes, and presence of ash, minerals, and char particles that can catalyze some of the aging reactions (2, 5-6, 8, 10, 12-13, 15, 19, 22).

Physical and chemical methods have been used to characterize bio-oils during storage or accelerated aging. The viscosity measurement (1-4, 6, 8, 10-11, 13-17, 19, 21-22) represents the most useful method to follow aging. In addition, Karl-Fischer methods (1, 3-4, 6, 8, 11, 13-14, 16-19, 21) have been used for obtaining accurate values for water content. FT-IR (3, 5-7, 14, 16-17, 21-22), and <sup>1</sup>H-NMR and <sup>13</sup>C-NMR (3, 7, 16-17, 21, 23) have been used to evaluate functional group and chemical structure changes. GC-MS

(2,6,8,10,16,18,21-22) has been used for analysis of changes of chemical composition of volatiles. GPC (1, 3-5, 7-8, 10-11, 14-15, 17, 21-22) has been used to measure the changes on average M.wt. pH (2-4, 10-14, 16-17, 22), TGA (2-3, 5, 7, 10-11, 17), and CHN elemental analysis (2, 6-7, 10, 13, 21), have all been used in prior aging studies.

The objectives of this study were to study the effect of accelerated aging of two different types of bio-oil samples: one from ash wood produced from a pilot-scale continuous auger pyrolyzer and the other from birch wood produced in a static lab-scale tube furnace. The two bio-oils are significantly different enough in chemical nature to allow for useful aging comparisons. Accelerated aging was performed by storage of freshly made bio-oils at 80 °C for 1, 3 and 7 days. Several analytical techniques were used to follow the physical and chemical changes of bio-oil aging.

## **4.2. Methods and Materials**

### **4.2.1. Materials**

Birch wood samples were ground to 2 mm by a cutting mill (Pulverisette 15, Fritsch GmbH, Oberstein, Germany), and ash wood was obtained as sawdust produced from a furniture factory. The moisture content was 3.4 and 5.0%, while the ash content was 0.58 and 0.53%, for the ash and birch wood feedstocks, respectively. The NMR solvent (methanol-d<sub>4</sub>, 99.96 atom % D with 0.03% (v/v) tetramethylsilane (TMS)) and all other solvents were from Sigma-Aldrich (USA).

#### 4.2.2. Bio-oil samples and accelerated aging

Fresh birch wood bio-oil was obtained using a tube-furnace pyrolyzer, as shown in Figure 4.1. The sample load was 3-4 g/run, and the tube-furnace pyrolyzer was operated at 500 °C under a nitrogen gas flow of 300 mL/min. The produced vapors were trapped and collected as liquid in two cold regions: the water-cooled condenser, and the liquid-nitrogen cold trap. The incondensable gases were vented to a fume-hood. The produced liquids (bio-oil) in two traps were combined together after ten consecutive runs.

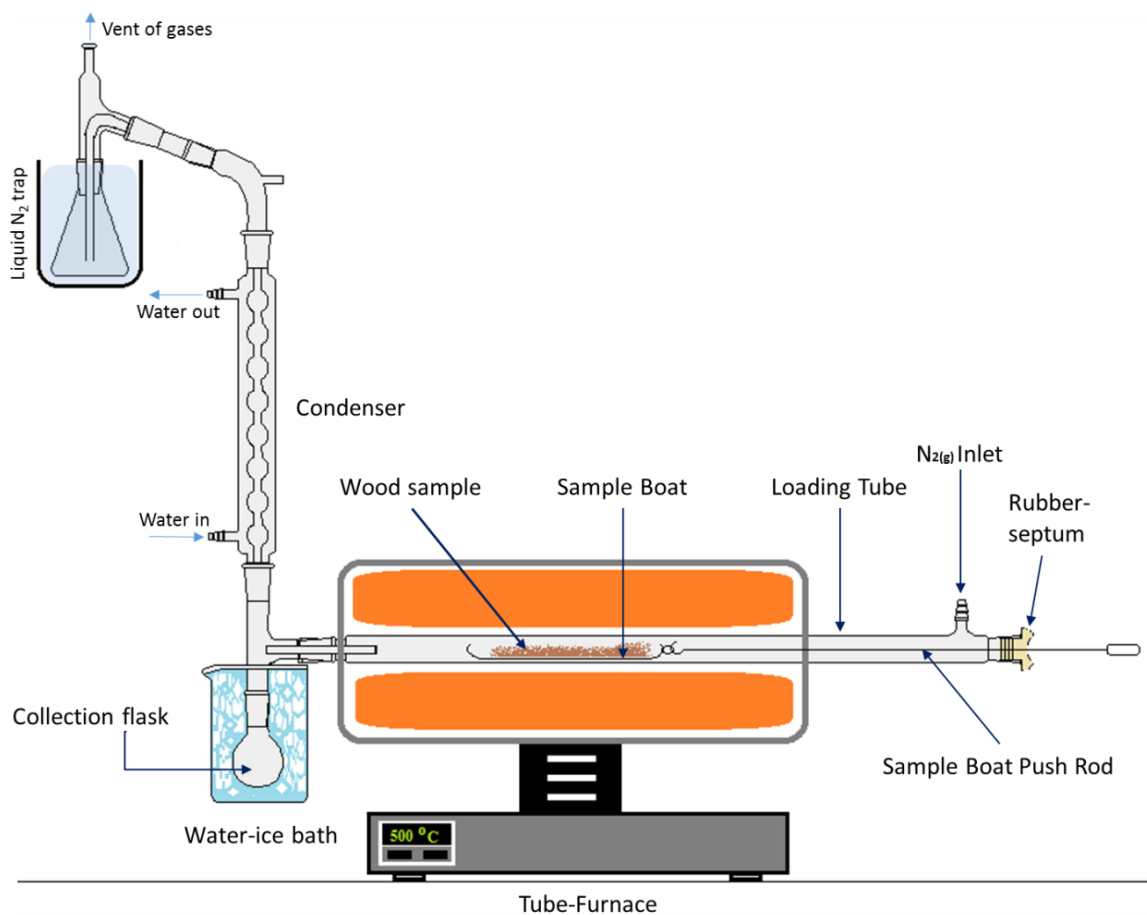


Figure 4.1. Lab scale pyrolysis unit.

The ash bio-oil samples were obtained from Dr. P. Fransham (Abri-Tech., Quebec Canada). Their auger pyrolyzer (2 kg/h) was set at 480 °C, and the bio-oil was collected in a water-cooled metal condenser. A fresh bio-oil was quickly frozen in a dry ice pack and delivered to the lab within 24 h. The particle (mainly fine char) content was measured by filtration through a glass filter after oils were diluted in methanol 1:1 (v/v). The filtrated samples (10 mL) purged with nitrogen were stored in Nalgene bottles (20 mL) in the freezer (-10 °C), until used.

For accelerated aging experiments, nine separate samples (10 g each) from each bio-oil (ash and birch) were placed in airtight Nalgene bottles. Then, three replicate samples were stored at 80 °C for 1, 3, or 7 days. Sample coding: example AB-1; AB=ash bio-oil, BB= birch bio-oil; -0,-1,-3,-7 represent fresh, 1, 3 and 7 day aged bio-oils. After the storage period, the aged bio-oil samples were rapidly cooled in ice water and weighted to ensure that weight loss was less than 2 %. The viscosity and water content were then measured. Followed by storage at -5 °C until further analysis.

#### 4.2.3. Analysis

4.2.3.1. Physiochemical properties: The kinematic viscosity was measured by capillary-type viscometer at 25 °C. Water content was determined by Karl-Fischer coulometric titration (Mettler Toledo V30 Coulometric KF titrator) using a Hydranal<sup>®</sup>-Composite 5 solution after the bio-oils had been diluted in dry acetonitrile solvent. A microscope (Carl Zeiss Microscopy GmbH, Jena, Germany) with polarized light was used to obtain digitalized microscopic images of bio-oils. The pH of the bio-oils was measured using a

digital pH meter (PICCOLO ATC pH testers, Hanna Instruments). Ash content was measured by burning a 1g oil on muffle-furnace at 600 °C.

4.2.3.2. Py-GC/MS analysis: A  $1.25 \pm 0.05$  mg bio-oil sample was weighed using a micro balance into a Py cup and then introduced into a vertical micro-furnace pyrolyzer (PY-2020D, Frontier laboratories Ltd., Yoriyama, Japan), coupled to a gas chromatography/mass spectrometry (GC/MS) (HP 5890 II/HP 5971A, Hewlett Packard, Palo Alto, CA, USA). The MSD w interface temperature was 270 °C, EI 70 eV and scan range of  $m/z$  40–550. The pyrolysis furnace, interface temperature and GC injector port were maintained at 270 °C. The capillary flow was 2 mL/min and split flow 40 mL/min. A GC capillary column (Zebron™ ZB-1701, 30 m  $\times$  0.25 mm i.d.  $\times$  0.25  $\mu$ m, Phenomenex, Inc., USA) was used. The GC oven was held at 50 °C for 6 minutes to trap and focus the volatile components, and then the temperature increased to 260 °C at 5 °C/min and held for 4 minutes. The Py cup was removed, cooled and weighed on a micro-balance to measure the nonvolatile residue fraction. In case of pyrolysis of residues, same method for Py-GC/MS was used with changing the temperature of pyrolysis furnace to 550°C.

4.2.3.3. Thermogravimetric analysis (TGA): A 10–15 mg bio-oil sample was placed on a Pt-sample pan. The pan was introduced into the TGA instrument (TA Instruments Q500, USA) and heated from 30 °C to 600 °C at 20 °C/min under a 10 mL/min flow of N<sub>2</sub>.

2.3.4. FTIR analysis: Samples were analyzed using an OPUS spectrometer (Thermo Scientific, USA) operating in the wavelength range of 4000–650  $\text{cm}^{-1}$  with a resolution of 4  $\text{cm}^{-1}$ .

4.2.3.5. <sup>13</sup>C-NMR analysis: Bio-oil samples (50%) were prepared in methanol-d<sub>4</sub> (99.96 atom % D with TMS). The spectra were acquired using a Bruker AVANCE 300

spectrometer (Bruker, Germany) at 60 °C. Suitable  $^{13}\text{C}$  NMR spectra required an acquisition time of 7.5 h (20,000 scans).

### **4.3. Results and Discussions**

#### **4.3.1. Fresh bio-oil samples**

The birch wood pyrolysis products obtained by the tube-furnace pyrolyzer were  $63 \pm 3\%$  oil and  $18 \pm 2\%$  char. The yield of bio-oil from the auger pyrolyzer of ash wood was approximately 65% (the yield of char was not recorded). Table 1 shows the analytical data of filtered fresh bio-oil properties and percentage of solids before filtration. The solids content (mainly char) in non-filtered ash wood bio oil is much higher than that in birch wood bio-oil because the later was performed under static conditions. All oil samples tested for aging were first filtered to remove particulates that could catalyze the aging process. Both bio-oils had comparable viscosity and water content (Table 1). All bio-oil samples were weighed before and after thermal aging to ensure that there was no significant loss of water or other volatiles. The results showed that sample lost amounted to no more than 2.0% of their original masses. Before any analysis, the samples were well-shaken to ensure homogenization. The color of bio-oil turned darker as the aging period increased. The pH measurements for aged bio-oil samples were not significantly different from that of fresh samples.

Table 4.1. Initial bio-oil properties.

Biomass feedstock	Raw oil*	Filtered oil*						
	Char (%)	Oil code	Char (%)	water cont.(%)	Visc (cSt)	Ash (%)	Density (g/ml)	pH
Ash	3.0	AB-0	< 0.1	30.3	11.5	0.3	1.2	2.7
Birch	< 0.1	BB-0	n.d**	32.3	10.4	> 0.1	1.1	2.2

\* average of duplicate analysis,  $\pm 5\%$ , \*\* not detected

#### 4.3.2. Change in water content

Figure 4.2 (a) shows that fresh bio-oil from ash (AB-0) had initially lower H<sub>2</sub>O % than the bio-oil produced from birch (BB-0). Both samples showed significant increases in their H<sub>2</sub>O content as the aging (at 80°C) period increased. This suggests that, condensation and esterification reactions take place to produce water during thermal aging (2,10). The rate of H<sub>2</sub>O production was high for both bio-oils at 1 and 3-days. However, ash bio-oil showed a much more rapid increase in H<sub>2</sub>O content than that from birch. This can be explained in terms of ash bio-oil's higher solids (e.g., infiltrated char) and ash content, which would assist in catalyzing condensation reactions (10).

#### 4.3.3. Viscosity

The viscosity measurements for the fresh and aged samples after storage at 80 °C are shown in Figure 4.2 (b). The reason for using low temperature (25 °C) in viscosity measurements was to avoid further changes in bio-oil chemistry occurring when higher temperatures are used (12). Even so, the viscosity measurements were still high at 25 °C because of the low oil-fluidity caused by the presence of high M.wt polar components (e.g., oligomers) with strong intermolecular forces, i.e., hydrogen bonding and dipole-dipole

interaction (8, 10). Results showed that the viscosity increased as the storage period increased generally from 10 to 30 cSt for all samples. The increase in viscosity indicates that polymerization and condensation reactions have occurred within bio-oil to form larger molecules (6). The viscosities for fresh samples were found to be significantly less than were previously reported for wood bio-oil (4, 12). This may be explained by the high water content in the present bio-oils.(8) The biggest change in viscosity occurred within an initial 3-day period increasing ca. 3-fold viscosity change and reached a slow increasing by 7-days as shown in Figure 4.2 (b).

The 7-days aged ash bio-oil (AB-7) showed the highest viscosity at the end of 7-days of aging, which indicates that this particular bio-oil is more reactive (less stable) during storage. This could again be catalyzed by the presence of higher char and solids content catalyzing more condensation reactions as described in previous research (8, 12, 14, 19). Although oil samples were filtered, this may not have removed non-filtrated char particles in the ash bio-oil, which had high solids content in its infiltrated oil.

#### 4.3.4. TGA

TGA is a proximate analysis (5), which can be used to study the difference in the thermal degradation of samples under nitrogen, in this case, differences between fresh and aged bio-oil samples. Typical TGA curves for bio-oils are shown in Figure 4.3. The loss in mass begins at low temperature with mass loss maxima between 50 to 100 °C, because of the loss of water (30-35 %) and volatile compounds. More than half of the samples mass was lost (vaporized) before 300°C was reached. The TGA curves suggest a significant increase in the bio-oil thermal decomposition temperature from fresh-bio-oil to



increasingly aged oil, as discussed in a previous report (3). The TGA-curves shift would support evidence that polymerization and condensation reactions have changed the volatility\thermal decomposition properties of the bio-oil components with accelerated aging (17). The mass loss percent of residues of samples at temperatures 270 (GC-volatile) and 500 °C (classified as non-volatiles residue) (10) are labeled in Figure 4.3. The % residue at these temperatures increased as aging progressed, i.e. the curve shifts to the right with aging.

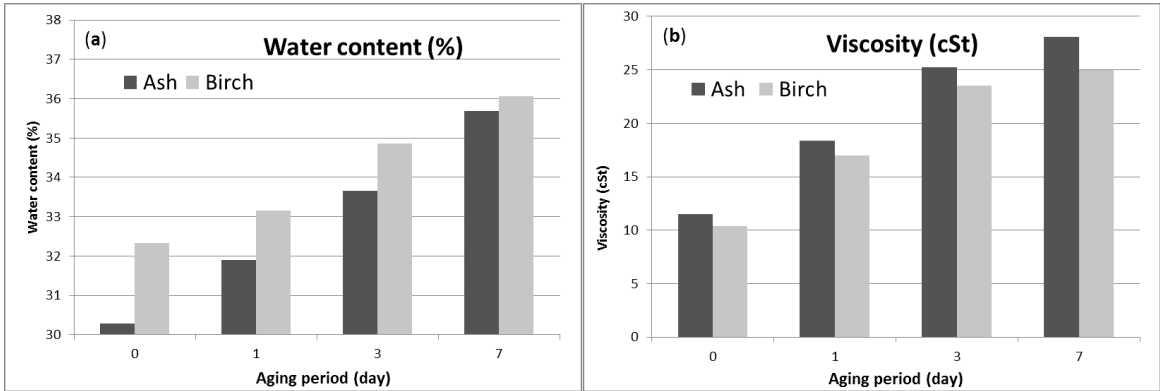


Figure 4.2. (a) Water content (% wt/wt) for fresh and aged (at 80°C) bio-oil samples. (b) viscosity measurements (at 25 °C) for the fresh and aged bio-oil samples. Average of triplicate runs with %RSD between 5-8%.

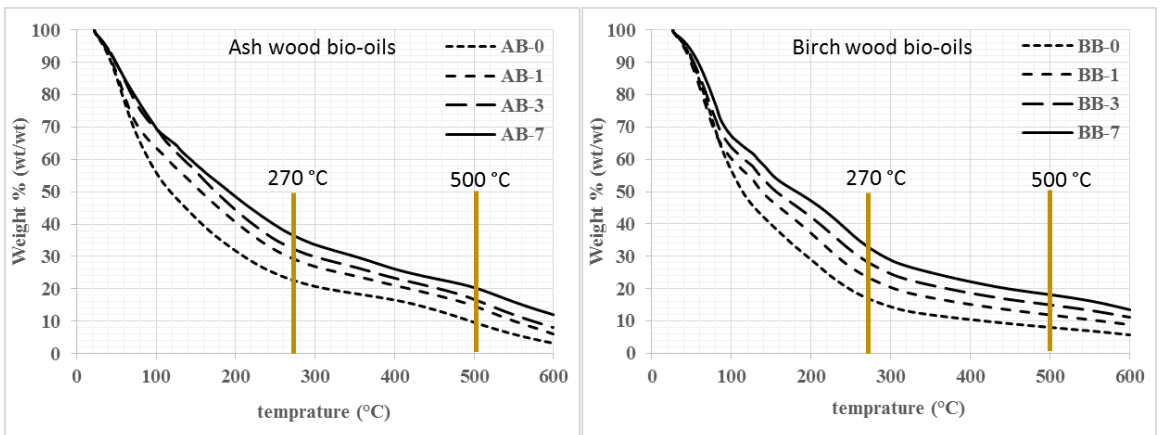


Figure 4.3. TGA curves for the control and aged (at 80°C) bio-oil samples from ash and birch woods [sample code: AB=ash bio-oil, BB= birch bio-oil; -0,-1,-3,-7 present fresh, 1, 3 and 7 day aged bio-oils]. Curves represent average of duplicate runs.

#### 4.3.5. Py-GC/MS

A pyrolysis interface that uses a sample cup was used in this study, so that whole bio-oil samples could be analyzed without the need to dilute the sample in (injection) solvent. In addition, the residue remaining in the cup after GC/MS could be re-analyzed by subjecting the sample to analytical pyrolysis, as described below. The use of this approach to bio-oil analysis can be found in chapter 2 (24). GC/MS analysis for all bio-oil samples was performed with the goal to identify and quantify the changes in bio-oil composition with aging. Figure 4.4 gives the TIC GC/MS of the fresh bio-oils and the identities of the labeled peaks are given in Table 4.2. Figure 4.5 shows the changes in relative peak areas of significantly abundant compounds with aging of both bio-oils. Many of the components in both bio-oil samples showed reduced peak areas (or intensities) with aging. The compounds which saw the largest drop in abundance were further considered as important precursors in aging reactions as discussed below.

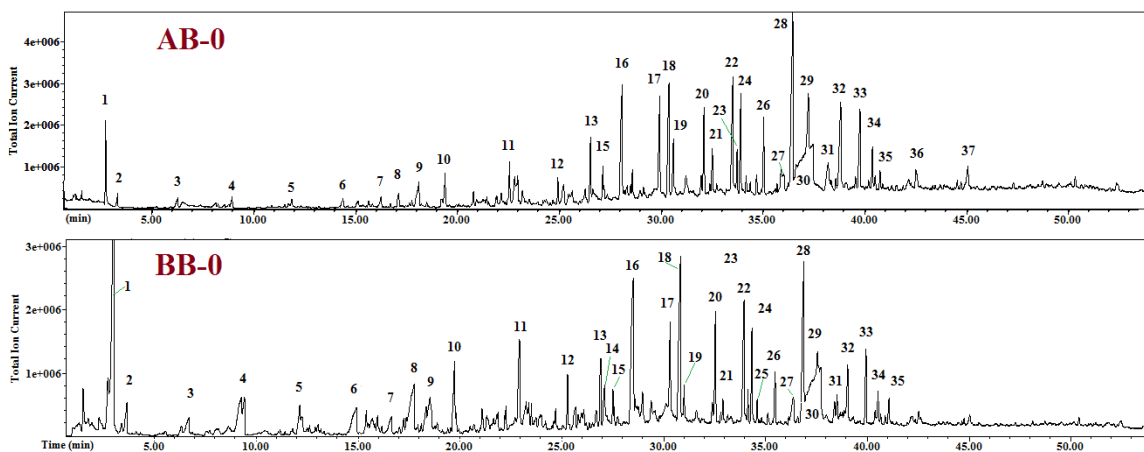


Figure 4.4. GC/MS TIC for the fresh bio-oil samples. [Labeled peaks are identified in Table 4.2, AB-0: fresh ash bio-oil (control) and BB-0: fresh birch bio-oil (control)].

Table 4.2 lists several identified compounds in birch bio-oil aging with notable decreases in abundance (Figure 4.5) with aging, i.e., compounds **3, 5, 6, 8, 13, 14, 17, 18, 22, 26, 28, and 29**. In contrast, some compounds had an increase in abundance within the first day of aging; those being compounds **1, 2, 4, 30, 31, 32, and 33**. In the case of ash bio-oil, compounds **13, 17, 22, 24, 26, 28, 36, and 37** decreased significantly with aging, while compounds **1, 2, 16, 29, and 30** increased in abundance during the first day, then decreased as aging progressed.

From these analyses, it can be seen that the lignin products with double bond side chains showed a significant decrease in their abundance with aging for both bio-oils. These compounds were 4-vinylguaiacol (**13**), cis-Isoeugenol or 4-allyl-guaiacol (**15**), trans-isoeugenol (**17**), 4-vinyl-syringol (**22**), 4-allyl-syringol (**24**), cis-4-propenyl-syringol (**26**) and trans-4-propenyl-syringol (**28**). All of these compounds contain olefins, which can react with each other or with other functional groups to produce larger M.wt compounds such as dimers and oligomers. All identified aldehydes, i.e., 2-furaldehyde (**4**), vanillin (**19**), syringaldehyde (**29**), homo-syringaldehyde (**31**), and sinapaldehyde (**37**), reduced in abundance with aging. Aldehyde species are known to be reactive in bio-oils (*12*). It has also been reported (*18*) that furfural and vanillin have a strong tendency to polymerize, due to their carbonyl group.

The initial increase in abundance in some compounds suggests some degradation of susceptible components to hydrolysis compounds (*12, 21*). For example, acetic acid (**1**), acetol (**2**), and levoglucosan (**30**) levels increased quickly as the bio-oil was subjected to 80 °C heat likely from acid hydrolysis/oxidation and in the case of levoglucosan the decomposition of sugar derivatives. With further aging anhydrosugars, such as,

levoglucosan, could participate in the polymerization reactions or can undergo hydrolysis to glucose during heating (18). Furthermore, if glucose is formed it could undergo dehydration reactions to form potentially reactive intermediates.

Figure 4.6 illustrates some suggested (aging) reactions occurring during wood bio-oil storage (21, 25). All lignin compounds shown have been identified in the bio-oils and have an olefin side group, which can undergo to self-condensation/polymerization reactions as shown in first three reactions. Aldehydes can undergo condensation reactions as well as shown in reaction 4 while aldehydes and alcohols can react to produce acetals as shown in reaction 5.

The residue in the Py cup, measured after each GC/MS analysis with a 270 °C furnace temperature, represents the material remaining after vaporization of the GC fraction of oil samples. The weight percent for these residues were 18 (AB-0), 23 (AB-1), 24 (AB-3), 30 (AB-7), 9 (AB-0), 13 (BB-1), 16 (BB-3), and 22 (BB-7). These results followed the same trend obtained by TGA at 270 °C (Figure 4.3).

Subsequently, the residues were analyzed by Py-GC/MS at a pyrolysis temperature of 550 °C in the same pyrolysis unit described in the experimental. As the aging progressed, more pyrolysis products were observed in the pyrogram as shown in Figure 4.7, which shows fresh versus 7-day aged bio-oils. All identified compounds were related to lignin pyrolysates, in which their amount were higher in aged samples. This indicates that the residue was mainly composed of products of lignin pyrolysates during aging. These identified compounds include primarily cresols, and cuaiacols and syringols, which can be

produced during the depolymerization reactions that occur at the pyrolysis temperature (550 °C).

Table 4.2. Identified compounds in bio-oil samples from ash and birch wood.

Peak #	RT (min)	compound	Peak #	RT (min)	compound
1	2.71	Acetic acid	21	33.16	Acetoguaiacone
2	3.31	1-Hydroxy-2-propanone (acetol)	22	34.20	4-Vinyl-syringol
3	6.69	3-Hydroxy-propanal	23	34.42	Guaiacylacetone
4	9.44	2-Furaldehyde	24	34.60	4-Allyl-syringol
5	12.18	2-Furanmethanol	25	34.91	6-Hydroxy-Hydrocoumarin
6	14.96	Dihydro-methyl-furanone	26	35.77	( <i>cis</i> )-4-propenyl-syringol
7	16.71	2(5 <i>H</i> )-Furanone	27	36.77	Unknown
8	17.36	4-Hydroxy-5,6-di-hydro-(2 <i>H</i> )-pyran-2-one	28	37.20	( <i>trans</i> )-4-Propenyl-syringol
9	18.37	2-Hydroxy-3-methyl-2-Cyclopenten-1-one	29	37.95	Syringaldehyde
10	19.69	Phenol & Guaiacol	30	38.08	Levoglucosan
11	22.94	4-Methylguaiacol	31	38.87	Homo-syringaldehyde
12	25.37	4-Ethylguaiacol	32	39.45	Acetosyringone
13	27.01	4-Vinylguaiacol	33	40.35	Syringyl acetone
14	27.30	3,4-Dihydro-6-methyl-2H-pyran-5-yl methyl ketone	34	40.93	Propio-syringone
15	27.64	( <i>cis</i> )-Isoeugenol or 4-allyl-guaiacol	35	41.29	Sinapyl alcohol
16	28.61	Syringol	36	42.97	Homosyringic acid
17	30.51	( <i>trans</i> )-Isoeugenol	37	45.39	Sinapaldehyde
18	30.96	4-Methyl-syringol			
19	31.20	Vanillin			
20	32.74	4-Ethyl-syringol			

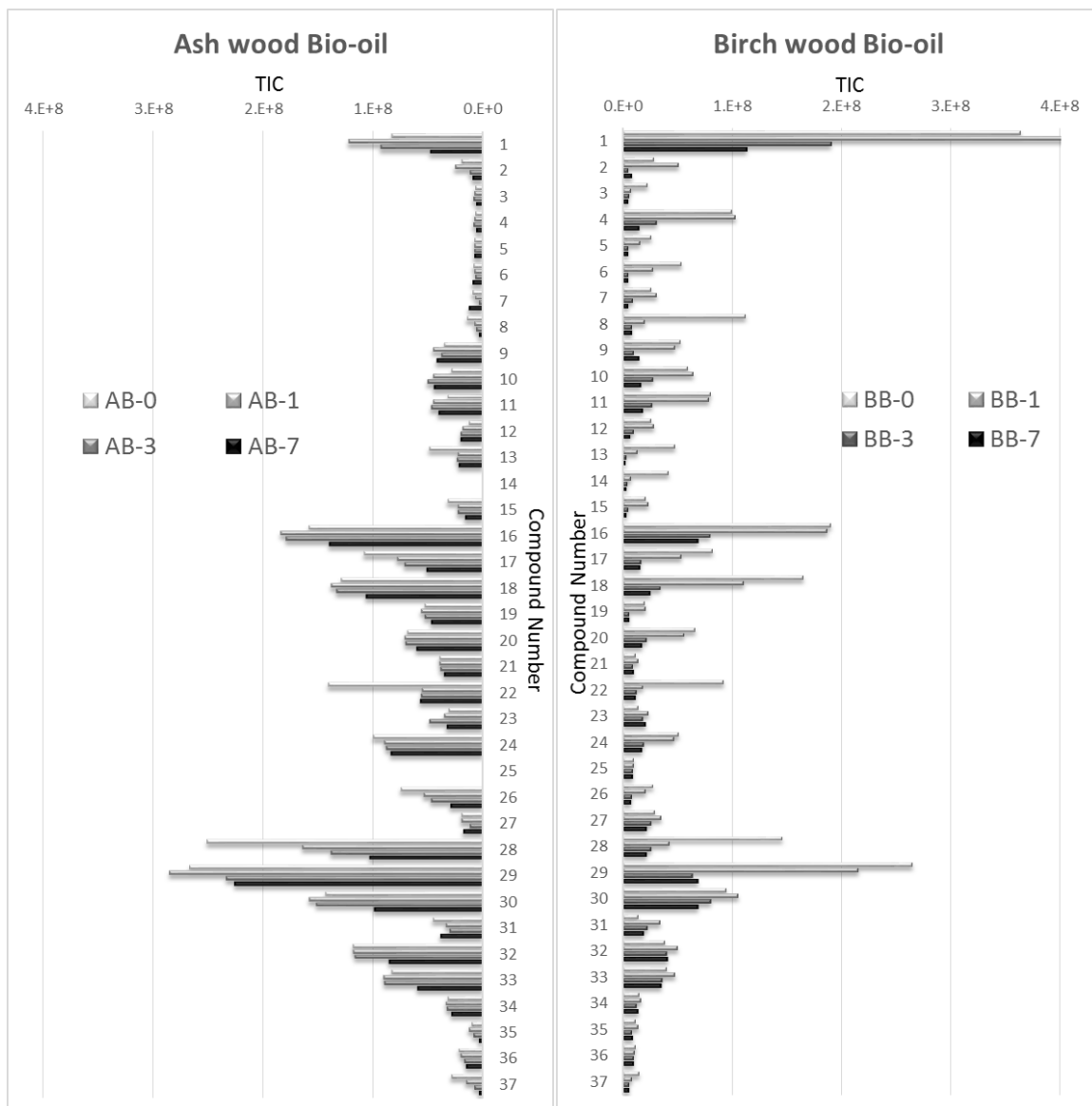


Figure 4.5. Relative peak area changes for identified compounds during accelerated aging (at 80°C) for bio-oil samples (see Table 4.2 for identification of numbered compounds in Figure 4.4). Bars represent average of duplicate runs; %RSD < 5%.

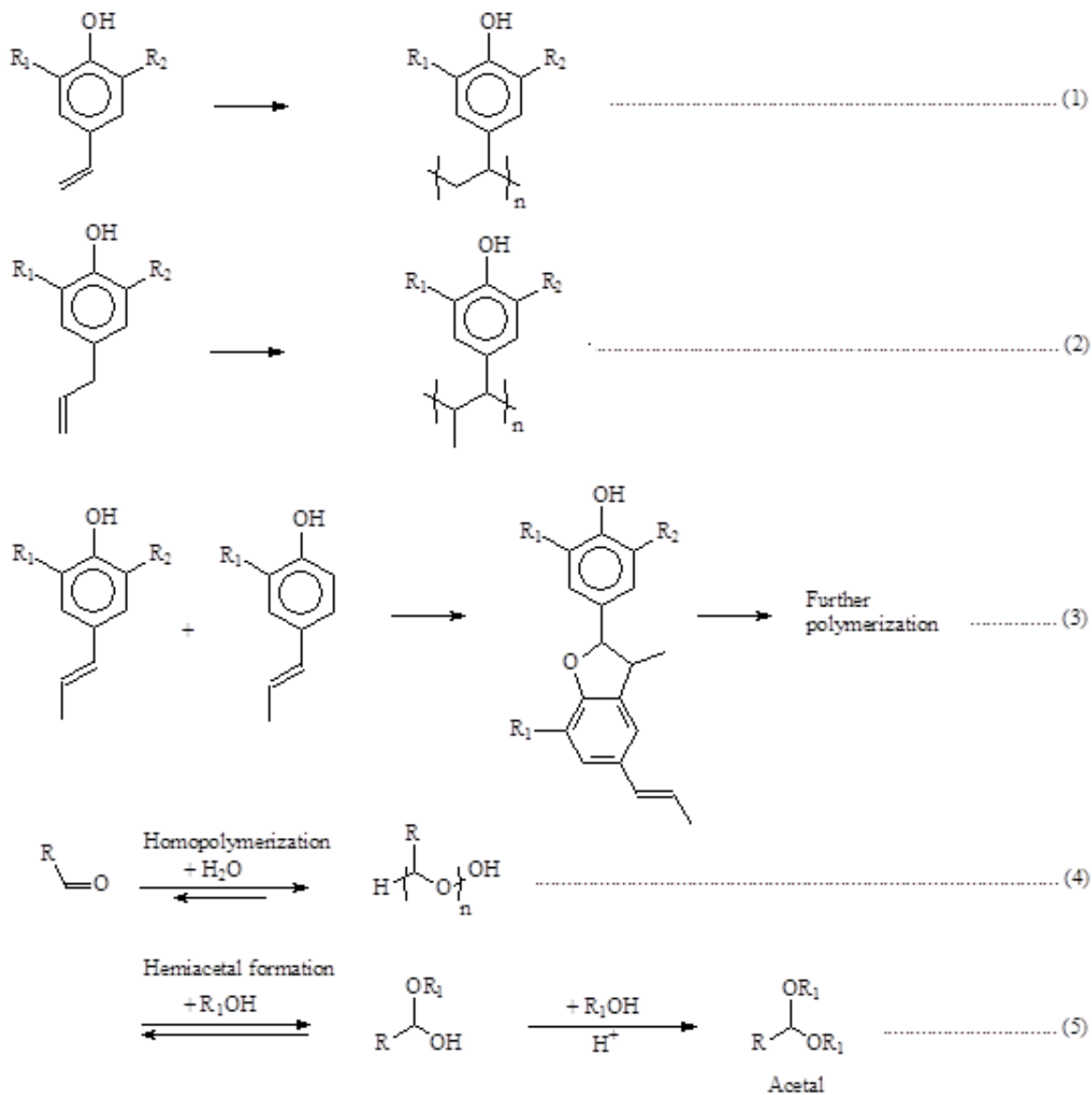


Figure 4.6. Possible chemical reactions that may occur during bio-oil accelerated aging (at 80°C) (21, 25).

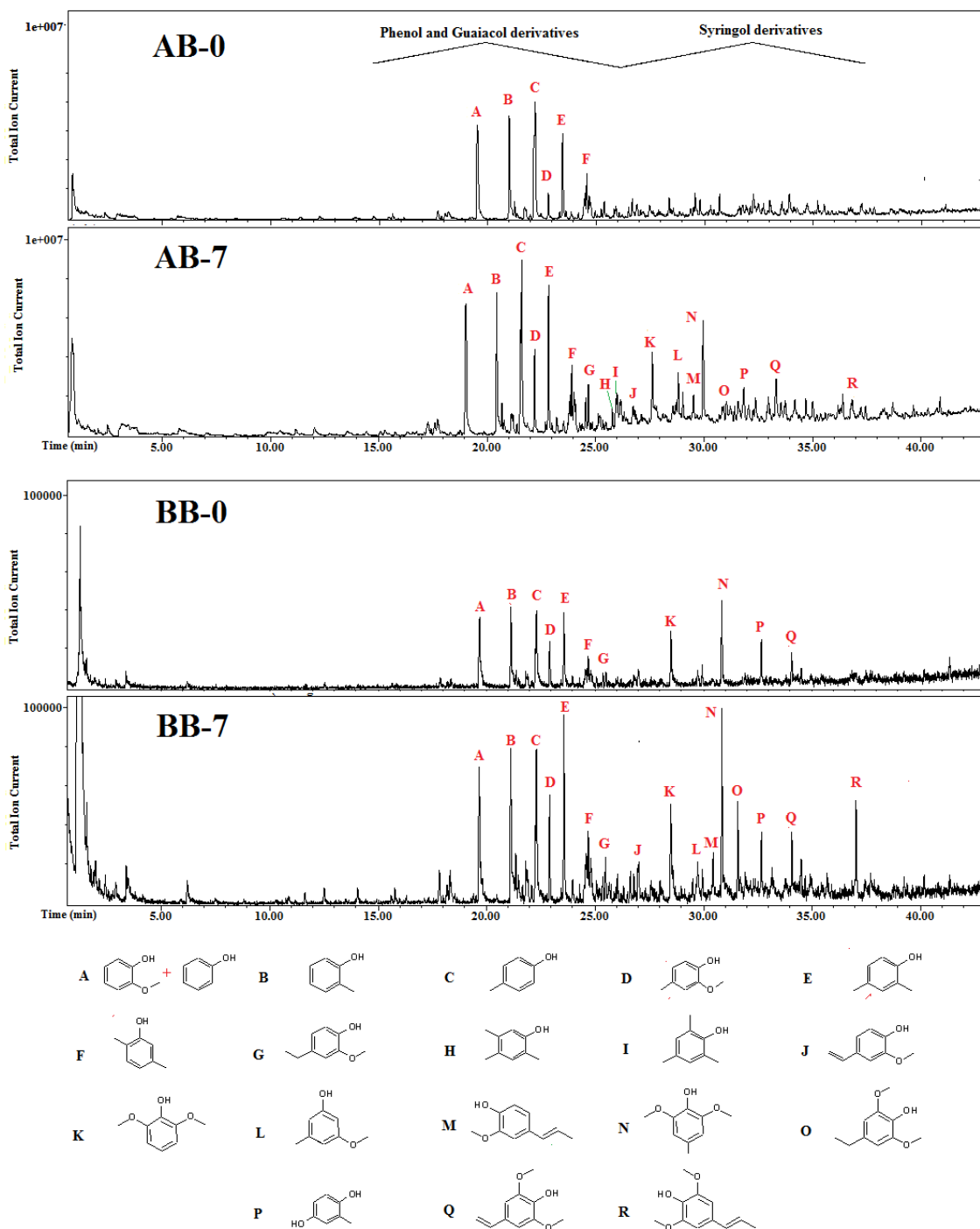


Figure 4.7. Py GC/MS TIC at 550 °C for residues from Py-GC/MS analysis at 270 °C [AB-0: fresh ash bio-oil (control), AB-7: 7-days aged ash bio-oil (at 80°C), BB-0: fresh Ash bio-oil (control) and BB-7: 7-days aged birch bio-oil (at 80°C)].



#### 4.3.6. FTIR

The FTIR spectral changes of specific functional groups among the aged samples were evaluated as shown in Figure 4.8. The % transmittance-intensities in the spectra can be used to represent the relative concentrations of selected functional groups (6). The highest intensity bands were observed for carbonyls and hydroxyls groups.

The broad band for hydroxyl groups ( $3000\text{--}3650\text{ cm}^{-1}$ ) indicates the large presence of water, and to a smaller extent alcohols, carboxyl acids and phenols (3, 5, 9, 16-17, 21). The carbonyl band ( $1710$  and  $1640\text{ cm}^{-1}$ ) indicates the presence of aldehydes, ketones, carboxylic acids and esters (6, 26-27). Many of the bands' intensities increased during the accelerated aging particularly the hydroxyl band and it could be attributed to increased water content as shown in water content values (Figure 4.2 (a)). The bands at  $1635$ ,  $1265$ , and  $1217\text{ cm}^{-1}$  also increased, while bands at  $1045$  and  $1015\text{ cm}^{-1}$  have decreased with aging. These changes can be assigned to the formation of new ester and ether groups in the bio-oils during aging, producing water molecules as a byproduct (26). The increasing carbonyl bands' intensities ( $1710$  and  $1640\text{ cm}^{-1}$ ) can mostly be related to the formation of carbonyls through oxidation reactions (6, 12). Only the 7-day aged ash bio-oil (AB-7) showed significant band intensity at  $1610\text{ cm}^{-1}$  and at  $1515\text{ cm}^{-1}$ . These two bands could correspond to aromatic skeletal vibrations (6, 7, 21, 26-27). This spectral information can point to the formation of new aromatic rings or to the formation of conjugated bonds with carbonyl groups. Finally, there is FTIR evidence that etherification or esterification reactions occurred in the bio-oil during the accelerated aging as suggested above (28).

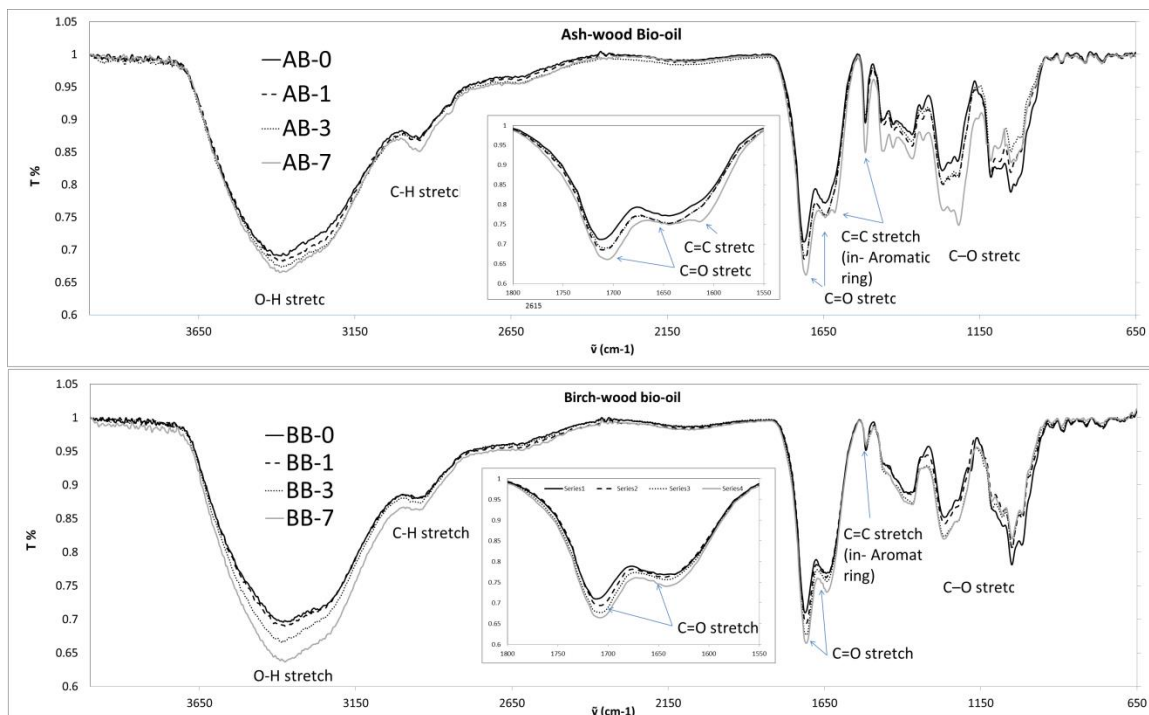


Figure 4.8. FTIR spectra of fresh and aged (at 80°C) bio-oil samples.

#### 4.3.7. $^{13}\text{C}$ -NMR analysis

NMR analysis can help to provide information about the entire bio-oil samples. However, the interpretation of NMR spectra is difficult for complex mixtures like bio-oils due to the overlapping of the chemical shift regions for some  $^{13}\text{C}$  classes (29). Both bio-oils' fresh (control) samples and the 7-day aged samples were analyzed. The  $^{13}\text{C}$ -NMR spectra of samples AB-0, BB-0, AB-7 and BB-7 are shown in Figure 4.9 and 4.10. Typically, the intensity of most signals are significantly reduced or disappear after the bio-oil aging which strongly indicates the thermal instability of bio-oils during storage (3, 23).

Since all samples were prepared at the same concentration, it is possible some of the aged samples had high M.wt components that did not dissolve in the NMR solvent. In particular signals at 55 and 66 ppm due to hydroxyl carbon (C-OH) decreased possibly due to condensation reactions of alcohol-containing compounds. The signal at 92 ppm indicating

the possible presence of carbohydrate-related carbon and the signal at 99 ppm indicating olefinic carbons (30), both decreased in intensity with aging, an observation, which is also discussed in the GC/MS section. In contrast, new peaks were observed in  $^{13}\text{C}$ -NMR spectra for samples AB-7 and BB-7. In the case of ash bio-oil new signals at 23, 53 and 178 ppm, and for birch bio-oils at 23 and 53 indicated the formation of alkyl carbons ( $-\text{CH}_3$ ,  $-\text{CH}_2-$ , or  $-\text{CH}-$ ) connected to an oxygen atom or aromatic moiety. Also, the signal at 178 ppm in both aged oils indicate the possible formation of ester groups (23). Finally, the signal for aldehydes, 160-215 ppm was reduced in both aged bio-oil spectra. Many if not all of these spectral observations could be explained by etherification, esterification or condensation reactions, which would take place during accelerated aging.

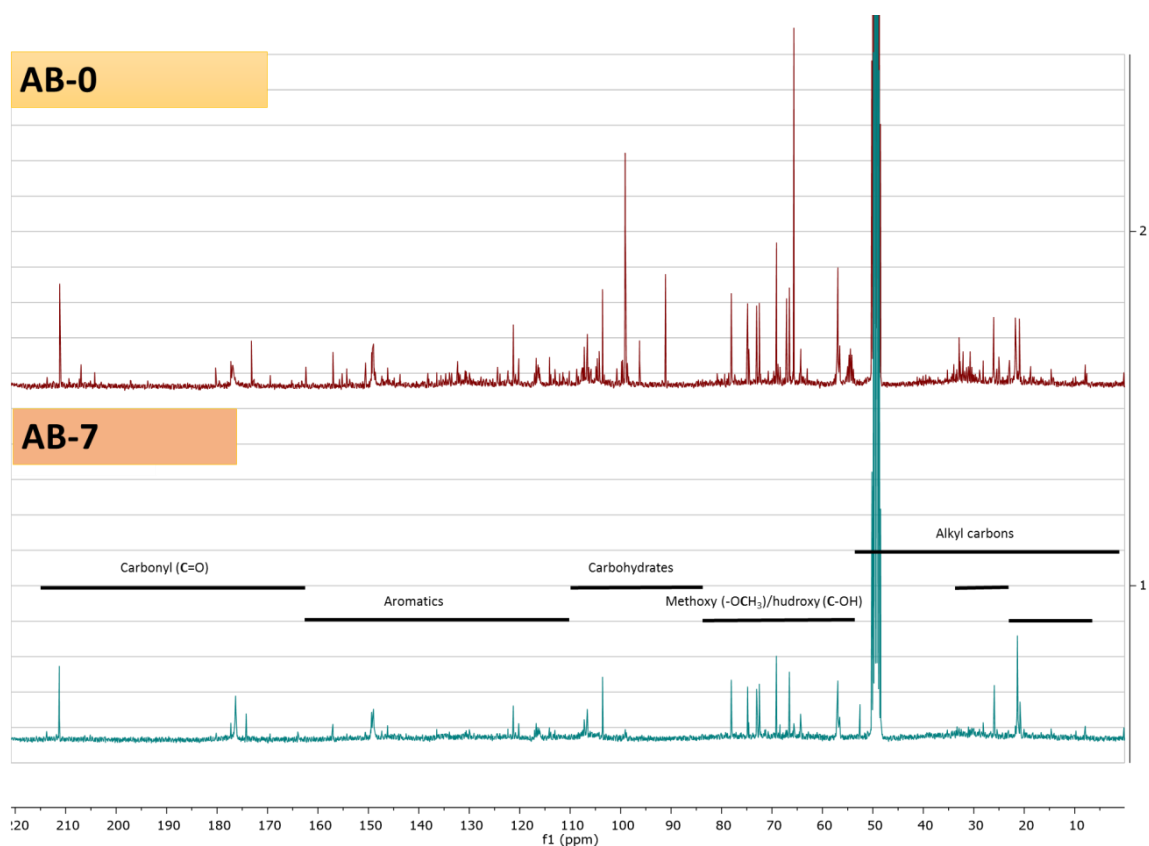


Figure 4.9.  $^{13}\text{C}$  NMR spectra for the fresh (AB-0) and 7-day aged (at  $80^\circ\text{C}$ ) bio-oil (AB-7) sample from ash wood.

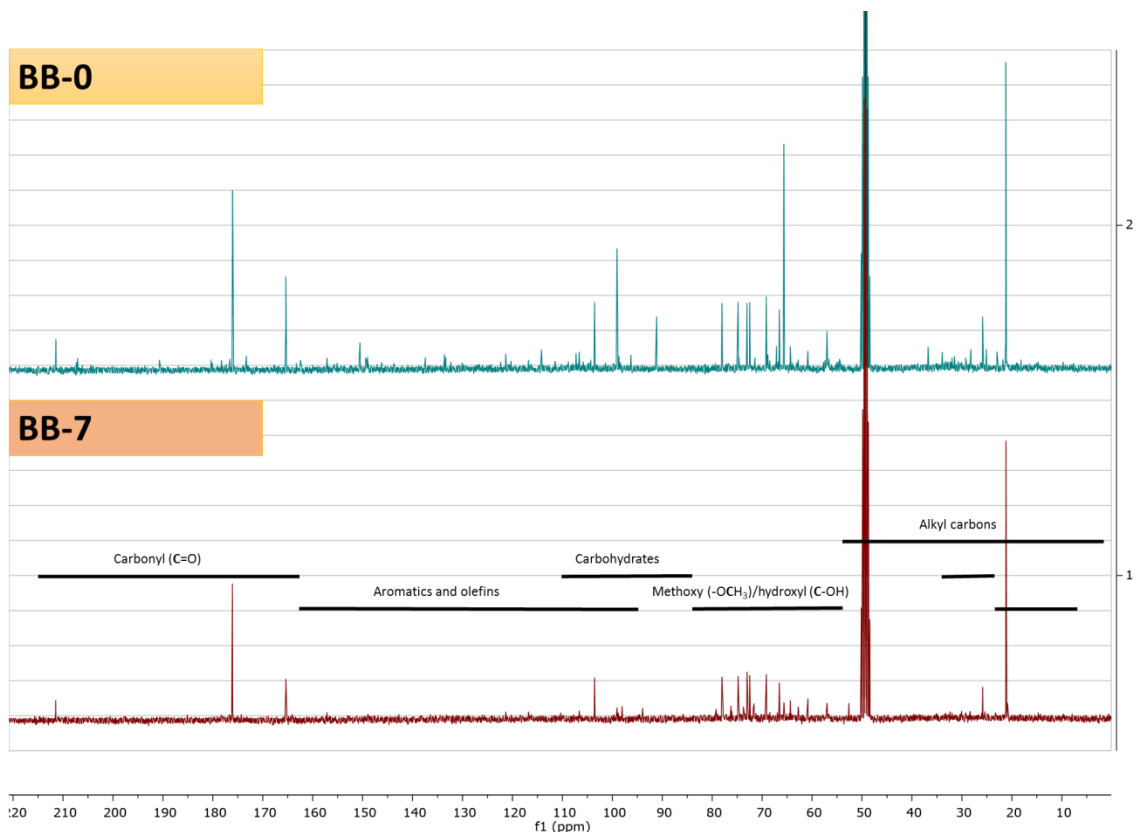


Figure 4.10.  $^{13}\text{C}$  NMR spectra for the fresh (BB-0) and 7-days aged (at  $80^\circ\text{C}$ ) bio-oil (BB-7) sample from birch wood.

#### 4.3.8. Homogeneity

Microscopic images of fresh and aged bio-oil samples at magnifications of  $\times 10$  (Figure 4.11 and 4.12) show some clear changes with aging. The colour of bio-oils became darker during the aging period. Except for the 7-day aged samples, all show a single liquid phase with some suspended black or waxy particles. Phase separation was evident with AB-7 and BB-7 possibly due to increased water content and/or aggregation of higher M.wt components from the aging process and phase separation (11). It has been suggested that lignin-rich oligomers polymerize during storage and separate out of the bio-oil medium as a viscous material (20).

The microscopic images clearly show the increase in size and amount of solid particles with aging. Some of these solids are most likely char residues, ash or minerals carried over in the pyrolytic vapors and could be formed via precipitation after condensation reactions during aging. A possible reason for increasing particle-size with aging has been suggested due to aggregation of small particles formed by polymerization (10-11, 20). The bio-oils from ash wood showed more solids possibly due to biochar-catalyzed polymerization reactions since significant amounts of biochar were not filtered out from the ash bio-oil.

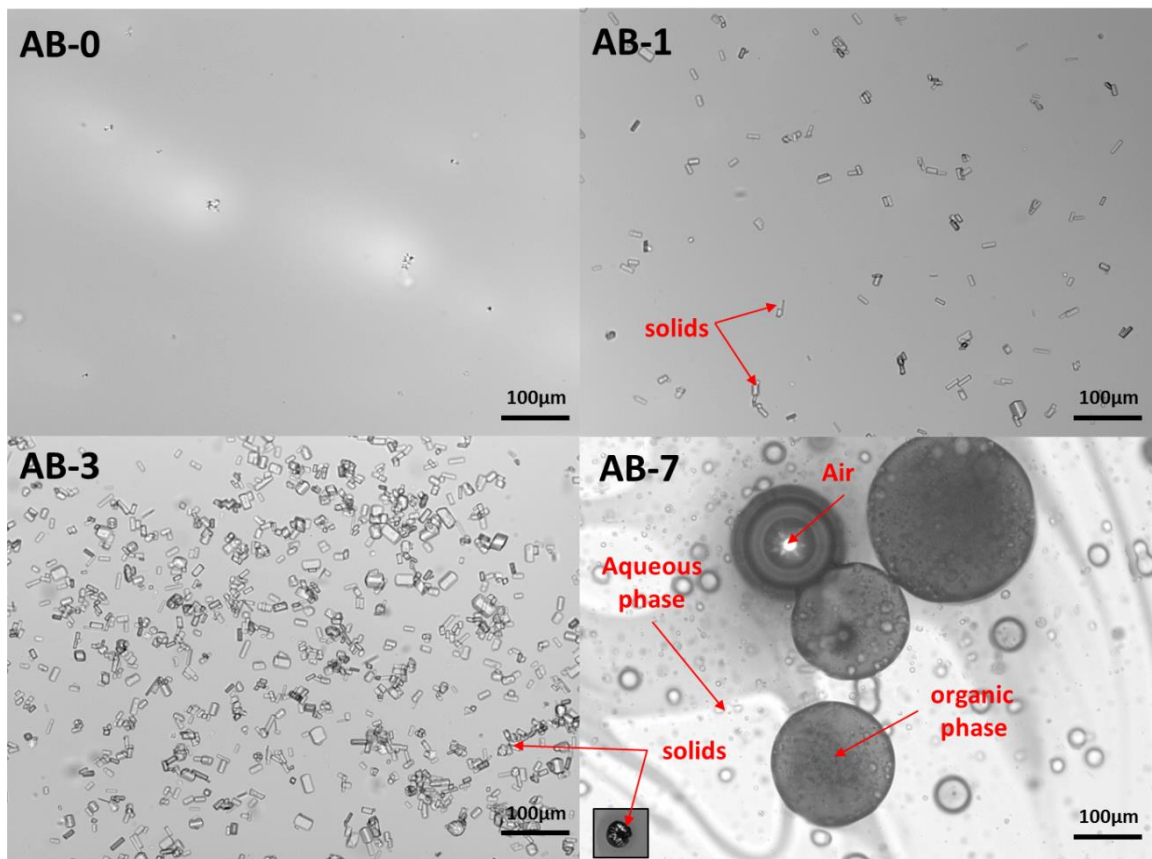


Figure 4.11. Microscopic images ( $\times 10$ ) for fresh and aged ash bio-oil (at  $80^{\circ}\text{C}$ ).

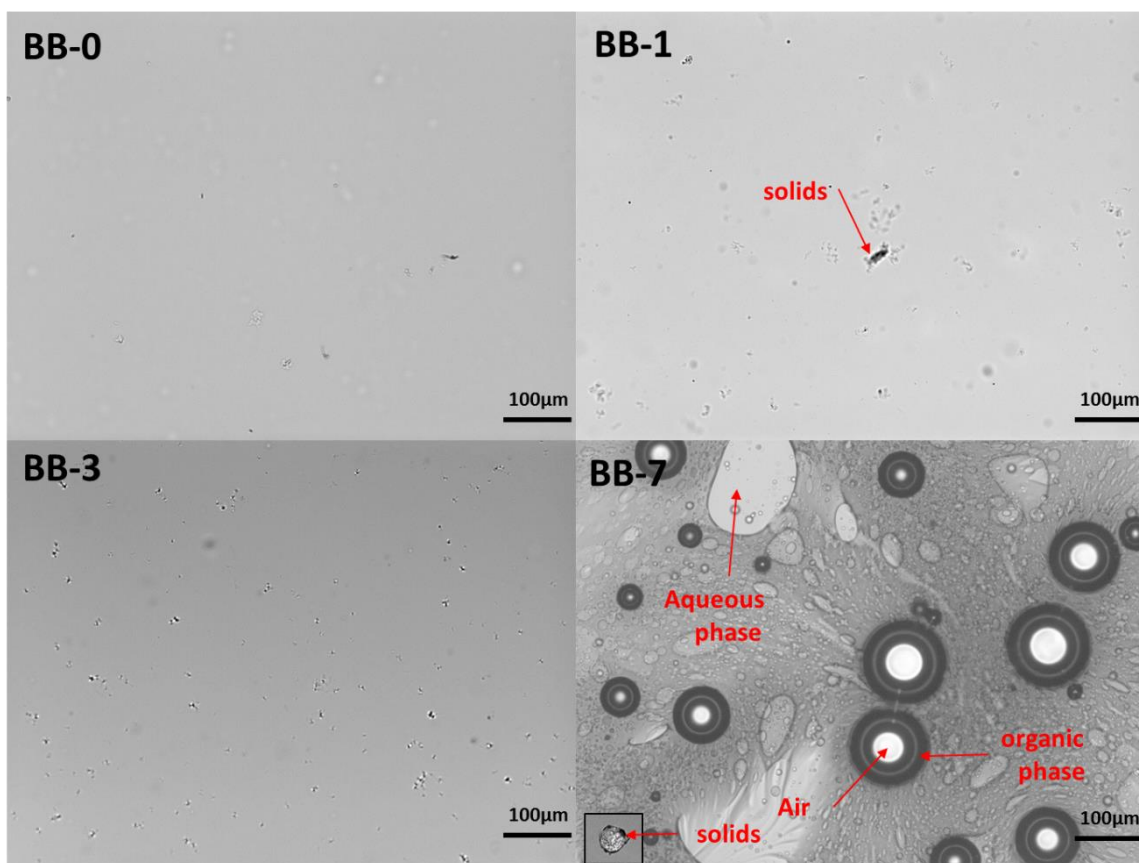


Figure 4.12. Microscopic images ( $\times 10$ ) for fresh and aged birch bio-oil (at  $80^{\circ}\text{C}$ ).

#### 4.4. Conclusion:

In this chapter, the effect of accelerated aging (at  $80^{\circ}\text{C}$ ) on bio-oils produced from ash and birch using an auger or tube furnace pyrolyzer was investigated. The bio-oil's physicochemical properties, i.e., water content, viscosity, homogeneity and chemical composition i.e., GC/MS,  $^{13}\text{C}$ -NMR, TGA and FTIR were measured and correlated with aging periods. Results shows no significant difference between the accelerated aging (at  $80^{\circ}\text{C}$ ) of ash and birch bio-oils. The two bio-oil's properties were changing via reactions between chemically reactive components including (typically the acids, alcohols, aldehydes and alkenes). Water content and viscosity increased during aging and Py-GC/MS, FTIR and  $^{13}\text{C}$ -NMR all show changes in chemical composition related to the aging

process. The largest change observed by Py-GC/MS analysis of the bio-oil was the reduction in the amount of olefinic-containing compounds, while FTIR analysis indicated products aging reactions formed through etherification and esterification. These types of reactions were confirmed by the increase in water content. FTIR showed decreases in carbonyl and other groups with aging while NMR analysis results were more difficult to interpret due to solubility issues. However, reduction in aldehyde and hydroxyl carbon signals indicated condensation reactions during aging. TGA analysis showed increasing thermal degradation temperatures in oils with age while the amount of residue left after GC/MS analysis significantly increased. Microscopic images showed solids content and homogeneity changed with aging. By 7-days, the samples underwent phase separation, which was especially apparent for ash bio-oils. Considering all these results, it could be inferred that polymerization and condensation reactions occurred (i.e., esterification, etherification and olefinic condensation).

#### 4.5. References

1. Nolte, M. W.; Liberatore, M. W. Real-Time Viscosity Measurements during the Accelerated Aging of Biomass Pyrolysis Oil. *Energy Fuels* **2011**, *25*, 3314-3317.
2. Ortega, J. V.; Renehan, A. M.; Liberatore, M. W.; Herring, A. M. Physical and chemical characteristics of aging pyrolysis oils produced from hardwood and softwood feedstocks. *J. Anal. Appl. Pyrolysis* **2011**, *91*, 190-198.
3. Jiang, X.; Zhong, Z.; Ellis, N.; Wang, Q. Aging and Thermal Stability of the Mixed Product of the Ether-Soluble Fraction of Bio-Oil and Bio-Diesel. *Chem. Eng. Technol.* **2011**, *34*, 727-736.
4. Trinh, T. N.; Jensen, P. A.; Dam-Johansen, K.; Knudsen, N. O.; Soerensen, H. R.; Hvilsted, S. Comparison of Lignin, Macroalgae, Wood, and Straw Fast Pyrolysis. *Energy Fuels* **2013**, *27*, 1399-1409.
5. Cordella, M.; Berrueco, C.; Santarelli, F.; Paterson, N.; Kandiyoti, R.; Millan, M. Yields and ageing of the liquids obtained by slow pyrolysis of sorghum, switchgrass and corn stalks. *J. Anal. Appl. Pyrolysis* **2013**, *104*, 316-324.

6. Hilten, R. N.; Das, K. C. Comparison of three accelerated aging procedures to assess bio-oil stability. *Fuel* **2010**, *89*, 2741-2749.
7. Jiang, X. X.; Naoko, E.; Zhong, Z. P. Structure properties of pyrolytic lignin extracted from aged bio-oil. *Chin. Sci. Bull.* **2011**, *56*, 1417-1421.
8. Boucher, M. E.; Chaala, A.; Pakdel, H.; Roy, C. Bio-oils obtained by vacuum pyrolysis of softwood bark as a liquid fuel for gas turbines. Part II: Stability and ageing of bio-oil and its blends with methanol and a pyrolytic aqueous phase. *Biomass Bioenergy* **2000**, *19*, 351-361.
9. Bridgwater, A. Upgrading biomass fast pyrolysis liquids. *Environ. Prog. Sustain. Energy* **2012**, *31*, 261-268.
10. Fahmi, R.; Bridgwater, A. V.; Donnison, I.; Yates, N.; Jones, J. M. The effect of lignin and inorganic species in biomass on pyrolysis oil yields, quality and stability. *Fuel* **2008**, *87*, 1230-1240.
11. Chaala, A.; Ba, T.; Garcia-Perez, M.; Roy, C. Colloidal Properties of Bio-oils Obtained by Vacuum Pyrolysis of Softwood Bark: Aging and Thermal Stability. *Energy Fuels* **2004**, *18*, 1535-1542.
12. Diebold, J.P. (2002). A review of the chemical and physical mechanisms of the storage stability of fast pyrolysis bio-oils, in *Fast Pyrolysis of Biomass: A Handbook*, vol. 2 (ed. A.V. Bridgwater), CPL Press, Newbury, pp. 243-292.
13. Yu, F.; Deng, S.; Chen, P.; Liu, Y.; Wan, Y.; Olson, A.; Kittelson, D.; Ruan, R. Physical and chemical properties of bio-oils from microwave pyrolysis of corn stover. *Appl. Biochem. Biotechnol.* **2007**, *137-140*, 957-970.
14. Elliott, D. C.; Oasmaa, A.; Preto, F.; Meier, D.; Bridgwater, A. V. Results of the IEA Round Robin on Viscosity and Stability of Fast Pyrolysis Bio-oils. *Energy Fuels* **2012**, *26*, 3769-3776.
15. Baldwin, R. M.; Feik, C. J. Bio-oil Stabilization and Upgrading by Hot Gas Filtration. *Energy Fuels* **2013**, *27*, 3224-3238.
16. Xu, J.; Jiang, J.; Sun, Y.; Lu, Y. Bio-oil upgrading by means of ethyl ester production in reactive distillation to remove water and to improve storage and fuel characteristics. *Biomass Bioenergy* **2008**, *32*, 1056-1061.
17. Jiang, X.; Ellis, N. Upgrading Bio-oil through Emulsification with Biodiesel: Thermal Stability. *Energy Fuels* **2010**, *24*, 2699-2706.
18. Hu, X.; Wang, Y.; Mourant, D.; Gunawan, R.; Lievens, C.; Chaiwat, W.; Gholizadeh, M.; Wu, L.; Li, X.; Li, C. Polymerization on heating up of bio-oil: A model compound study. *AIChE J.* **2013**, *59*, 888-900.
19. Javaid, A.; Ryan, T.; Berg, G.; Pan, X.; Vispute, T.; Bhatia, S. R.; Huber, G. W.; Ford, D. M. Removal of char particles from fast pyrolysis bio-oil by microfiltration. *J. Membr. Sci.* **2010**, *363*, 120-127.
20. Fratini, E.; Bonini, M.; Oasmaa, A.; Solantausta, Y.; Teixeira, J.; Baglioni, P. SANS Analysis of the Microstructural Evolution during the Aging of Pyrolysis Oils from Biomass. *Langmuir* **2006**, *22*, 306-312.
21. Kim, T.; Kim, J.; Kim, K.; Lee, S.; Choi, D.; Choi, I.; Choi, J. W. The effect of storage duration on bio-oil properties. *J. Anal. Appl. Pyrolysis* **2012**, *95*, 118-125.



22. Xu, J.; Jiang, J.; Dai, W.; Zhang, T.; Xu, Y. Bio-Oil Upgrading by Means of Ozone Oxidation and Esterification to Remove Water and to Improve Fuel Characteristics. *Energy Fuels* **2011**, *25*, 1798-1801.
23. Ben, H.; Ragauskas, A. J. In Situ NMR Characterization of Pyrolysis Oil during Accelerated Aging. *ChemSusChem* **2012**, *5*, 1687-1693.
24. Alsbou, E.; Helleur, R. Whole sample analysis of bio-oils and thermal cracking fractions by Py-GC/MS and TLC-FID. *J. Anal. Appl. Pyrolysis* **2013**, *101*, 222-231.
25. Bhattacharya, P.; Hassan, E. B.; Steele, P.; Cooper, J.; Ingram, L. Effect of acid catalysts and accelerated aging on the reaction of methanol with hydroxy-acetaldehyde in bio-oil. *BioResources* **2010**, *5*, 0908-0919.
26. Volli, V.; Singh, R. K. Production of bio-oil from de-oiled cakes by thermal pyrolysis. *Fuel* **2012**, *96*, 579-585.
27. Lievens, C.; Mourant, D.; He, M.; Gunawan, R.; Li, X.; Li, C. An FT-IR spectroscopic study of carbonyl functionalities in bio-oils. *Fuel* **2011**, *90*, 3417-3423.
28. Czernik, S.; Johnson, D. K.; Black, S. Stability of wood fast pyrolysis oil. *Biomass Bioenergy* **1994**, *7*, 187-192.
29. Pittman, C. U., Jr.; Mohan, D.; Eseyin, A.; Li, Q.; Ingram, L.; Hassan, E. M.; Mitchell, B.; Guo, H.; Steele, P. H. Characterization of Bio-oils Produced from Fast Pyrolysis of Corn Stalks in an Auger Reactor. *Energy Fuels* **2012**, *26*, 3816-3825.
30. Mullen, C.; Strahan G.; Boateng A. Characterization of Various Fast-Pyrolysis Bio-Oils by NMR Spectroscopy. *Energy Fuels* **2009**, *23*, 2707-2718.

# **Chapter 5**

## **Summary and Future work**

## 5.1. Summary of research

Bio-oils are a complex mixture of highly oxygenated compounds. They can be produced by fast pyrolysis from renewable biomass feedstock such as wood, forest residue and agricultural wastes. It is necessary to understand the physical and chemical nature of bio-oils in order to enhance its production yields, quality and end-uses.

This study has used several analytical techniques to characterize bio-oil samples from different biomass feedstock, especially from woody biomass and to study bio-oil stability during storage through accelerated aging.

In the second chapter, Py-GC-MS and TLC-FID were used together to rapidly profile “whole” bio-oil samples with minimal sample preparation. TLC-FID analysis, for the first time, was carefully optimized for rapid, two solvent development, analysis. Both techniques could distinguish general and specific differences among bio-oil samples based on their feedstock origin. TLC-FID showed good (polar) band differences among hardwood, softwood and straw bio-oils, and, further, among the thermal cracking fractions of forest residue bio-oil. Lignin pyrolysates were shown to separate with the least polarity zone, carbohydrates in the medium zone. The intensity of origin point (biochar and macromolecular material) was highest for barley straw bio-oil compared to other bio-oils. The technique was shown to be complimentary to Py-GC/MS analysis. The Py-GC/MS unit was adapted for “whole” sample bio-oil characterization whereby the non-volatile fraction (residue after thermal desorption at 270 °C) can be accurately measured.

In the third chapter, ESI-Ion Trap MS and ESI-Ion Trap MS<sup>2</sup> have been successfully used to analyze bio-oil components and to distinguish between carbohydrate and lignin-derived products. Different dopants (formic acid, NH<sub>4</sub>Cl, NaCl, and NaOH)

were used alongside model compounds (levoglucosan, glucose, cellobiose, guaiacol, vanillin and syringol) and representative bio-oil samples from lignin and cellulose fast pyrolysis. Doped bio-oil samples with  $\text{NH}_4\text{Cl}$ ,  $\text{NaCl}$ , and  $\text{NaOH}$  resulted in enhancement in sensitivity and peak intensity obtained in positive ion compared to negative ion mode. Meanwhile, negative ion mode provided more interpretative ESI  $\text{MS}^n$  results for the analysis of bio-oil samples for distinguishing between pyrolysates based on their origin.  $\text{NaOH}$ -doped samples resulted in intense peaks for deprotonated ions, especially for lignin products compared to non-doped samples.  $\text{NH}_4\text{Cl}$  dopant showed promising results, as it was found that carbohydrate products can readily form ammonium adducts and chloride adducts, while lignin-derived products did not. The fractionation of bio-oil successfully provided less complex spectra for bio-oil fractions leading to more useful  $\text{MS}^2$  analysis. SPE provided the best results for the water fraction (carbohydrate-derived products), while the lignin fraction was best obtained from the lignin precipitation method. This study provides a base for other studies to expand on the analysis of bio-oil by ESI-MS using low resolution MS or with higher resolving power instruments, such as FT-ICR MS that can be used to better confirm the chemical formula for bio-oil components.

In Chapter 4, an accelerated aging study was applied to bio-oil at  $80\text{ }^\circ\text{C}$ . The results showed important instability parameters that can affect bio-oil during storage. Samples of bio-oil from woody biomass (ash and birch using an auger and tube furnace pyrolyzer, respectively) were produced through fast pyrolysis. The fresh samples were filtrated and placed in an oven at  $80\text{ }^\circ\text{C}$  in air tight vials for different periods (1, 3 and 7 days). The bio-oil's physicochemical properties, i.e., water content, viscosity, homogeneity and chemical composition (GC/MS,  $^{13}\text{C}$ -NMR, TGA and FTIR) were analyzed and correlated with aging

periods. The results clearly showed that the bio-oil's properties were changed with increasing aging-period due to chemical reactions of certain bio-oil components. Water content and viscosity increased during aging and Py-GC/MS, FTIR and  $^{13}\text{C}$ -NMR all showed changes related to chemical composition. The increase in water content with aging period can be explained by condensation reactions. The largest change was observed by Py-GC/MS analysis of the bio-oil via a reduction in olefinic compounds, while FTIR analysis indicated aging products through etherification and esterification. Again, these types of reactions were supported by the increase in water content. FTIR showed a decrease in carbonyl and other groups with aging, while NMR results were more difficult to interpret due to solubility issues. However, reduction in aldehyde and hydroxyl carbon signals indicated condensation reactions occurred during aging. TGA analysis showed increasing thermal degradation temperatures in oils with age while the amount of residue left after GC/MS analysis significantly increased. Microscopic images showed solids content and homogeneity changed with age by 7 days, where samples underwent phase separation. Considering all these results, it could be inferred that polymerization and condensation reactions occurred with accelerated aging (i.e., esterification, etherification and olefinic condensation).

## 5.2. Future work

Although extensive research work that has been done on the characterization of bio-oil in this study and by others, further analyses for its components are needed due to its complexity and variability based on feedstock origin. Bio-oil contains only 30-40% GC-amenable fraction and 20-30% water content (1). These fractions have been already well characterized by a large number of researchers. The remaining bio-oil fraction remains poorly characterized due to its non-volatility and high molecular weight range. Although this thesis has satisfactorily addressed its analysis, this complex fraction remains one of the goals of future work by chemists.

The use of different mass spectrometric ionization and mass analyzer techniques should be investigated for bio-oil analysis. The combination of using different ionization techniques and high resolution MS can provide valuable compositional information. For example, desorption electrospray ionization (DESI) technique would be a useful approach to bio-oil component ionization (2). Bio-oil samples can be embedded on an appropriate surface, such as a TLC plate, and then exposed to DESI MS. Also, the bio-oil sample can be first fractionated by TLC plate (or rod) using the two solvent system developed in Chapter 2. Reactive DESI is another approach and it could be used to selectively analyze targeted species in bio-oils such as phenols or aldehydes (3). The second MS ionization method which could be investigated is MALDI/LDI. MALDI and LDI can both be applied to provide ionization of large molecular weight components in bio-oils. Different matrixes with different dopants can be studied for bio-oil analysis. The challenge is the sample spot preparation due to fact that the bio-oil when dissolved in an appropriate matrix/solvent is difficult to co-crystallize with the matrix (unreported by author). Sample fractionation as

described in Chapter 3 may make sample spot preparation easier, particularly for analysis of bio-oil fractions by LDI. A TOF/TOF mass analyzer provides higher mass resolution (20,000+ resolving power) compared to the Ion Trap analyzer (2,000-4,000) that has been used in Chapter 3. Even higher resolution MS such as Fourier transform ion-cyclotron (FT ICR) MS and Q-TOF MS analyzers can be utilized for compound formula and accurate mass data (4-5).

Based on the results from Chapter 2, TLC rods can be used in combination with Py-GC/MS as a hybrid technique, in which the bio-oil sample is first separated along a chromarod, then the separated bands analyzed by Py-GC/MS. This method was successfully used for analyses of petroleum oil and lipids (6).

The second field of bio-oil research could be focused on is bio-oil fractionation. Fractionation can greatly enhance the characterization of oxygen-containing species in bio-oils (7). As found in Chapter 3, SPE and precipitation for py-lignin can simplify the analysis of bio-oil. Py-lignin fractionation using a preparative column will be investigated based on size and polarity of its components. Further fractionation will result in much simpler and more informative spectra. Py-lignin (water insoluble fraction) is an important fraction in bio-oils. It is considered as the major component for the oligomers in bio-oils and not analyzable by GC. Additional investigation on its composition using different analytical methods should be utilized such as thermal-desorption-Q-TOF MS (accurate mass technique) and APCI/ESI- Ion Trap MS after further fractionation. Thermally-assisted hydrolysis/methylation-GC/MS can also be used to analyze dimers and trimers in this fraction (8).

Py-lignin contains several extractable chemicals, including flavors such as vanillin, and raw compounds for resin synthesis. Several fractionation procedures can be employed in order to recover some of these compounds.

It has been shown in Chapter 4 that bio-oil's composition changes during storage and this change is due to the presence of reactive compounds and of char. Long-term aging at room temperature (e.g. 6 months) should be studied in addition to accelerated aging at 80 °C to further understand stability issues of the liquid product.

Other stability parameters that should be studied include: (i) the pH and total acidity of aged bio-oils, (ii) measuring the abundance of reactive species such as furfuraldehyde, 5-hydroxymethyl furfuraldehyde, levoglucosan, vanillin and phenol-olefinic compounds, (iii) examine the exposure of bio-oil to air vs. N<sub>2</sub>, (iv) cationic content such as Na<sup>+</sup> and Ca<sup>2+</sup> which could catalyze reactions, (v) py-lignin yield and (vi) the addition of a reducing agent to reduce some of the reactive groups. Further investigations aimed at bio-oil stabilization should be attempted, including fractionation, solvent addition, and ultrafiltration. It was found that the presence of methanol or ethanol in the bio-oil and using any emulsification process provides a control over the viscosity of the bio-oil (1).

### 5.3. References

1. Mohan, D.; Pittman, C. U., Jr.; Steele, P. H. Pyrolysis of Wood/Biomass for Bio-oil: A Critical Review. *Energy Fuels* **2006**, *20*, 848-889.
2. Eckert, P. A.; Roach, P. J.; Laskin, A.; Laskin, J. Chemical Characterization of Crude Petroleum Using Nanospray Desorption Electrospray Ionization Coupled with High-Resolution Mass Spectrometry. *Anal. Chem.* **2012**, *84*, 1517-1525.
3. Zhang, Y.; Chen, H. Detection of saccharides by reactive desorption electrospray ionization (DESI) using modified phenylboronic acids. *Int. J. Mass spectrom.* **2010**, *289*, 98-107.



4. Smith, E. A.; Lee, Y. J. Petroleomic Analysis of Bio-oils from the Fast Pyrolysis of Biomass: Laser Desorption Ionization-Linear Ion Trap-Orbitrap Mass Spectrometry Approach. *Energy Fuels* **2010**, *24*, 5190-5198.
5. Smith, E. A.; Park, S.; Klein, A. T.; Lee, Y. J. Bio-oil Analysis Using Negative Electrospray Ionization: Comparative Study of High-Resolution Mass Spectrometers and Phenolic versus Sugaric Components. *Energy Fuels* **2012**, *26*, 3796-3802.
6. S. L. Estévez and R. Helleur, "Fatty acid profiling of lipid classes by silica rod TLC-thermally assisted hydrolysis and methylation-GC/MS," *Journal of Analytical and Applied Pyrolysis*, vol. 74, no. 1-2, pp. 3-10, 2005.
7. Mohan, D.; Pittman, C. U., Jr.; Steele, P. H. Characterization of Pine Pellet and Peanut Hull Pyrolysis Bio-oils by Negative-Ion Electrospray Ionization Fourier Transform Ion Cyclotron Resonance Mass Spectrometry. *Energy Fuels* **2012**, *26*, 3810-3815.
8. Shadkani, F.; Estevez, S.; Helleur, R.J. Analysis of Catechins and Condensed Tannins by Thermally-Assisted Hydrolysis/Methylation-GC/MS and by a Novel Two Step Methylation. *J. Anal. Appl. Pyrolysis* **2009**, *85*, 54-65.

# Appendix

### Supporting Information for Chapter 3

Table S3.1. MS methods that have been used in characterization of bio-oils.

Ionization mode	Ion Mode	Mass analyzer	Sample	Ref <sup>a</sup>
APCI	-ve	Liner quadrupole Ion Trap (LQIT)	Carbohydrates**	13
APPI	*	Liner Ion Trap-orbitrap	Toluene extract from Biochar**	7
ESI	+ve	Liner quadrupole Ion Trap (LQIT)	Model compounds from lignin degradation products**	14
		Triple-quadrupole	Chicken manure	9
	+ve/-ve	Quadrupole	Lignin	15
		-ve	FT-ICR	Pine and peanut hulls pellets
	Red oak			12
	Red pine			2
	-ve	Liner Ion Trap-orbitrap	Water/Methanol extract from biochar**	7
		Liner quadrupole Ion Trap (LQIT)	Carbohydrates**	13
			Model compounds from lignin degradation products**	14
		Orbitrap	Red oak	12
Q-TOF	12			
FD	*	Double focusing	Chicken manure	10
FI	*			10
LDI	*	Liner Ion Trap-orbitrap	Loblolly pine	5
		TOF	Pyrolytic lignin**	6
	+ve	Liner Ion Trap-orbitrap	Toluene extract from Biochar**	7
MALDI	*	TOF	Pyrolytic lignin**	6

<sup>a</sup> See chapter 3's references, \* N/A, \*\*Not bio-oil sample.

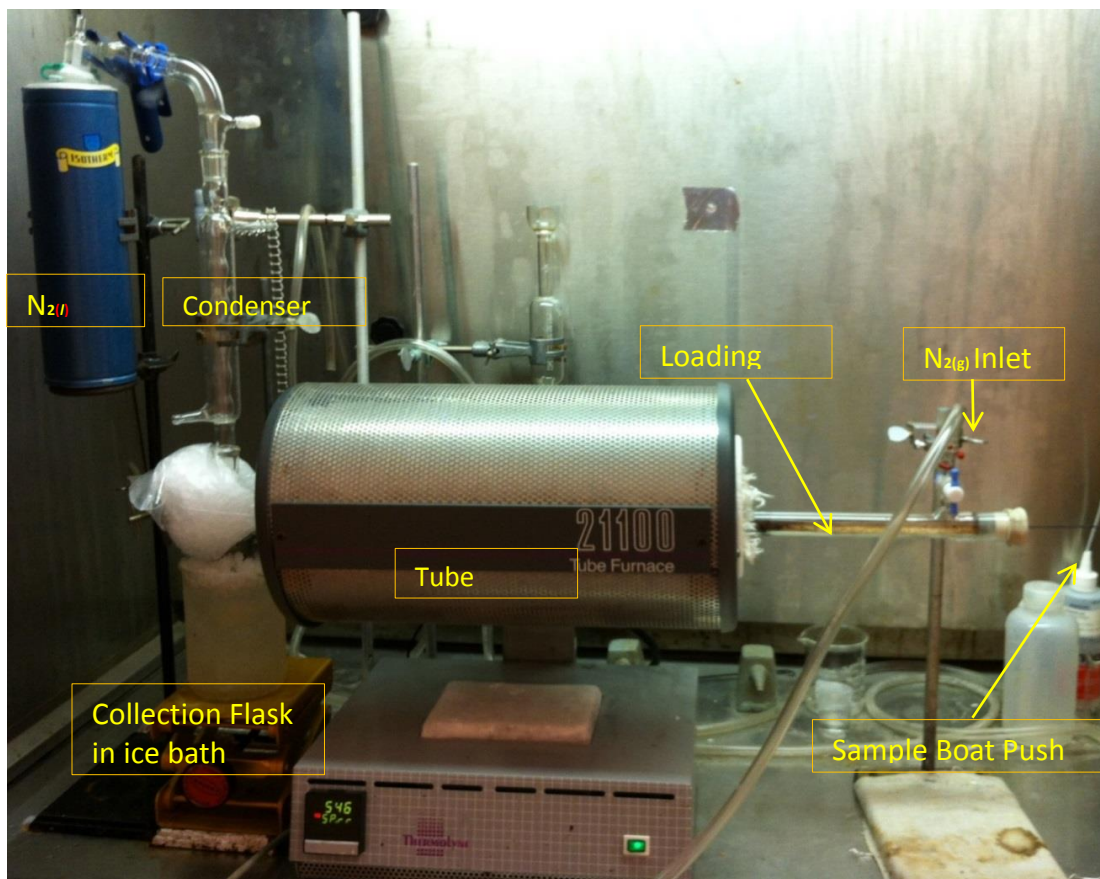


Figure S3.1. Small-scale tube-furnace pyrolysis unit.

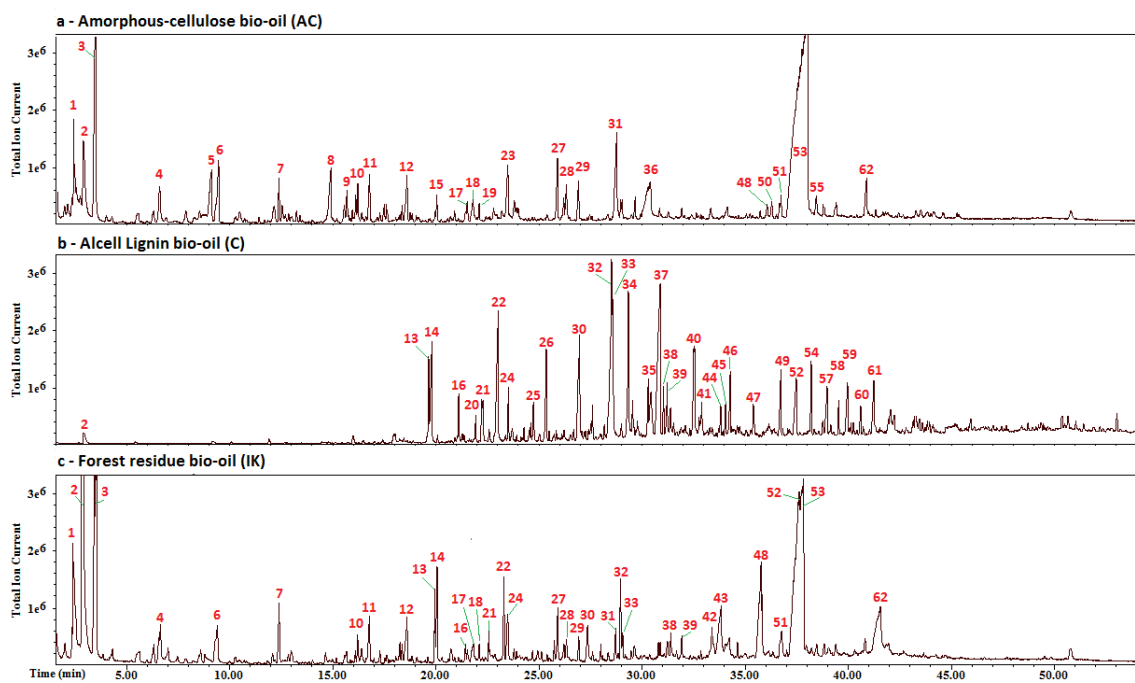


Figure S3.2. GC-MS: Individual products in bio-oils from a) cellulose, b) lignin and c) Forest residue.

Table S3.2. Products identified in bio-oil samples labeled in Figure S2.

Peak No.	Bio-oil feedstock	Cellulose	Alcell Lignin	Forest residue
	Compound	detected peaks		
1	2-hydroxyacetaldehyde	*		*
2	Acetic acid	*	*	*
3	Hydroxypropanone	*		*
4	Propanoic acid	*		*
5	Pyruvic acid	*		
6	2-furaldehyde	*		*
7	Tetrahydro-4-pyrone	*		*
8	2-methyl-2-cyclopentene-1-one	*		
9	5-methyl-2-furaldehyde	*		
10	4-methyl-Cyclohexanol	*		*
11	2(5H)-Furanone	*		*
12	2-hydroxy-3-methyl-2-Cyclopenten-1-one	*		*
13	Phenol		*	*
14	Guaiacol		*	*
15	2,3-Dihydro-5-hydroxy-6-methyl-(4H)-pyran-4-one	*		
16	2-methyl phenol		*	*
17	3-hydroxy-2-methyl-4H-Pyran-4-one	*		*
18	2,5-Furandicarboxaldehyde	*		*
19	2(3H)-Furanone, dihydro-3-methylene-	*		
20	3-methyl-guaiacol		*	*
21	4-methyl-phenol		*	*
22	4-methyl-guaiacol		*	*
23	2,3-dihydroxy-1-hexen-4-one	*		
24	dimethyl-phenol		*	*
25	4-ethyl-guaiacol		*	
26	Dimethyl-guaiacol		*	
27	1-hydroxy-3,6-dioxabicyclo[3.2.1]octan-2-one	*		*
28	3,4-anhydro-d-galactosan	*		*
29	1,4:3,6-dianhydro- $\alpha$ -d-glucopyranose	*		*
30	3-methoxy-1,2-Benzenediol		*	*
31	5-(Hydroxymethyl)-2-furanecarboxaldehyde	*		*
32	1,2-Benzenediol	*	*	*
33	Syringol		*	*
34	6-methoxy-1,2-Benzenediol		*	
35	Isoeugenol		*	
36	2-hydroxymethyl-5-hydroxy-2,3-dihydro-(4H)-pyran	*		

Table S3.2 contd.

	Bio-oil feedstock	Cellulose (C)	Alcell Lignin (L)	Forest residue (FR)
Peak No.	Compound	detected peaks		
37	4-methyl-syringol		*	
38	Vanillin		*	*
39	Hydroquinone		*	*
40	4-ethyl-syringol		*	
41	Methyl vanillate		*	
42	Acetoguaiacone			*
43	1,6-Anhydro- $\beta$ -d-talopyranose	*		*
44	4-vinyl-syringol		*	
45	Guaiacylacetone		*	
46	4-propenyl syringol		*	
47	4-allyl-syringol		*	
48	1,6-Anhydro- $\beta$ -d-mannopyranose	*		*
49	4-propenyl syringol		*	
50	1,6-dianhydro- $\alpha$ -d-galactofuranose	*		
51	3,4-Altrosan	*		*
52	Syringaldehyde		*	
53	Levoglucosan	*		*
54	Unknown		*	
55	1,6-Anhydro- $\alpha$ -d-talopyranose	*		*
56	Methyl syringate		*	
57	Acetosyringone		*	
58	Unknown		*	
59	Syringyl acetone		*	
60	Propio - syringone		*	
61	Unknown			
62	Unknown	*		*

Table S3.3. Model compounds: Positive ion mode ESI MS, with and without dopants.

#	Compd. (M.wt - g/mol )	None	Formic acid	NaCl	NH <sub>4</sub> Cl
1	LG (162)	[M+Na] <sup>+</sup> (100%, 1.5e7), [2M+Na] <sup>+</sup> (10%)	[M+Na] <sup>+</sup> (100%, 7e6) [2M+Na] <sup>+</sup> (10%)	[M+Na] <sup>+</sup> (100%, 1.25e7), [2M+Na] <sup>+</sup> (10%)	[M+NH <sub>4</sub> ] <sup>+</sup> (100%, 2.1e6), [M+Na] <sup>+</sup> (75%), [2M+Na] <sup>+</sup> (15%)
2	Glu (180)	[M+Na] <sup>+</sup> (100%, 1.2e7), [2M+Na] <sup>+</sup> (20%)	[M+Na] <sup>+</sup> (100%, 9e6), [2M+Na] <sup>+</sup> (20%)	[M+Na] <sup>+</sup> (100%, 9e6), [2M+Na] <sup>+</sup> (15%)	[M+NH <sub>4</sub> ] <sup>+</sup> (100%, 3e6), [M+Na] <sup>+</sup> (80%) [LG+NH <sub>4</sub> ] <sup>+</sup> (40%), [LG+H] <sup>+</sup> (10%)
3	Cbio (342)	[M+Na] <sup>+</sup> (100%, 1e6), [2M+Na] <sup>+</sup> (10%), [M+H] <sup>+</sup> (5%), [M-H <sub>2</sub> O+H] <sup>+</sup> (70%)	[M+Na] <sup>+</sup> (5%), [M+H] <sup>+</sup> (10%), [M-H <sub>2</sub> O+H] <sup>+</sup> (100%, 5e5).	[M+Na] <sup>+</sup> (100%, 2e6), [2M+Na] <sup>+</sup> (5%)	[M+NH <sub>4</sub> ] <sup>+</sup> (100%, 2.5e6), [M+H] <sup>+</sup> (15%), [M-H <sub>2</sub> O+H] <sup>+</sup> (90%)
4	G (124)	[M+Na] <sup>+</sup> (100%, 2e5)	[M+Na] <sup>+</sup> (50%, 2e5), [M+H] <sup>+</sup> (25%)	[M+Na] <sup>+</sup> (100%, 3e5)	ND
5	S (154)	[M+Na] <sup>+</sup> (100%, 3e7), [M+H] <sup>+</sup> (10%), [2M+Na] <sup>+</sup> (15%).	[M+Na] <sup>+</sup> (100%, 3e7), [M+H] <sup>+</sup> (15%), [2M+Na] <sup>+</sup> (10%).	[M+Na] <sup>+</sup> (100%, 4e7), [2M+Na] <sup>+</sup> (10%).	[M+H] <sup>+</sup> (100%, 1e7), [M+Na] <sup>+</sup> (50%)
6	V (152)	[M+Na] <sup>+</sup> (100%, 1e7), [M+H] <sup>+</sup> (20%), [2M+Na] <sup>+</sup> (5%)	[M+Na] <sup>+</sup> (100%, 4.7e6), [M+H] <sup>+</sup> (95%)	[M+Na] <sup>+</sup> (100%, 2e7)	[M+H] <sup>+</sup> (100%, 6e6), [M+Na] <sup>+</sup> (5%)



Table S3.4. Model compounds: Negative ion mode ESI MS, with and without dopants.

#	Compd. (M.wt - g/mol)	None	NaOH	NH <sub>4</sub> Cl
1	LG (162)	[M-H] <sup>-</sup> (80%), [2M-H] <sup>-</sup> (100%, 6e5)	[M-H] <sup>-</sup> (100%, 5e5), [2M-H] <sup>-</sup> (50%)	[M+Cl] <sup>-</sup> (100%, 4e5)
2	Glu (180)	[M-H] <sup>-</sup> (100%, 7e5), [2M-H] <sup>-</sup> (15%)	[M-H] <sup>-</sup> (100%, 4e5), [2M-H] <sup>-</sup> (25%)	[M+Cl] <sup>-</sup> (100%, 7e5)
3	Cbio (342)	[M-H] <sup>-</sup> (95%), [LG-H] <sup>-</sup> (100%, 2e5), [Glu-H] <sup>-</sup> (15%)	[M-H] <sup>-</sup> (40%), [LG-H] <sup>-</sup> (100%, 7e5), [Glu-H] <sup>-</sup> (15%)	[M+Cl] <sup>-</sup> (100%, 8e5)
4	G (124)	M-H] <sup>-</sup> (100%, 1.4e4)	[M-H] <sup>-</sup> (100%, 4e4)	poor
5	S (154)	[M-H] <sup>-</sup> (70%), [2M-H] <sup>-</sup> (100%, 1.6e5)	[M-H] <sup>-</sup> (50%,2.5e5)	[M-H] <sup>-</sup> (40%, 1.5e4)
6	V (152)	[M-H] <sup>-</sup> (100%, 1.4e6)	[M-H] <sup>-</sup> (100%, 1.6e6)	[M-H] <sup>-</sup> (100%, 1e6)

Table S3.5. Tandem mass spectra in positive and negative modes for model compounds.

Compound (m/z of [M-H] <sup>-</sup> )	MS <sup>2</sup> fragmentation (product ions' m/z) relative abundance	MS <sup>3</sup> fragmentations (product ions' m/z) relative abundance
Guaiacol (123)	123-CH <sub>3</sub> (108) 100%	
Vanilline (151)	151-CH <sub>3</sub> (136) 100%	136-CO (108) 100%
		136-CO <sub>2</sub> (96) 80%
Syringol (153)	153-CH <sub>3</sub> (138) 100%	138-CH <sub>3</sub> (123) 100%
	153-CO (125) 5%	
Levogulcosan (161)	161-H <sub>2</sub> O (143) 40%	143-H <sub>2</sub> O (125) 30%
		143-CO (113) 100%
		143-CH <sub>2</sub> O <sub>2</sub> (97) 60%
		143-CH <sub>6</sub> O <sub>2</sub> (71) 50%
	161-2H <sub>2</sub> O (125) 5%	
	161-CH <sub>4</sub> O <sub>2</sub> (113) 75%	113-H <sub>2</sub> O (95) 100%
		113-CO (85) 80%
		113-CH <sub>4</sub> O (71) 20%
161-C <sub>2</sub> H <sub>4</sub> O <sub>2</sub> (101) 100%		
161-C <sub>3</sub> H <sub>4</sub> O <sub>3</sub> (73) 40%		
161-C <sub>3</sub> H <sub>6</sub> O <sub>3</sub> (71) 20%		
Glucose (179)	179-H <sub>6</sub> O (161) 90%	161-H <sub>2</sub> O (143) 50%
		161-CH <sub>2</sub> O (131) 40%
		161-2H <sub>2</sub> O (125) 10%
		161-CH <sub>4</sub> O <sub>2</sub> (113) 100%
		161-C <sub>2</sub> H <sub>4</sub> O <sub>2</sub> (101) 100%
		161-C <sub>3</sub> H <sub>4</sub> O <sub>3</sub> (73) 40%
	179-2H <sub>2</sub> O (143) 100%	
	179-CH <sub>2</sub> O (149) 20%	
	179-CH <sub>4</sub> O <sub>2</sub> (131) 50%	
	179-C <sub>2</sub> H <sub>4</sub> O <sub>2</sub> (119) 70%	119-H <sub>2</sub> O (101) 100%
		119-CH <sub>2</sub> O (89) 10%
	179-CH <sub>6</sub> O <sub>3</sub> (113) 60%	
179-C <sub>2</sub> H <sub>6</sub> O <sub>3</sub> (101) 20%		
179-C <sub>3</sub> H <sub>6</sub> O <sub>3</sub> (89) 90%		

Table S3.5 contd.

Compound (m/z of [M-H] <sup>-</sup> )	MS <sup>2</sup> fragmentation (product ions' m/z) relative abundance	MS <sup>3</sup> fragmentations (product ions' m/z) relative abundance
Cellobiose (341)	341-C <sub>6</sub> H <sub>10</sub> O <sub>5</sub> (Glu, 179) 25%	179-H <sub>2</sub> O (161) 95%
		179-2H <sub>2</sub> O (143) 100%
		179-CH <sub>2</sub> O (149) 25%
		179-CH <sub>4</sub> O <sub>2</sub> (131) 50%
		179-C <sub>2</sub> H <sub>4</sub> O <sub>2</sub> (119) 65%
		179-CH <sub>6</sub> O <sub>3</sub> (113) 60%
		179-C <sub>2</sub> H <sub>6</sub> O <sub>3</sub> (101) 25%
		179-C <sub>3</sub> H <sub>6</sub> O <sub>3</sub> (89) 80%
	341-C <sub>6</sub> H <sub>12</sub> O <sub>6</sub> (LG, 161) 100%	161-H <sub>2</sub> O (143) 30%
		161-CH <sub>4</sub> O <sub>2</sub> (113) 75%
161-C <sub>2</sub> H <sub>4</sub> O <sub>2</sub> (101) 100%		
161-C <sub>3</sub> H <sub>4</sub> O <sub>3</sub> (73) 40%		
341-C <sub>7</sub> H <sub>12</sub> O <sub>6</sub> (149) <5%		
341-C <sub>8</sub> H <sub>16</sub> O <sub>8</sub> (101) <5%		
Tandem mass spectra in positive mode for model compounds		
Compound (m/z of [M+Na] <sup>+</sup> )	MS <sup>2</sup> fragmentations (product ions' m/z) relative abundance	MS <sup>3</sup> fragmentations (product ions' m/z) relative abundance
Guaiacol (147)	147 (100%), No fragments	
Vanilline (175)	(175) 100%, No fragments	
Syringol (177)	(177) 100%, No fragments	
Levogulcosan (185)	(185) 100%, No fragments	
Glucose (203)	(203) 25%	
	203-H <sub>2</sub> O (185) 20%	
	203-C <sub>2</sub> H <sub>4</sub> O <sub>2</sub> (143) 100%	
	203-C <sub>3</sub> H <sub>6</sub> O <sub>3</sub> (113) 10%	
Cellobiose (365)	365-H <sub>2</sub> O (347) 80%	347-CH <sub>2</sub> O (317) 60%
		347-C <sub>6</sub> H <sub>8</sub> O <sub>4</sub> (Glu, 203) 100%
		347-C <sub>6</sub> H <sub>10</sub> O <sub>5</sub> (LG, 185) 10%
	365-CH <sub>2</sub> O (335) <5%	
	365-C <sub>2</sub> H <sub>4</sub> O <sub>2</sub> (317) <5%	
	365-C <sub>2</sub> H <sub>4</sub> O <sub>2</sub> (305) 100%	305-C <sub>2</sub> H <sub>4</sub> O <sub>2</sub> (245) 100%
	365-C <sub>4</sub> H <sub>8</sub> O <sub>4</sub> (245) 10%	
	365-C <sub>6</sub> H <sub>10</sub> O <sub>5</sub> (Glu, 203) 20%	
365-C <sub>6</sub> H <sub>12</sub> O <sub>6</sub> (LG, 185) 10%		

Table S3.6. Negative mode MS<sup>2</sup> product ions resulting from ESI-Ion Trap MS of selected ions from the mass spectra of cellulose-bio-oil.

m/z of parent	m/z values of product ions													
	Relative ion abundance (%)													
161	143	129	127	113	101	97								
	25	25	50	95	100	20								
173	155	145	141	129	113	111	97							
	5	20	100	80	10	10	80							
177	159	149	143	139	133	131	117	115						
	40	100	18	10	30	30	15	20						
191	173	171	163	157	147	135	131	113						
	10	10	100	40	50	10	20	20						
197	179	165	153	151	135	125	121	109	97					
	40	40	100	30	10	15	15	20	<5					
205	185	177	171	161	159	145	127	115						
	15	15	25	50	30	100	10	15						
213	195	181	169	151	127	87								
	10	10	100	60	20	70								
221	203	191	187	177	175	161	145							
	25	25	30	100	20	40	30							
235	217	215	205	203	191	189	175	161	145	137	125	115		
	20	20	20	25	100	70	15	20	20	15	15	20		
237	219	217	205	193	191	177	175	163	161					
	20	15	50	50	100	20	20	20	25					
251	233	218	207	191	177	163	161	149	139	123	113			
	50	85	90	25	100	20	10	50	15	15	5			
263	245	243	233	231	229	219	217	203	191	175	173	161	145	135
	10	30	30	30	100	40	70	35	15	15	15	45	30	30
277	259	257	247	245	243	233	231	215	203	189	177	161	153	145
	30	40	25	25	40	45	100	15	30	10	10	40	30	30

Table S3.6 contd.

m/z of parent ions	m/z values of product ions													
	<i>Relative ion abundance (%)</i>													
279	261	259	247	245	235	233	217	215	205	191	179	161	145	
	60	50	100	40	40	90	20	20	20	20	20	40	15	
293	289	275	273	263	261	259	255	249	247	231	229	219	203	191
	50	40	80	20	70	75	25	75	100	30	30	40	30	20
	179	167	161											
	25	75	60											
307	289	275	263	247	234	219	205	191	161	145	133	115	101	
	30	50	40	10	10	10	10	10	100	10	10	10	5	
323	305	303	301	291	289	279	277	265	245	219	203	179	161	145
	40	35	40	50	100	35	40	80	40	35	20	20	60	5
335	317	305	289	275	261	245	233	217	205	177	161	143	131	113
	15	40	30	10	20	10	10	10	10	10	100	15	10	5
353	335	321	309	295	277	249	219	205	189	161	149	131	115	
	40	10	90	30	20	20	15	15	15	40	20	10	5	
341	323	309	307	297	295	281	279	179	161	143				
	30	25	40	20	25	10	15	100	30	30				
365	347	333	321	305	289	277	263	249	233	219	203	189	175	161
	30	40	50	<5	<5	<5	<5	<5	<5	<5	<5	<5	<5	100

Table S3.7. Positive mode MS<sup>2</sup> product ions resulting from ESI-Ion Trap MS of selected ions from the mass spectra of cellulose-bio-oil.

m/z of parent ions	m/z values of product ions													
	Relative ion abundance (%)													
127	109	99	81											
	100	10	10											
149	131	129	121	115	101	87	71							
	100	30	10	20	10	5	25							
161	143	141	131	129	127	115	101	99	85	71				
	50	55	30	100	80	30	75	50	15	20				
171	153	151	143	141	139	137	123	111	109					
	50	100	20	20	60	40	20	30	60					
185	167	163	139	125	111	99								
	40	100	10	25	10	5								
193	175	173	165	163	161	151	147	131	123					
	100	100	30	50	20	25	40	50	20					
199	181	169	167	151	139	127	109	97						
	70	75	100	5	10	10	5	5						
201	183	169	155	141	127	117	109							
	40	100	<5	<5	<5	<5	<5							
203	185	183	171	169	159	143	129							
	30	25	10	100	25	20	10							
215	197	183	173	165	155	141	125	109						
	50	100	<5	<5	<5	<5	<5	<5						
217	197	185	183											
	10	100	50											
229	211	197	183	169	155	143	127	109						
	50	100	<5	5	<5	<5	<5	<5						
231	211	199	197	167										
	10	100	50	5										
245	227	213	203	185	177	163	153	143	127	117	109	101		
	40	100	20	20	15	10	10	5	5	5	5	10		

Table S3.7 contd.

m/z of parent ions	m/z values of product ions													
	Relative ion abundance (%)													
257	239	225	207	197	189	155	147	109						
	30	100	10	10	5	5	5	5						
287	269	267	255	253	225	211	185	169	139					
	20	20	100	80	5	5	15	5	5					
281	263	249	245	231	221	213	203	189	175	161	143	129	117	101
	90	100	80	40	20	20	20	20	20	20	30	5	5	5
289	271	257	239	225										
	25	100	5	5										
301	283	269	251	241	227	209	199	185	173	157				
	40	100	10	10	10	10	10	30	5	5				
317	299	285	267	257	243	225	207	173						
	30	100	<5	<5	<5	<5	<5	<5						
331	313	299	281	271	257	239	229	205	185					
	20	100	<5	<5	<5	<5	<5	<5	10					
343	325	311	307	293	283	261	251	233	215	201	185	163	145	
	566	298	<5	<5	<5	<5	<5	<5	<5	<5	5	<5	<5	
347	329	327	315	313	297	287	261	245	231	219	201	191	185	167
	80	100	80	100	40	30	20	20	20	30	25	20	40	10
	165	151	127	111										
	10	5	5	5										
359	341	327	297	297	259	241	231	213	197	185	173	149	127	
	30	100	<5	<5	<5	<5	<5	<5	<5	20	<5	<5	<5	
365	361	359	347	345	333	331	329	301	259	225	303	195	185	
	5	5	25	100	10	<5	<5	<5	<5	<5	<5	<5	20	
401	383	369	341	327	299	285	257	243	225	210	173	158	186	
	25	100	10	10	10	<5	<5	<5	<5	<5	<5	<5	<5	
413	407	395	393	391	381	379	377	351	301	281	249	185		
	40	20	20	60	45	100	60	20	25	25	15	20		

Table S3.8. Negative mode MS<sup>2</sup> product ions resulting from ESI-Ion Trap MS of selected ions from the mass spectra of lignin-bio-oil.

m/z of parent ions	m/z values of product ions												
	Relative ion abundance (%)												
123	108												
	100												
137	122	109	93										
	100	25	60										
151	136	123	107										
	100	<5	5										
165	150	137	121										
	100	20	40										
167	152	137	135	123									
	100	20	30	20									
181	166	149	137										
	100	99	20										
195	180	178	163	161	151	149	136	123					
	100	50	80	25	20	25	5	<5					
197	182	180	165	163	153	138	121						
	100	40	95	50	50	20	10						
209	194	192	177	165	163	150	137						
	100	30	75	40	40	<5	<5						
241	226	223	213	209	208	197	196	185	153	121	110	95	
	65	50	20	50	100	40	40	45	20	10	50	20	
255	253	251	240	239	238	237	235	227	223	221	211	209	193
	40	100	80	40	75	45	50	30	95	90	70	70	20
	185	166	152	139	111	95							
	25	20	10	<5	50	<5							
293	289	276	273	259	247	232	219	189	167	153			
	100	30	25	35	60	10	15	40	<5	<5			
311	294	291	277	265	247	233	209	195	185	171			
	100	95	75	50	15	20	20	20	15	10			



Table S3.8 contd.

m/z of parent ions	m/z values of product ions												
	<i>Relative ion abundance (%)</i>												
317	302	300	285	283	273	271	257	241	191	179	163	149	137
	50	100	50	85	40	50	20	25	10	15	40	30	20
325	310	308	295	293	291	279	255	247					
	15	100	15	15	70	50	20	15					
339	324	322	319	309	307	305	293	275	261	247	>>		
	20	100	20	30	30	90	60	25	30	25	<5		
345	330	328	315	313	311	301	299	281	269	241	231	219	205
	40	100	20	50	70	40	70	20	20	20	20	15	20
	191	179	163										
	35	35	20										
355	340	322	309	295	277								
	100	50	60	10	15								
365	350	349	332	320	305								
	65	70	100	50	10								
367	352	351	338	334	322	309	290						
	100	80	20	70	50	10	<5						
383	368	367	351	350	337	307	293	276	259	246	231	215	179
	100	50	50	60	60	20	<5	<5	<5	<5	<5	<5	10
389	374	373	356	344	329	312	298	283	268	235	222	191	178
	100	50	50	25	10	<5	<5	<5	<5	<5	<5	5	<5
393	378	377	360	348	335								
	100	50	50	30	10								
417	402	385	384	373	357	341							
	100	30	40	40	20	<5							

Table S3.9. Positive mode MS<sup>2</sup> product ions resulting from ESI-Ion Trap MS of selected ions from the mass spectra of lignin-bio-oil.

m/z of parent ions	m/z values of product ions												
	Relative ion abundance (%)												
169	154	149	141	139	137	125	109						
	5	<5	20	5	100	<5	20						
177	195	177	160	159	149	147	143						
	50	100	30	40	90	20	50						
183	168	163	155	151	137	123	95						
	15	10	35	100	5	10	10						
191	191	174	173	163	147								
	100	5	45	30	15								
205	205	189	187	185	177	175	173	171	157	149	143		
	100	30	45	35	20	30	50	35	35	90	35		
219	219	203	201	199	191	189	187	173	171	161	159	157	
	50	50	60	80	20	40	100	20	40	20	25	20	
233	233	218	215	213	203	201	191	185	171	159			
	50	50	70	60	60	100	65	50	40	40			
253	221												
	100												
269	237	235	163										
	100	95	10										
283	251	249											
	100	30											
301	283	269	240	237	191	177							
	25	100	20	25	30	30							
331	313	299	298	297	205	191	177	167					
	5	10	10	100	10	15	50	15					
345	327	325	313	312	311	207	191	177					
	<5	<5	10	5	20	5	100	30					
345	327	325	313	311	297	283	219	205	191	189	177	175	167
	15	30	15	30	20	20	10	10	100	20	35	50	20
359	344	342	341	339	327	325	205	191	189	177			
	<5	<5	<5	<5	5	5	30	100	10				
359	341	325	311	297	233	219	205	207	191	189	175		
	20	20	10	10	10	10	30	25	100	35	20		
359>191	191	174	131	121	105								
	100	30	30	10	10								

Table S3.9 contd.

m/z of parent ions	m/z values of product ions												
	<i>Relative ion abundance (%)</i>												
373	355	341	339	219	217	205	203	191	189	177			
		15	15	20	30	100	30	90	20	15			
391	373	371	357	235	221	205	191	177					
	10	10	50	50	70	70	100	30					
401	384	383	369	367	355	339	325	247	245	233	231	219	217
	20	20	25	25	10	10	10	20	30	90	70	70	70
	205	204	191	175									
	100	65	70	20									
413	395	381	379	339	301	287	257	243	229	217	205	191	175
	15	40	40	10	20	5	60	100	40	50	40	50	20

Table S3.10. Negative mode MS<sup>2</sup> product ions resulting from ESI-Ion Trap MS of selected ions from the mass spectra of forest residue-bio-oil.

m/z of parent ions	m/z values of product ions													
	Relative ion abundance (%)													
151	136	123	107	103										
	100	10	10	<5										
161	143	129	113	101	99	97	87	85	73	71				
	40	35	50	100	10	10	15	15	10	10				
177	162	159	149	131	115	103	97							
	100	20	5	<5	<5	<5	<5							
191	173	176	159	157	151	147	145	131	129	127				
	60	75	55	55	40	45	100	50	45	60				
221	203	201	191	189	187	177	175	161	159	157	145			
	25	330	20	75	40	80	100	50	40	30	40			
259	244	241	226	215	196	186								
	100	50	50	60	40	20								
265	247	245	235	233	231	221	219	203	191	153	131	97		
	50	40	40	60	70	100	100	50	60	40	40	80		
299	284	282	281	279	269	267	265	255	253	237	235	223	209	193
	60	60	30	70	30	50	75	45	100	40	50	35	20	20
	179	167	161	151										
	20	20	20	20										
313	298	296	295	293	281	279	269	267	251	250	249	237	221	203
	40	20	10	50	30	50	50	55	20	20	100	10	10	5
	191	179	167	151	137	125	109							
	5	5	5	10	20	15	10							
323	319	307	303	291	289	279	277	263	261	249	247	245	233	223
	5	25	50	75	80	40	70	30	50	20	40	40	35	20
	205	179	161	143										
	15	20	100	10										
325	310	309	307	306	292	280	262	248	221	205	189	179	161	145
	70	40	40	80	90	100	50	40	20	20	15	15	10	30

Table S3.11. Positive mode MS<sup>2</sup> product ions resulting from ESI-Ion Trap MS of selected ions from the mass spectra of forest residue-bio-oil.

m/z of parent ions	m/z values of product ions												
	Relative ion abundance (%)												
171	153	139	125	111	97								
	40	100	20	30	20								
185	167	153	125	111									
	25	100	5	5									
199	181	167	153	139	125	111	97						
	50	100	10	5	10	5	5						
201	183	181	169	167	153	139	125						
	20	25	100	60	5	5	5						
215	197	183	155	137	127								
	20	100	<5	<5	<5								
227	209	195	191	181	167	152	109	98					
	50	100	10	5	10	<5	<5	<5					
247	229	228	215	214	197	186	172	154	137	123	112		
	30	50	95	100	5	10	5	70	10	5	20		
259	241	240	227	226	208	195	185	145	151	140	122	95	
	60	70	80	100	10	15	10	15	25	10	5	5	
273	255	254	241	240	222	212	198	181	155	140	121	112	100
	50	70	100	95	10	20	5	5	10	5	10	5	5
301	283	282	269	268	255	237	227	215	199	187	176	150	136
	50	30	100	70	<5	<5	<5	<5	<5	35	<5	<5	<5
301	283	282	281	280	269	268	267	253	227				
	25	25	50	25	80	40	100	10	20				
315	297	296	283	282	269	255	227	205	187	176	164	151	137
	40	50	100	60	<5	<5	<5	<5	<5	<5	<5	<5	<5
347	343	329	327	315	313	185	163						
	20	10	15	35	100	10	20						
379	361	360	359	358	357	356	345	317	275	215	185		
	50	40	90	40	70	50	100	20	20	25	25		

